ABSTRACT

Title of Document: KINETIC AND STRUCTURAL CHARACTERIZATION OF GLUTAMINE-DEPENDENT NAD SYNTHETASES

Melissa Resto, Doctor of Philosophy, 2010

Directed By: Dr. Barbara Gerratana, Department of Chemistry and Biochemistry

Multifunctional enzymes catalyzing successive reactions have evolved several mechanisms for the transport of intermediates between active sites. One mechanism, substrate channeling, allows the transport of the intermediate without releasing it into the solvent. Members of the glutamine amidotransferase (GAT) family often utilize substrate channeling for the transport of intermediates. GAT enzymes hydrolyze glutamine to ammonia, which is transported to an acceptor domain preventing wasteful hydrolysis of glutamine and increasing the efficiency of the reaction. Many GAT enzymes utilize molecular tunnels to shuttle ammonia between active sites. Often GAT enzymes synchronize the active site through conformational changes that occur during catalysis.

Glutamine-dependent NAD synthetases are GAT enzymes and catalyze the last step in the biosynthesis of NAD, utilizing nicotinic acid adenine dinucleotide (NaAD), ATP and glutamine. Steady-state kinetic characterizations and

stoichiometric analysis of NAD synthetase from *Mycobacterium tuberculosis* (NAD synthetase^{TB}) revealed a substrate channeling mechanism for ammonia transport and tight coordination of the active sites resulting in an enzyme that is highly efficient in the use of glutamine. The crystal structure of NAD synthetase^{TB} has revealed a 40 Å tunnel that connects the active sites and is postulated to play a role in the synchronized activities. Several regions of the enzyme were identified that may be important for regulation, such as the YRE loop which contacts the glutamine active site and key regions of the tunnel. Mutations of tunnel residues, such as D656A, show that interruption of important interactions can result in compromise in transfer of ammonia or active site communication.

Phylogenetic analysis revealed that glutamine-dependent NAD synthetases have different levels of regulation. Three groups of enzymes were identified represented by NAD synthetase from *M. tuberculosis*, *S. cerevisiae* (NAD synthetase^{Yeast}) and *Thermotoga maritima* (NAD synthetase^{TM}). Steady-state kinetic characterizations and stoichiometric analysis of NAD synthetase^{TM} has revealed a compromised coordination of the active sites compared to the highly synchronized NAD synthetase^{TB} and the moderate synchronization of NAD synthetase^{Yeast}. Sequence alignment of these groups has allowed identification of residues that line the tunnel that may be responsible for the differences observed in active site coordination and are, therefore, important for active site communication.

KINETIC AND STRUCTURAL CHARACTERIZATION OF GLUTAMINE-DEPENDENT NAD SYNTHETASES

By

Melissa Resto

Dissertation submitted to the Faculty of the Graduate School of the
University of Maryland, College Park, in partial fulfillment
of the requirements for the degree of
Doctor of Philosophy
2010

Advisory Committee:
Professor Barbara Gerratana, Chair
Professor Douglas Julin
Professor Jason Kahn
Professor Steven Rokita
Professor Marco Colombini

Acknowledgements

I would like to thank my advisor Dr. Barbara Gerratana for her guidance and support throughout my graduate career. I have learned a great deal over the years I have worked in her lab and believe that the experiences I have could not have been obtained in anywhere else.

I would also like to thank members of my lab for their assistance and friendship. Dr. Wei Li for the companionship over the several years we spent working in the same lab. Jason Yaffe and Andrew Chang for the assistance they provided with my project. Kaiti Chang for enthusiastically taking on the task of picking up my project. Dr. Watchalee Chuenchor for her assistance in the crystallization of my protein and most importantly for her humor and the positive outlook she would bring. Katie Connor for her making it a wonderful experience working with her and getting to know her.

I thank my friends and family. Dr. Sara Lioi for being my friend, housemate and sounding board. Kathy Goodson for our many entertaining conversations and her much needed humor. Dr. Kelly Daggett for all the experiences we have shared both in and out of the lab and for the always welcomed distractions from the lab next door. I thank my family for supporting me in every possible way. They have given me encouragement and have always taught me to not give up on my goals.

Table of Contents

Acknowledgements ii
Table of Contents iii
List of Tables v
List of Figures vii
List of Abbreviations xi
Chapter 1: Introduction 1
1.1 Multifunctional Enzymes 1
1.2 Substrate Channeling 2
1.3 Enzymes with Molecular Tunnels 4
1.4 Glutamine Amidotransferase Family 6
1.5 NAD Synthetase 14
1.5.1 *Ammonia-Dependent NAD Synthetase* 15
1.5.2 *Glutamine-Dependent NAD synthetases* 18
Chapter 2: Kinetic Characterization of NAD Synthetase from *M. tuberculosis* 21
2.1 Mycobacterium tuberculosis 21
2.2 Nicotinamide Adenine Dinucleotide 25
2.3 NAD Biosynthesis 27
2.4 Goals of Study 29
2.5 Cloning and Purification 29
2.6 Quaternary Structural Characterization 33
2.7 Assay Development 34
2.8 Order of Substrate Binding: Binding Studies 41
2.9 Ordering of Substrate Binding: Inhibition Studies 44
2.10 Kinetics Analysis Shows Optimal Kinetics Synergism 47
2.11 Affect of Glutaminase on Synthetase Domain 53
2.12 Kinetic Mechanism of NAD Synthetase^{TB} 56
Chapter 3: Structural and Mutagenesis Studies of NAD Synthetase^{TB} 58
3.1 Structure of NAD Synthetase^{TB} 58
3.2 The Quaternary Structure of NAD synthetase^{TB} 58
3.3 The Glutaminase Domain and the Glutamine Tunnel 62
3.4 The Ammonia Tunnel and NAD Synthetase^{TB} Mutants 70
3.5 The Synthetase Domain of NAD Synthetase^{TB} 83
Chapter 4: Comparative Study of Glutamine Dependent NAD Synthetases 88
4.1 Thermophilic Proteins and Structural Stability 88
4.2 Thermotoga maritima 90
4.3 Phylogentic Analysis of Glutamine-Dependent NAD Synthetases 90
4.4 Cloning, Expression and Purification of NAD Synthetase^{TM} 94
4.5 Temperature Dependence of NAD Synthetase^{TM} 95
4.6 Steady State Kinetic Characterization of NAD Synthetase^{TM} 96
4.7 Structural Studies of Glutamine-Dependent NAD synthetases 101
4.8 Conclusion 104
Chapter 5: NaADH Assay Development 106

5.1 Necessity for the Development of Continuous Direct Assays 106
5.2 Cloning Expression and Purification of Enzymes Involved in the Biosynthesis of NaAD 108
5.3 The Biosynthesis of NaAD 111
5.4 Reduction of NaAD 113
Chapter 6: Materials and Methods 118
6.1 Materials 118
6.2 Cloning and Expression of Wild Type and Mutant NAD Synthetases 119
6.3 Purification of Wild Type and Mutant NAD Synthetases^{TB} and NAD Synthetases^{TM} 122
6.4 Protein Crystallization 126
6.5 NAD synthetase Activity Assays 127
6.6 Calculation for Assay Detection Limits 132
6.7 Initial Velocity Studies 133
6.8 Temperature Dependent Studies 134
6.9 Inhibition Studies 134
6.10 Binding Studies 135
6.11 Steady-State Kinetic Analysis 136
6.12 Stoichiometry Analysis 137
6.13 Glutaminase Effectors 137
6.14 DON Progress Curve 137
6.15 Inactivation by DON 138
6.16 Phylogenetic analysis 139

List of Tables

Table 1.1. The activation of the glutaminase activity of several GAT enzymes. 13

Table 2.1 Inhibitor constants for the substrate analogs..... 47

Table 2.2 Steady state kinetic parameters of the wild-type NAD synthetase^{TB} catalyzed reactions[a] 49

Table 2.3 Activation of the glutaminase domain of NAD synthetase$^{TB\ a}$ 52

Table 2.4 Stoichiometry analysis for NAD synthetase^{TB} catalyzed reaction[a] 53

Table 2.5 Steady state kinetic parameters of the C176A NAD 55

Table 3.1 Steady state kinetic parameters of the D656A NAD synthetase^{TM} catalyzed reactions 76

Table 3.2 Stoichiometry analysis for wild type and D656A NAD synthetase^{TB} catalyzed reaction[a] 77

Table 3.3 Steady state kinetic parameters of the L486A NAD synthetase^{TM} catalyzed reactions 79

Table 3.4 Steady state kinetic parameters of the L486F NAD synthetase^{TM} catalyzed reactions 80

Table 3.5 Stoichiometry analysis for NAD synthetase^{TB} catalyzed 80

Table 4.1 Steady state kinetic parameters of the NAD synthetase^{TM} catalyzed reactions 98

Table 4.2 The channeling efficiency of NAD synthetases from *T. maritima* , *M. tuberculosis* and yeast. 100

Table 6.1 The purification yields of the wild type and mutant NAD synthetase^{TB} and NAD synthetase^{TM}. 123

List of Figures

Figure 1.1 The four mechanisms of intermediate transport in multifunctional enzymes..... 4

Figure 1.2 The mechanism for glutamine amidotransferase enzymes..... 8

Figure 1.3. Examples of reactions catalyzed by the synthase/synthetase domains of GAT enzymes. 9

Figure 1.4 The reaction catalyzed by the glutaminase and synthetase domains of NAD synthetase. 14

Figure 1.5 The types of NAD synthetases. 15

Figure 1.6 The ordering of the P2 loop of ammonia-dependent NAD synthetase from *B. subtilis*..... 17

Figure 1.7. The first tethered dimer inhibitors of NAD synthetase^{NH3} developed..... 18

Figure 2.1 The spread of *M. tuberculosis* in the lungs..... 23

Figure 2.2 The four first line drugs for treatment of M. TB infection. 25

Figure 2.3 NAD utilization in the cell. NAD is utilized as a coenzyme and for regulation of proteins and signaling pathways in the cell. 26

Figure 2.4 The biosynthetic pathways of NAD formation for *Mycobacterium tuberculosis* and Eukaryotic organisms. 28

Figure 2.5 The protein expression systems utilized for the expression and purification of NAD synthetase^{TB}. 31

Figure 2.6 The purification gel of NAD synthetase^{TB} (expected molecular weight is 74.682 KDa)..... 32

Figure 2.7 The chromatograph of the quaternary structure determination of NAD synthetase^{TB}. 34

Figure 2.8 The coupling assays for NAD synthetase monitoring NAD formation. ... 37

Figure 2.9 The coupling assays for NAD synthetase monitoring glutamine formation. 38

Figure 2.10 The coupling assays for NAD synthetase monitoring pyrophosphate/ inorganic phosphate formation. 39

Figure 2.11 The HPLC chromatograph for the substrates and products of NAD synthetase monitored at 254 nm. 40

Figure 2.12 The intrinsic fluorescent titration data for glutamine. 41

Figure 2.13 NADH concentration based fluorescent intensity. 43

Figure 2.14 The possible inhibition patterns for an enzyme with two substrates. 45

Figure 2.15 The effectors of GAT activation. 51

Figure 2.16 The formation of glutamate or NAD production versus glutamine concentration. 53

Figure 2.17 The inactivation of NAD synthetase^{TB} by DON. 55

Figure 2.18 The kinetic mechanism of NAD synthetase^{TB} 57

Figure 3.1 Oligomeric assembly of NAD synthetase^{TB}. 60

Figure 3.2 Superposition of the synthetase domain (residues 320-679) with NAD synthetase^{NH3} with different ligands. 61

Figure 3.3 Right: Backbone superposition of G5 and G1 (1-320 residues) in green on PH0642 (PDB code 1J31) in blue slate with r.m.s.d. of 1.66 Å for 230 matched residues per subunit. 63

Figure 3.4 DON inhibition of the glutaminase domain. 64

Figure 3.5 Sequence alignments by ClustalW of the glutaminase (a) and synthetase (b) domains of NAD synthetase^{TB} with prokaryotic and eukaryotic NAD synthetases. 66

Figure 3.6 Superposition of the proposed catalytic triad (Glu52-Lys121-Cys176), of the side chain of the DON adduct and of Glu177-Tyr127 residues of the four glutaminase domains in the asymmetric unit.

..... 69

Figure 3.8 The homooctameric structure of NAD synthetase^{TB} with all eight intersubunit tunnels. 70

Figure 3.9 The ammonia tunnel and the synthetase active site. Subunits 1, 5 and 6 are in magenta, green and orange, respectively. 73

Figure 3.10 The YRE loop in of the glutaminase domain (G5) of NAD synthetase^{TB}. 76

Figure 3.11 The CD spectra of wild type and mutant NAD synthetase^{TB}. 77

Figure 3.12 Connecting elements between glutaminase and synthetase active sites.. 81

Figure 3.13 Mapping of the mutations of yeast NAD synthetase reported in Brenner *et al*.(*139*) on S1 and G5 of NAD synthetase^{TB}. 83

Figure 3.14 Superposition of the synthetase domains of NAD synthetase^{TB} with GMP synthetase and with asparagine synthetase. 84

Figure 3.15 Cartoon representation of one subunit of NAD synthetase^{TB} 86

Figure 4.1 The phylogenetic tree for glutamine-dependent NAD synthetase. 94

Figure 4.2 The protein gel of the purification of NAD synthetase^{TM}. 95

Figure 4.3 The temperature dependent profile of NAD synthetase^{TM}.. 96

Figure 4.4 The kinetic scheme for glutamine-dependent NAD synthetase^{TM} reaction. 98

Figure 4.5 The mechanisms of groups A, B and C as represented by NAD synthetase^{TB}, NAD synthetase^{Yeast} and NAD synthetase^{TM} respectively..... 101

Figure 4.6 The amino acid sequence alignment of selected glutamine-dependent NAD synthetases. 103

Figure 4.7 The crystals obtained from crystallization of DON modified NAD synthetase^{TM} bound with NaAD. 104

Figure 5.1 A) The biosynthetic scheme for the synthesis of NaAD. B) The 1, 4 reduction of NaAD to NaADH. 108

Figure 5.2 The chromatograph of the purifiaction of the NaAD synthesis reaction. 113

Figure 5.3 The completed reduction of NaAD to NaADH monitored by HPLC. 114

Figure 5.4 The UV scan of NaADH and NADH at 0.1 mM concentration..... 116

Figure 6.1 The protein gels of the mutants of NAD synthetase^{TB}. 124

Figure 6.2. The MALDI-TOF spectrum of NAD synthetase^{TB}. 126

Figure 6.3 The calibration curve for the cycling assay. 128

Figure 6.4 The calibration curve for the glutaminase assay. 129

Figure 6.5 The calibration curve for the ion paired HPLC assay monitoring ADP, AMP and NAD formation..... 130

Figure 6.6 The calibration curve for the malachite green assay. 131

List of Abbreviations

acetyl-NAD	3-acetylpyridine adenine dinucleotide
AlCAR	5'-(5-aminoimidazole-4-carboxamide) ribonucleotide
AMPCPP	α,β-methyleneadenosine 5'-triphosphate
AMPPCP	β,γ-methyleneadenosine 5'-triphosphate
ATIC	5-amino-4-imidazolecarboxamide ribonucleotide transformylase /inosine 5-monophosphate cyclohydrolase
CPS	carbamyl phosphate synthetase
DON	6-diazo-5-oxo-L-norleucine
GAT	glutamine amidotransferase
Glutamine	L-glutamine
GPATase	glutamine phosphoribosylpyrophosphate amidotransferase
IGPS	imidazole glycerol phosphate synthase
M. TB	*Mycobacterium tuberculosis*
NaAD	nicotinic acid adenine dinucleotide ($NaAD^+$)
NAD	nicotinamide adenine dinucleotide (NAD^+)
PFAR	N'-(5'- phosphoribosyl)-formimino-5-aminoimidazole-4-carboxamide ribonucleotide
PPi	pyrophosphate
PRPP	phosphoribosylpyrophosphate

Chapter 1: Introduction

1.1 Multifunctional Enzymes

In many biosynthetic pathways it is necessary for enzymes to catalyze more than one reaction. In these cases the enzyme may contain multiple active sites expressed on one polypeptide chain in order to facilitate the reaction (*1*). These multifunctional enzymes catalyze the synthesis of many important biological molecules such as amino acids (*1-3*), nucleotides (*4*), cofactors (*5*) and a variety of metabolites in the cell. Examples of multifunctional enzymes can be found performing a variety of functions. 6-phosphofructose-2 kinase/fructose-2,6-bisphosphatase is an important enzyme in the regulation of the glycolytic and gluconeogenesis pathways and catalyzes two opposing reactions, the breakdown and formation of fructose 2,6-bisphosphate that each occur in two separate catalytic domains (*6*). The bifunctional β-lactamase $bla_{\text{LR-13}\Lambda}$ cleaves β-lactams conferring antibiotic resistance to the organism. The two domains of the β-lactamase have two different specificities toward β-lactam subclasses giving the enzyme a wider substrate specificity (*1*). Many multifunctional enzymes catalyze sequential reactions and it is this category of multifunctional enzymes that shall be focused on. There are several benefits of multifunctionality including increased coordination of gene function (*7, 8*) and increased kinetic advantage due to the proximity effect (*8*). Substrate channeling (discussed in detail below) is also kinetically advantageous allowing direct transfer of intermediates between active sites without diffusion into the solvent. Many multifunctional enzymes are also able to regulate catalytic activities through coordination of the active sites (*8*).

1.2 Substrate Channeling

Enzymes that catalyze multiple reactions have evolved several mechanisms for shuttling intermediates between different active sites (Figure 1.1). The first mechanism involves the use of a "swinging arm" (Figure 1.1A). In these enzymes a prosthetic group is bound to the enzyme on which the substrate is bound. The prosthetic groups utilized are biotin, lipoic acid and pantetheine acid (*9*). The product of one active site is then transported where it becomes the substrate for the other active sites where it is extended and modified (*9*). This is exemplified in fatty acid and polyketide synthases, both utilize a phosphopantetheinyl group as part of an acyl carrier protein to carry the growing molecule to different active sites. Some fatty acid and polyketide synthases consist of monofunctional enzyme complexes; however, many others are complexes of multifunctional enzymes. Human fatty acid synthase is a dimer made up of seven domains per monomer. The type I erythromycin synthase contains three multifunctional enzymes performing seven reactions (*9*). The second mechanism involved the physical proximity of active sites in a multienzyme complex in which the intermediate would travel a short distance to the next active site (Figure 1.1B). In some cases formation of these multienzyme complexes have been shown *in vitro* (*10*). However, as in the case of purine biosynthesis, efforts to show the formation of such a multienzyme complex *in vitro* failed (*11*). A seminal work *(12)* recently showed that 5-amino-4-imidazolecarboxamide ribonucleotide transformylase/inosine 5-monophosphate cyclohydrolase (ATIC), a bifunctional enzyme that catalyzes the formation of inosine monophosphate through 5-

formylaminoimidazole-4-carboxamide ribonucleotide intermediate (*13*), is part of a multienzyme complex (the purinosome) with the trifunctional TrifGART and the bifunctional PAICS involved in *de novo* synthesis of purines (*12*). Low purine concentrations in human cancer cells were shown to induce co-localization of these enzymes (*12*). These results are significant because it indicates that multienzyme complex formation, and therefore substrate channeling and active site regulation, can be regulated by the product of the biosynthetic pathway, in this case by adenosine and guanosine nucleotides. It is also suggests that enzymes, which do not form a complex *in vitro*, may do so *in vivo* in the presence/absence of metabolites. A third mechanism involves the transport of a molecule, not covalently bound to the enzyme, between distant active sites through an internal "tunnel" (Figure 1.1C) (*1, 14*). The last mechanism involved the diffusion in solution of the intermediate to allow it to reach the second active site (*10*) (Figure 1.1D). After considering the case involving the purinosome discussed above it is possible that this mechanism is not used in the cell when the intermediate is unstable/toxic or when the intermediate/product formation needs to be tightly regulated.

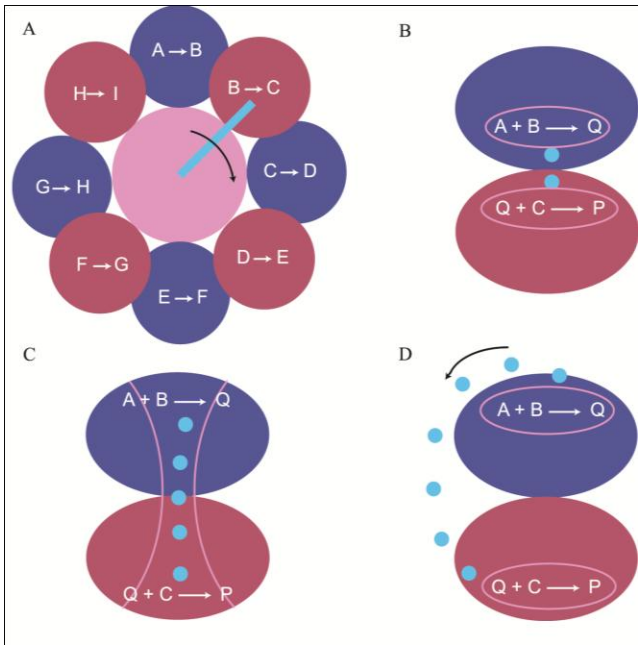

Figure 1.1 The four mechanisms of intermediate transport in multifunctional enzymes. A. A substrate is tethered to the enzyme and swings from one active site to another where modifications are made or the chain is extended. B. The active sites of the enzyme are situated adjacent to each other and the intermediate can pass from one active site to another. C. A molecular tunnel allows transport of the intermediate. D. An intermediate travels out of one active site, through the solvent to the second active site.

1.3 Enzymes with Molecular Tunnels

A molecular tunnel allows the passage of the intermediate by connecting two active sites that are located on different domains or subunits of an enzyme (*15*). The use of molecular tunnels for the transportation of intermediates has several advantages. Prevention of intermediates from release into the solvent increases the efficiency of the reaction since no intermediate can diffuse away (*16*). It protects unstable intermediates from solvent (*16, 17*) and sequesters toxic intermediates from

release into the cell (*16*) such as ammonia, which can be cytotoxic at high concentrations.

Currently enzymes that transfer intermediates through molecular tunnels are identified using a variety of techniques. Crystal structures can provide evidence for the possibility of a tunnel mechanism. In 1988 the crystal structure of tryptophan synthase was solved from *Salmonella typhimurium* (*18*). It was determined that the two subunits were separated by 25 Å and there existed a tunnel that was large enough to allow the passage of the indole intermediate. This was the first large piece of evidence for the use of a molecular tunnel to shuttle catalytic intermediates between different active sites. Since then a variety of enzymes have been identified that contain molecular tunnels utilizing crystal structures, kinetic and biochemical techniques. In order to confirm the use of the tunnels identified in crystal structure mutagenesis of residues proposed to line these tunnels have been performed in attempts to block the tunnel (*19-22*). Calculating the stoichiometry of product formation allows for the indirect determination of transport of an intermediate with in an enzyme. A one to one stoichiometry is indicative of transport within an enzyme in which the product of one active site is transported and utilized in the second reaction and, therefore, no intermediate is lost to solvent. However, if the stoichiometry is not one to one a method to determine whether there is some channeling in catalysis is a classic isotope dilution experiment, which involves the analysis of the competition between the intermediate species labeled with a radioisotope or heavy atom introduced into the bulk solvent and the unlabeled intermediate produced by the enzyme. For example with enzymes that transport ammonia exogenous $^{15}NH_3/^{14}NH_3$

and ammonia hydrolyzed from glutamine compete for incorporation into the final product. If the ratio of $^{15}NH_3/^{14}NH_3$ is the same ratio as the $^{15}NH_3/^{14}NH_3$ added to the bulk solvent then the ammonia formed from glutamine is allowed to equilibrate with the solvent. The $^{15}NH_3/^{14}NH_3$ can also be dictated by the ratio of the k_{cat}/K_M for glutamine and ammonia, which is the ratio of ammonia incorporated into NAD obtained from the solvent or glutamine hydrolysis. If the $^{15}NH_3/^{14}NH_3$ is dictated by the ratio of the k_{cat}/K_M the ammonia produced by glutamine hydrolysis is transported within the enzyme and does not equilibrate with ammonia in the solvent (*10*).

Enzymes that utilize molecular tunnels to shuttle intermediates catalyze a wide variety of reactions that are essential for cellular function. They are involved in the biosynthesis of amino acids, nucleic acids and coenzymes such as NAD. There are four classes of enzymes with molecular tunnels; enzymes that transport ammonia (glutamine amidotransferase) (*15*), one that transports indole (tryptophan synthase) (*23*), one enzyme that transports carbamate (carbamoyl phosphate synthetase) (*24*) and one that transports carbon monoxide (carbon monoxide dehydrogenase/acetyl-CoA synthase) (*25*). Of these four types of enzymes the most numerous are the enzymes that transport ammonia that belong to the glutamine amidotransferase (GAT) family (discussed below) (*14*).

1.4 Glutamine Amidotransferase Family

Members of the glutamine amidotransferase family contain two domains. The first domain is a glutamine amidotransferase domain, which produces ammonia through the hydrolysis of glutamine to glutamate. The ammonia is then shuttled to the synthase/ synthetase domain, which binds the acceptor molecule. Enzymes containing

GAT domains hydrolyze glutamine using Cys or Ser residue as a nucleophile (Figure 1.2). There are four classes of amidotransferases, the triad family, the N-terminal glutaminases or Ntn, the amidases and the nitrilase superfamily (*26*). The triad family, also called the class I or G-type, utilizes a Cys-His-Glu catalytic triad and Cys acts as a nucleophile to attack the amine of glutamine, examples are carbamoyl phosphate synthetase (CPS) and imidazole glycerol phosphate synthase (IGPS). The Ntn or class II enzymes do not utilize a catalytic triad but make use of an N-terminal cysteine as the nucleophile as is the case with asparagine synthetase B. The amidases utilized a nucleophilic serine residue (Figure 1.2 B) and is exemplified by glutamine-$tRNA^{gln}$ amidotransferase (*10*). The last class of amidotransferases is the nitrilases, which contain a catalytic triad of Glu-Lys-Cys, where Cys acts as a nucleophile, and of which glutamine-dependent NAD synthetase is the only member to date. The acceptor domains of GAT enzymes do not contain similarities in sequence, structure or mechanism since they catalyze a variety of reactions (Figure 1.3).

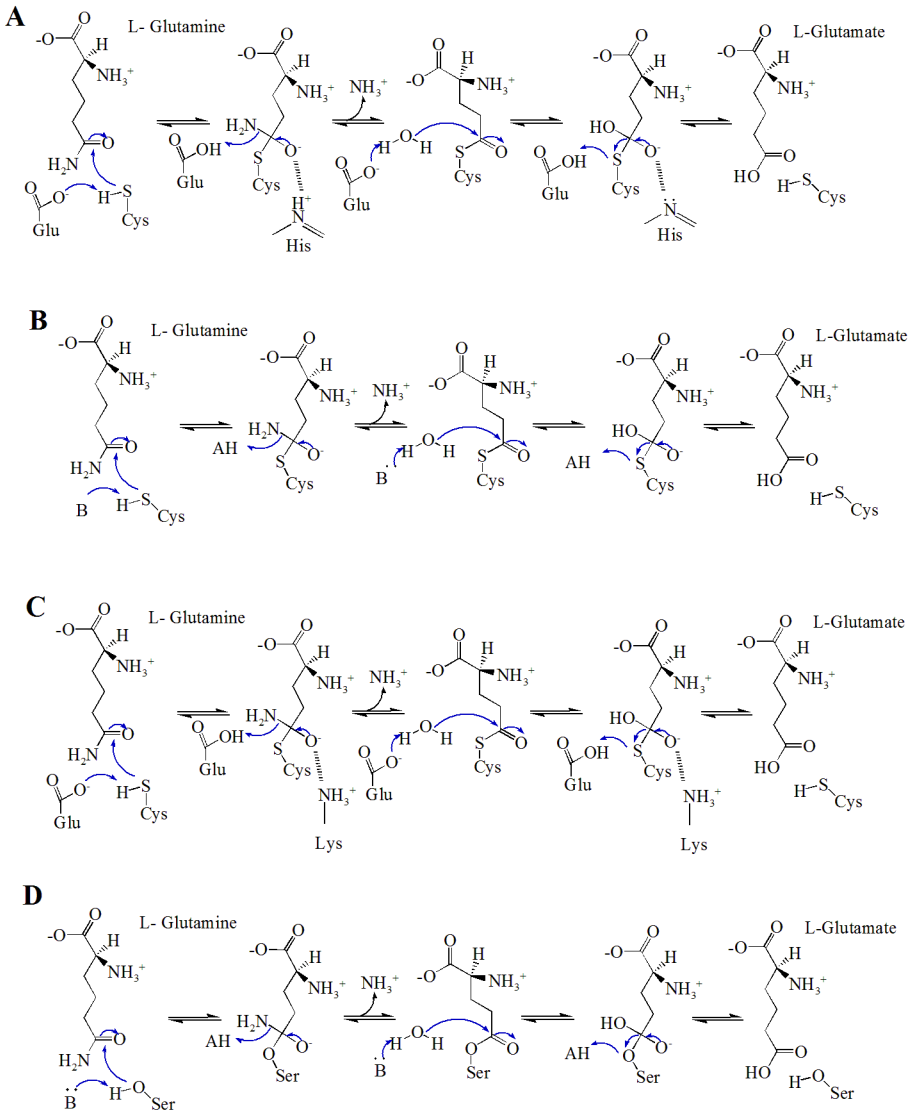

Figure 1.2 The mechanism for glutamine amidotransferase enzymes. A. In the class I enzymes a Cys is the nucleophile, Glu acts as the acid/base and His stabilizes the negative charge on the transition state. B. In the class II enzymes Cys is the nucleophile and there is no catalytic triad. C. In the nitrilases Glu acts as the acid/base and Lys stabilizes the negative charge on the transition state. D. The amidases utilize a nucleophilic serine residue**.**

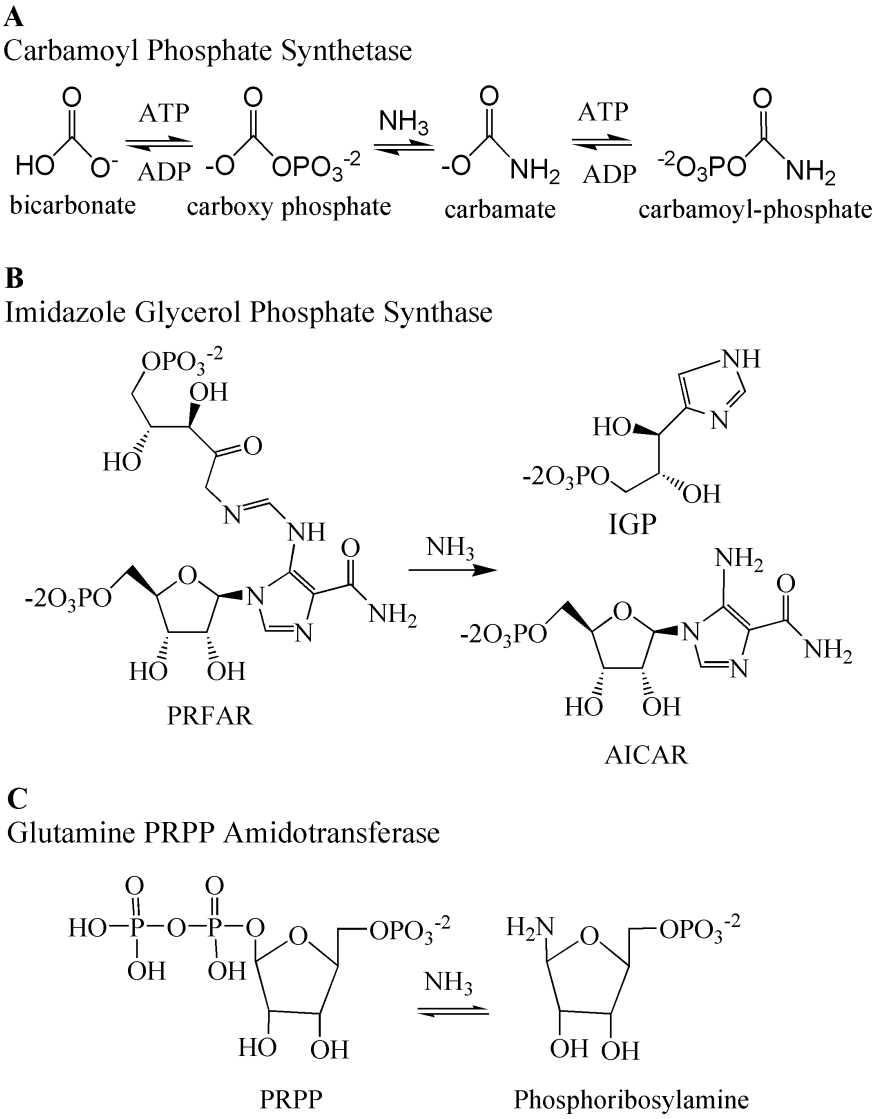

Figure 1.3. Examples of reactions catalyzed by the synthase/synthetase domains of GAT enzymes. A. The reaction catalyzed by the synthetase domain of carbamoyl phosphate synthetase. B. The reaction catalyzed by the synthase domain of imidazole glycerol phosphate synthase. C. The reaction catalyzed by the synthetase domain of glutamine PRPP amidotransferase.

As mentioned above, many of members of the GAT family utilize molecular tunnels in order to transport intermediates from the glutaminase domains to the

synthase/ synthetase domain. In the majority of GAT enzymes the molecular tunnels are primarily composed of the synthetase domains, therefore, the molecular tunnels have few similarities (*24*). In the majority of these enzymes the ammonia tunnel is lined with predominantly hydrophobic residues, such as in asparagine synthetase (*27*) and glutamine phosphoribosylpyrophosphate amidotransferase (GPATase) (*28*). In few examples (glutamine synthase (*29*), glutamyl-tRNA reductase (*30*) and the thymidylate synthase-dihydrofolate reductase (*31*)) the tunnel is lined with hydrophilic residues. The sequence of the residues that line the tunnels of GAT enzymes are strictly conserved in some enzymes, such as GPATase (*32*), and not strictly conserved in others, such as asparagine synthetase (*27*). In many GAT enzymes the ammonia tunnel is fully formed in the enzyme, however, in some cases the tunnel is transiently formed during catalysis. The tunnel in glutamine synthetase is formed by two cavities that are not connected (*29*). It is proposed that the residues separating the cavities and preventing ammonia passage act as a gating mechanism involved in signaling between the active sites (*10, 29*). The tunnel of both GMP synthetase and GPATase are not formed until substrate is bound. In the absence of phosphoribosylpyrophosphate (PRPP) no tunnel is observed in GPATase, however, the binding of PRPP causes of kink in the C-terminal helix resulting in a restructuring of a loop causing formation of ~20 Å long tunnel connecting the active sites (*32*). The crystal structure of *E. coli* GMP synthetase shows the active sites are separated by 30 Å but no tunnel was observed (*33*). However, it is proposed that the binding of the substrates, ATP and XMP, causes a major conformational change forming a tunnel between the active sites (*33, 34*). Molecular dynamic simulations of ammonia

transport through CPS revealed that ammonia is transported through the tunnel through hydrogen bonding interactions between the ammonia molecule and the side chains of the residues lining the tunnel (*35, 36*). The tunnel is sealed from solvent (*36*) and ammonia transport is fast occurring from 9.5 to 14 nsec over a 13 Å portion of the tunnel (*35*). Transport occurs in stages with the ammonia molecule frequently oscillating between residues and is favored by a free-energy potential (*36*). It was also shown that the ammonium ion could only proceed partially through the tunnel before becoming trapped (*35*). The tunnel of glucosamine-6-phosphate synthase was also analyzed by molecular dynamic simulation also showing fast transport of the ammonia molecule (*37*). It was also revealed that local conformational changes occur in the tunnel during ammonia transport (*37*). A narrow passage was widened through the flipping of an Ala sidechain suggesting that this region acted like a gate to the next region of the tunnel. Mutagenesis experiments have confirmed the importance of many of the residues involved in ammonia transport (*36, 37*). However, the results of these molecular dynamic simulations may not be applicable to ammonia tunnels from other enzymes due to the fact that the composition and method of formation of the tunnels for GAT enzyme varies a great deal.

Many GAT enzymes that utilize molecular tunnels synchronize the activities of the active sites during the reaction (*15, 38*) (Table 1.1). The coordination of active sites prevents the loss of an ammonia due to diffusion out of the active site into the solvent, reaction of the intermediate with the solvent or to conserve a scarce substrate. The synchronization of the active sites may occur due to conformational changes in the protein that may be the result of substrate binding or intermediate formation (*15,*

34). These can be the result of local changes in the glutamine active site or larger conformational changes throughout the enzyme. This coordination of the active sites is referred to as active site coupling. This activation of the glutaminase active site due to the presence of synthase/synthetase activity occurs in many GAT enzymes (Table 1.1). The activation can be only a few fold or large. Some examples of of enzymes that undergo glutaminase activation are GPATase, IGPS and glutamine synthase. GPATase exhibits coupling of the active sites as indicated by the 2.8 fold increase in the V_{max} of the glutaminase reaction in the presence of PRPP. PRPP binding induces a conformational change that modifies the glutaminase active site repositioning an Arg residue for glutamine binding and causing a kink in the C-terminal helix which causes restructuring of a loop resulting in formation of the ammonia tunnel. (*28*). IGPS undergoes a 4900-fold increase of the k_{cat} of glutaminase activity due to the binding of PRFAR, which causes small changes in loops that surround glutamine actives site and a conformational change in a partially ordered loop in the synthetase active site *(15, 42)*. Glutamine synthase undergoes active site synchronization indicated by the 22 fold increase in the V_{max} of the glutaminase, which occurs through the binding of ferredoxin and 2-oxoglutarate (*39*). It is proposed that glutamine synthase substrate binding induces a conformational change in a loop at the glutaminase active site, which causes a cascade of changes ending in the formation of a salt bridge and the activation of the N-terminal nucleophilic cys through a hydrogen bonding interaction (*40*).

Table 1.1. The activation of the glutaminase activity of several GAT enzymes.

Enzyme	Activation	Mechanism
CPS	6.5 fold (k_{cat}) (*17*)	Formation of bicarbonate phosphate triggers glutaminase activation (*41*).
IGPS	4900 fold (k_{cat}) (*42*)	PRFAR binding causes small changes in loops that surround glutamine actives site and conformational change in a partially ordered loop in the synthetase active site (*15, 42*).
GPATase	2.8 fold (V_{max})	PRPP binding repositions Arg residue in GAT active site for glutamine binding and causes a kink in the C-terminal helix which causes large restructuring of a loop causing formation of the ammonia tunnel.
Glutamine synthase	22 fold (V_{max}) (*43*)	Ferredoxin and 2-oxoglutarate binding causes a conformational change in a glutaminase active site loop, activating the N-terminal nucleophilic cys through H-bond formation.
Glucosamine-6-phosphate synthase	69 fold (k_{cat}) (*44*)	Binding of fructose-6-phosphate causes ordering of C-terminal tail then the glutaminase domains become ordered (*45*).
GMP synthetase		Binding of ATP and XMP forms the ammonia tunnel and stimulates catalysis (*33*).
Glu-tRNA^{Gln}	3 fold (k_{cat})	Formation of P-γ-Glu-tRNA^{Gln} intermediate

amidotransferase	(*26*)	triggers the motion of a hairpin in a adjacent subunit which positions a Thr residue for activation of the glutaminase active site (*46*).
Asparagine synthetase	No activation	The glutaminase and synthase active sites are uncoupled and no communication is observed (*47*).

1.5 NAD Synthetase

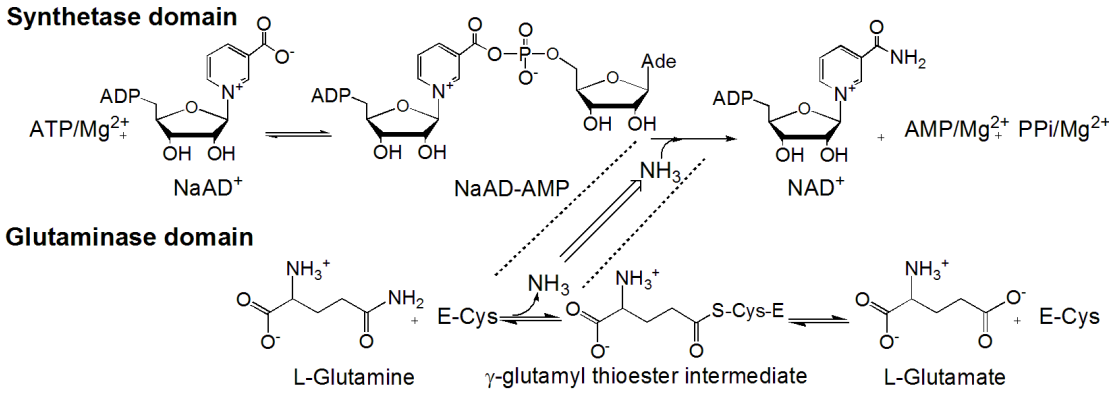

Figure 1.4 The reaction catalyzed by the glutaminase and synthetase domains of NAD synthetase.

NAD synthetase catalyzes the last step in the *de novo* biosynthesis of NAD. It is responsible for the formation of nicotinamide adenine dinucleotide (NAD) from nicotinic acid adenine dinucleotide (NaAD) and ATP (Figure 1.4). There are two forms of NAD synthetase: a strictly ammonia-dependent enzyme (NAD synthetase^{NH3}) and a glutamine-dependent enzyme (NAD synthetase^{Gln}), which is capable of utilizing glutamine as an ammonia donor. The ammonia dependent enzyme is found primarily in prokaryotes, such as *E. coli* (*48*) and *B. subtilis* (*49*), while the glutamine-dependent enzyme is found in eukaryotes and some prokaryotes,

such as *Mycobacterium tuberculosis* (*50*) and *Thermotoga maritima* and the archea *M. thermophila* (Figure 1.5). Recently a glutamine-dependent enzyme was identified from *Thermus thermophilus* that contained both active sites on separate subunits (personal communication with Andrei Osterman, Sanford-Burnham Medical Research Institute).

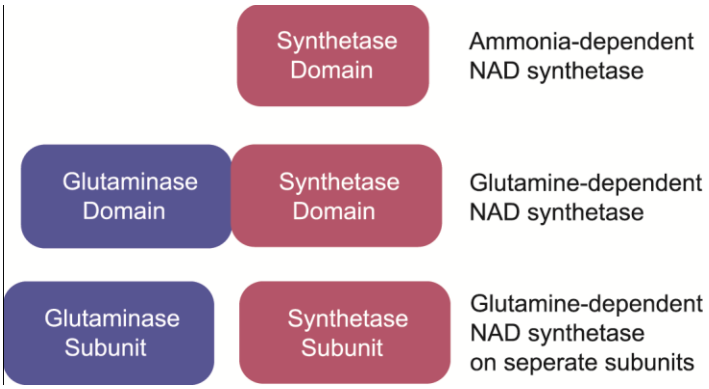

Figure 1.5 The types of NAD synthetases. A ammonia-dependent enzyme with only the synthetase domain, a glutamine-dependent enzyme with a synthetase and glutaminase domain in one subunit and a glutamine dependent enzyme with the synthetase and glutaminase domain on separate subunits.

1.5.1 *Ammonia-Dependent NAD Synthetase*

The ammonia-dependent NAD synthetase contains only the synthetase domain and utilizes exogenous ammonia as a nitrogen source. The synthetase domain is a member of the N-type ATP pyrophosphatases family (*51*). This family is characterized by a flexible nucleotide binding loop designated the P loop. Members of this family catalyze reactions that share the ATP-dependent activation of a carbonyl group by forming an acyladenylate intermediate and pyrophosphate (*52*). A

nitrogen nucleophile, in this case ammonia, attacks the acyladenylate intermediate releasing AMP (Figure 1.4).

The crystal structures of ammonia-dependent NAD synthetase from *B. subtilis* (NAD synthetase^{Bac}), *E. coli* (NAD synthetase^{Ecoli}), *H. pylori* (NAD synthetase^{HP}) and *B. anthracis* (NAD synthtase^{Ban}) has provided a great deal of information about the mechanism. NAD synthetase^{NH3} is a homodimer consisting of α-helices and β-sheets (*52-55*). The NaAD binding site is located at the interface of the dimer while the ATP binding site is within one subunit (*56*). The most interesting aspect of the enzyme structure is the presence of two flexible loop near the enzyme active site, designated loop P1 and P2. In the apo structures both P loops are disordered (*41, 44, 45*(*55*). In NAD synthetase^{Bac} when only NaAD is bound the P loops are also disordered (*52*) (Figure 1.6A). The P1 loop becomes ordered due to hydrogen bonding of Q84^{Bac} to the adenine base of ATP (*50, 53, 54*). P2 loop stabilization was observed in NAD synthetase^{Bac} and NAD synthetase^{HP} (*52-54*). The ordering of P2 loop involves coordination of the Mg^{2+} ions which coordinate to AMP/PPi. NAD synthetase^{Bac} and NAD synthetase^{Ban} crystal structures with AMP and pyrophosphate bound contains a second magnesium bound and the P2 loop partially ordered. This second active site magnesium ion is coordinated to the carbonyl backbone of T208^{Bac} in the P2 loop (*55-57*) (Figure 1.6C). When the NAD synthetase^{Bac} is crystallized with NaAD-AMP and pyrophosphate the P2 loop is completely ordered (*58, 59*) (Figure 1.6B). These structures indicate that the binding of ATP and the formation of the intermediate complex trigger conformational changes in the loops P1 and P2, respectively. The P

loops, when ordered, close over the active site. This ordering of the P loops protects the ATP molecule and the unstable NaAD-AMP intermediate from hydrolysis.

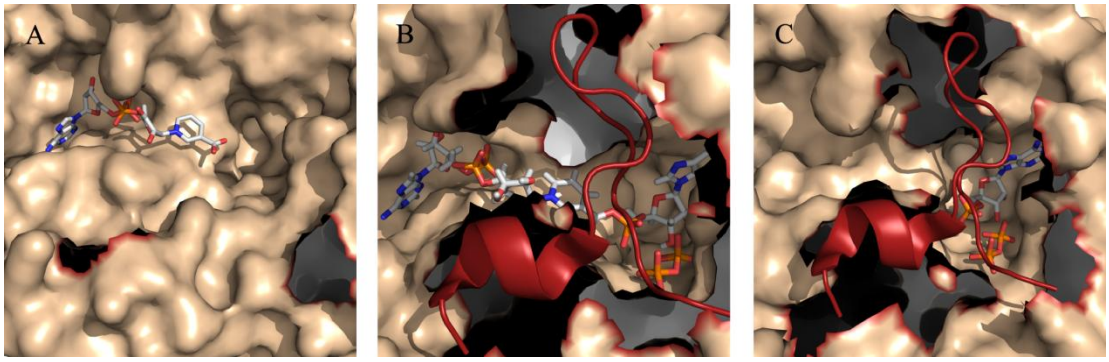

Figure 1.6 The ordering of the P2 loop of ammonia-dependent NAD synthetase from *B. subtilis*. A. In the presence of NaAD the P2 loop is disordered. B. In the presence of the acyladenylate intermediate the P2 loop is ordered. C. In the presence of AMP and pyrophosphate the P2 loop is ordered.

The ammonia dependent NAD synthetases from several organisms have undergone steady state kinetic characterization including those from *E. coli*, *B. stearothermophilus*, *S. typhimurium*, *B. anthracis* and *B. subtilis* (*55, 60-63*). NAD synthetase has been found to be critical for sporulation and vegetative growth of bacteria (*61, 64, 65*). NAD also plays an important role in many other processes in the cell (*66*) (discussed in chapter 2) This information coupled with the available structural data has allowed for ammonia dependent NAD synthetase to become targets for the development of inhibitors to combat the rise in antibiotic resistance. The first inhibitors developed were tethered dimmers (Figure 1.7), which contained hydrophobic groups, a polymethylene linker and a charged nitrogen (*67, 68*). The most effective of these compounds had measured IC_{50} values as low as 10 to 20 μM against NAD synthetase^{Bac} and resembled detergents (*67, 68*). The binding the

inhibitors were suggested to be the result of specific interactions (*68*). The tethered dimmers are bisubstrate inhibitors, which would bind to both the NaAD and ATP binding sites. However, the IC_{50} for the inhibitors are low. This could be because the inhibitors are substrate analogs and bind to an open conformation of the enzyme, disordered P2 loop, and an ordering of the P2 loop leading to a closed conformation may be needed in order to obtain a higher IC_{50}.

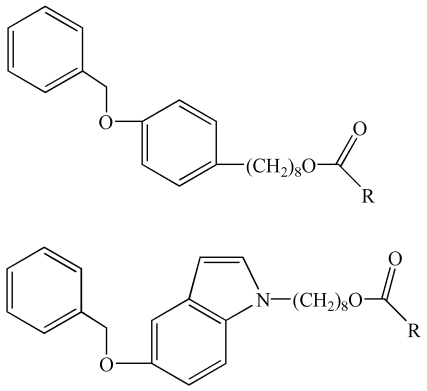

Figure 1.7. The first tethered dimer inhibitors of NAD synthetase^{NH3} developed. The R groups are aromatic with a charged nitrogen group. From these compound libraries were constructed to develop higher affinity inhibitors.

1.5.2 *Glutamine-Dependent NAD synthetases*

The glutamine dependent enzyme contains two domains, the GAT domain and the synthetase domain (Figure 1.5). Ammonia-dependent NAD synthetase from *B. subtilis*, while there is low sequence homology (25% homologous to yeast enzyme), it is structurally homologous to the synthetase domain of the glutamine-dependent enzyme (Chapter 3). The GAT domain is a member of the nitrilase superfamily, which catalyze carbon-nitrogen formation or hydrolysis through the attack of a cyano or carbonyl carbon by a nucleophilic cysteine (*5*). It was found that when mutating

E45, K114, C175 to alanine in NAD synthetase from *Saccharomyces cerevisiae* (NAD synthetase^{Yeast}) glutaminase specific activity was abolished confirming that these three amino acids are essential for glutamine hydrolysis (*5*). However, ammonia dependent activity was also reduced when these residues were mutated. This indicates that coupling of the active site may occur due to the fact that modification of the glutaminase active site results in changes in the synthetase activity.

NAD synthetase^{Yeast} was kinetically characterized. The glutaminase activity was activated 8 fold in the presence of NaAD. This indicates that there is some communication that occurs between the synthetase and glutaminase domain. The enzyme also has a 50% channeling efficiency. The channeling efficiency is the percentage of ammonia produced by glutamine hydrolysis that proceeds to form NAD (Equation 1.1). This percentage gives an indication of whether ammonia is transported within an enzyme or is released into solvent. A channeling efficiency of 100% is indicative of ammonia transport within the enzyme. NAD synthetase^{Yeast}, therefore, is an inefficient enzyme and undergoes wasteful glutamine hydrolysis.

$$\text{Channeling Efficiency} = \frac{[NAD^{\cdot}]}{[Gln]} \text{ X } 100$$

Equation 1.1

When I started to work on this project no crystal structure of any glutamine-dependent NAD synthetases had been solved. In 2003 Bieganowski *et al*. performed molecular modeling studies that threaded the sequence of NAD synthetase^{Yeast} to the nitrilase domain of worm NitFhit (15% identity with yeast enzyme) and the ammonia-dependent NAD synthetase from *B. subtilis* (25% identity with yeast enzyme) (*5*). The model obtained showed the presence of a ~45 Å tunnel connecting the two active

sites of NAD synthetase, however, the low sequence identity between the enzymes casted significant doubt on the validity of this model. The model was later shown to be incorrect upon determination of the crystal structure of NAD synthetase from *M. tuberculosis* (discussed in Chapter 3).

Chapter 2: Kinetic Characterization of NAD Synthetase from *M. tuberculosis*

2.1 Mycobacterium tuberculosis

Mycobacterium tuberculosis (M. TB) is the causative bacteria of the disease tuberculosis (*69*). Tuberculosis is spread when an infected individual coughs, spraying droplets containing bacteria into the air (*69-71*). These droplets can hang in the air for several minutes and be inhaled by another individual. The droplets enter the lungs and can penetrate the alveoli of the respiratory tract (*69, 71*). The bacteria are then engulfed by alveolar macrophages (*69-71*) (Figure 2.1), white blood cells that are involved in non-specific immune response by engulfing cellular debris. Once in the macrophage the bacteria are enclosed by phagosomes (*70, 71*), which are vacuoles formed to digest foreign organisms in the cell. There are several possible outcomes for the bacteria, hypothetically the phagosome can be activated and fuse with lysosomes (an organelle that contains digestive enzymes) leading to bacterial death (*70, 71*). The more accepted hypothesis is the phagosome are not activated and the bacteria continue to survive (*70, 71*). M. TB is capable of changing the intercellular conditions inside the phagosome to prevent maturation and fusion with a lysosome (*70-72*). This prevents the acidification of the environment and development of an immune response (*70-72*) allowing for the survival of the bacteria for long periods of time in the macrophages now hospitable environment (*69-71*). When the macrophages are lysed other macrophages, lymphocytes and T-cells are recruited and the bacterium is contained in tubercle (*70, 71*). At this time the immune

system of the host is capable of containing the infection. This is referred to as the latent or non-active stage in the lifecycle of M. TB in which the bacteria has reduced metabolic activity and the host is asymptomatic and not infectious (*70, 71*). This latent period in some cases can last for years (*69, 73*). When the hosts' immune system becomes compromised due to illness or age the macrophages are lysed and bacteria are spilled into the surrounding tissue and the individuals' immune system is not able to control the growth of M. TB (*70, 71*). The surrounding lung tissue is destroyed and the host begins showing symptoms of the disease and become infectious (*70*). At this time the bacteria can enter the blood stream and infect different parts of the host's body (*71, 72*).

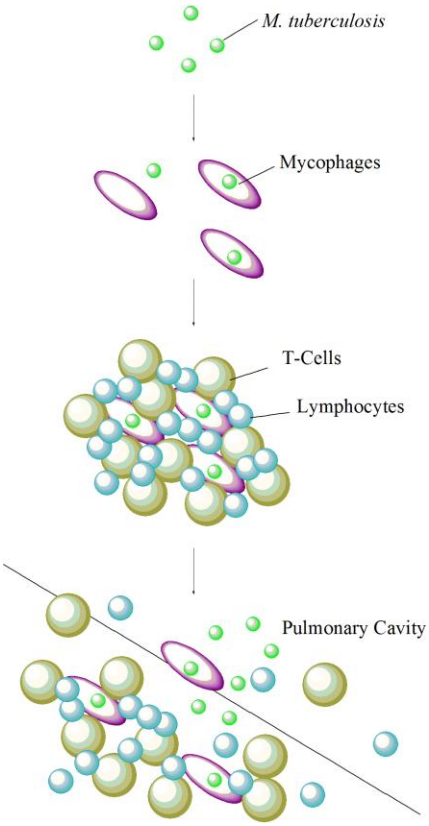

Figure 2.1 The spread of *M. tuberculosis* in the lungs. The bacteria enter the lungs and are engulfed by alveolar macrophages. Macrophages, lymphocytes and T-cells form tubercles to encase the bacteria. Once the cells are lysed the bacteria are capable of spreading to other parts of the body.

Tuberculosis is the leading cause of infectious death globally (*69*). As of 2002 it was estimated that 2 billion people were latently infected with the bacteria (*69, 73, 74*). An estimated 2 million people die of the disease every year (*69, 71*) with 9 million new cases diagnosed (*75*). Tuberculosis is most devastating in developing nations, where 95% of all cases occur (*69*). In many developing nations tuberculosis is the main cause of death and disability. However, in the United States alone an estimated 15 million people are infected with M. TB (*69*). Of the people infected with the bacteria only a small percentage (5% to 10%) will develop the active form of the

disease in their lifetime (*70, 71*). The occurrence of HIV has increased the likelihood of development of the disease. HIV or infected immunocompromised individuals have a 10% chance per year of developing active tuberculosis (*71, 74*).

Current treatments for tuberculosis include a six month regimen of chemotherapy utilizing a combination of the four first line tuberculosis drugs (*69, 70, 74, 76*) (Figure 2.2). Ineffective treatment of the disease due to noncompliance with the prescribed drug regimen has resulted in an increase in the occurrence of drug resistant tuberculosis (*69, 76*). Multi-drug resistant tuberculosis is resistant to three of the first line tuberculosis drugs (*77*) and is normally treatable (*69, 78, 79*). However, the treatment regimen involves two years of chemotherapy and in many cases resectional surgery (*69, 78, 79*). It is estimated that approximately 10% of M. TB is multi-drug resistant (*77*). Extreme drug resistant tuberculosis is resistant to all four first line tuberculosis drugs and several second line drugs and is often fatal (*76-78*). One high publicized case of drug resistant TB was that of Andrew Speaker who was initially believed to be infected with extreme drug resistant tuberculosis and left the United States against the regulation of the Center for Disease Control and Prevention (*80*). It was eventually determined that Mr. Speaker was infected with multi-drug resistant TB and received eight weeks of treatment before undergoing resection lung surgery to remove a tennis ball size of his lung (*81*). Mr. Speaker continued chemotherapy for two years (*80, 81*). Due to the increase in drug resistance it is important to find new drugs for treatment of tuberculosis. All current treatments are ineffective against latent tuberculosis (*70, 75*) that represents a reservoir for new

infection (*75*). Therefore, new drug targets need to be identified in order to develop drugs that are effective against active and latent tuberculosis infection.

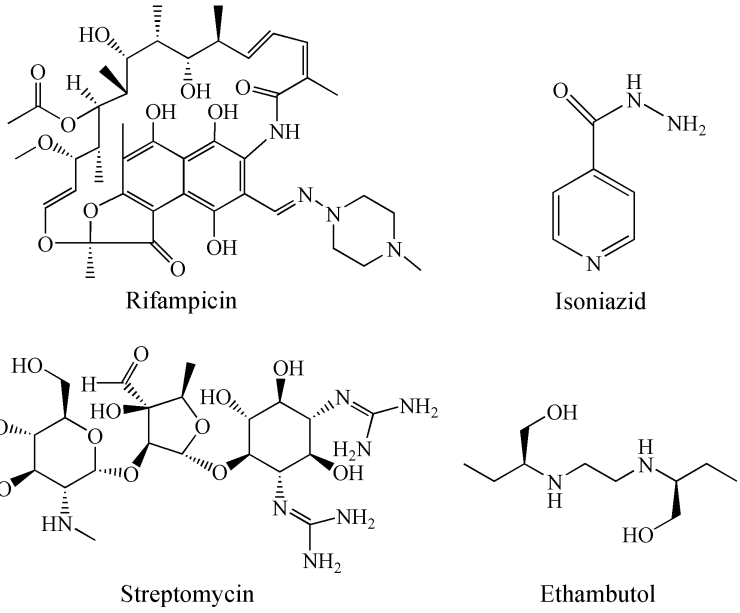

Figure 2.2 The four first line drugs for treatment of M. TB infection.

2.2 Nicotinamide Adenine Dinucleotide

NAD is utilized as a cofactor for many oxidation/reduction reactions in the cell and transfers two electron equivalents (*82, 83*). NAD cycles between the oxidized form of NAD and the reduced form of NADH (*84*). For example, NAD is the cofactor of enzymes involved in electron transport during glycolosis and the citric acid cycle for the synthesis of ATP from carbohydrates and fatty acids (*83*). On top of its role as a cofactor NAD is also utilized as a substrate in many biologically important reactions (Figure 2.3) such as NAD dependent DNA ligases (*84, 85*). Recently, it was determined that NAD is involved in histone deacetylation reactions, which are catalyzed by the yeast proteins Sir2 (*86-88*) and its mammalian homolog, mSir2α (*86*). Sir2 silences rDNA chromatin by the deacetylation of lysine residues on H3 and

H4 histones (*84, 86, 87*). Sir2 activity has been shown to extend the lifespan of yeast, *C. elegans* and *Drosophila* cells through maintenance of gene silencing (*87, 88*). NAD also acts as a substrate for ADP-ribosyl transferases (*84, 89-92*). ADP-ribosyl transferase catalyze the transfer of ADP from NAD to modify various cellular components such as proteins, nucleic acids and small molecules (*84*). ADP ribosylation of proteins has been shown to be important for a wide variety of functions including DNA repair (poly(ADP-ribose) polymerases) (*84, 90, 91*), transcription regulation (*91*), telomere length (Mono(ADP-ribosyl)transferases) (*84*), calcium efflux (*90*), protein degradation (*91*), vesicle trafficking (*91*) and apoptosis (*84, 91*). An ADP-ribosyl cyclase, CD38, is capable of hydrolyzing NAD to ADP-ribose as well as cyclizing NAD to form cADPR (cyclic ADP-ribose) (*84, 85, 89, 90*). It has been proposed that the CD38-cADPR system is involved in necrotic beta-cell death due to NAD depletion (*85*). cADPR levels are also associated with mediating calcium signals in the cell (*90, 92*).

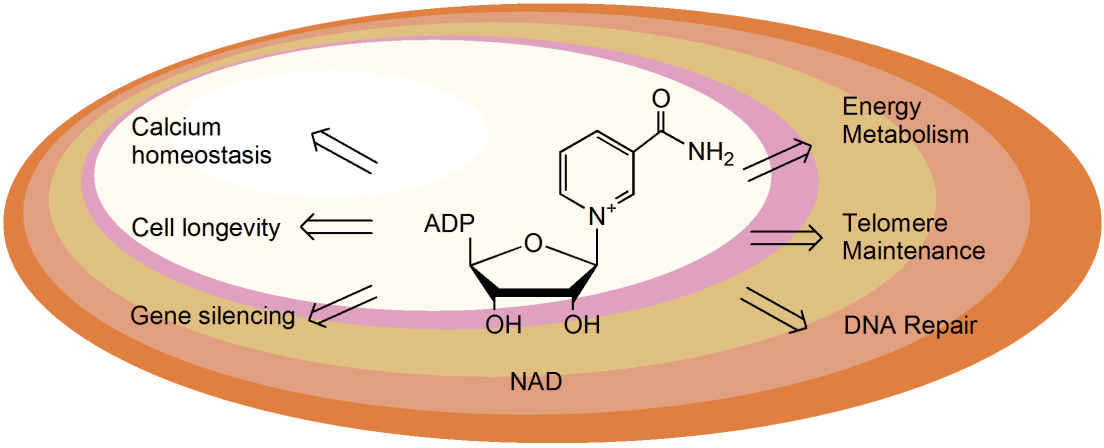

Figure 2.3 NAD utilization in the cell. NAD is utilized as a coenzyme and for regulation of proteins and signaling pathways in the cell.

Besides cADPR other metabolites derived from and involved in NAD biosynthesis are also important for cellular function. NaADP has been identified as a secondary messenger that modulates calcium in the cells (*85, 90, 93*). NaADP is formed through the base excision reaction performed by CD38 (*93*) and from NADP (*83*). NaADP is capable of releasing calcium stores in the cells. NaADP was shown to be associated with glucose levels in pancreatic β–cells, modulation of membrane structure and neurotransmitter release (*93*). Nicotinamide has been shown to inhibit poly(ADP-ribose) polymerases, mono(ADP-ribosyl) transferases and members of the Sir2 protein family (*89*), therefore, regulating NAD utilization. Nicotinic acid has also been shown to have a role in modulating levels of lipids in cells (*89*).

2.3 NAD Biosynthesis

NAD biosynthesis is a complex and organism specific biosynthetic pathway, which consists of *de novo* pathways and recycling pathways (*94, 95*). Depending on the organism the precursor of the pathway can differ (*94, 95*). Prokaryotes utilize L-aspartate while it was thought that only eukaryotes utilize L-tryptophan (*95*). However, it was recently discovered that some prokaryotic organisms can use tryptophan as a precursor as well (*96*). NAD biosynthesis in *Mycobacterium tuberculosis* proceeds through two pathways, the *de novo* pathway that proceeds from aspartate and the recycling pathway that utilizes nicotinamide/nicotinic acid (*97, 98*) (Figure 2.4). Knocking out nicotinic acid phosphoribosyltransferase activity in the recycling pathway or the genes *nadA-C* in the *de novo* pathway, leads to viable cells showing that neither the *de novo* nor recycling pathways are essential for NAD production (*94*). Knocking out the *de novo* pathway and not providing nicotinamide/

nicotinic acid to the cells resulted in cell death both for latent and active M. TB (*94*). This indicates that the last two enzymes in the biosynthetic pathway are essential for NAD production (Figure 2.4). This is further supported by the inhibition of NAD synthetase by indole derivatives showing decrease NAD production (*94*). Therefore, the inhibition of either nicotinic acid mononucleotide adenyltransferase or NAD synthetase would result in cell death and these enzymes are good targets for drug development.

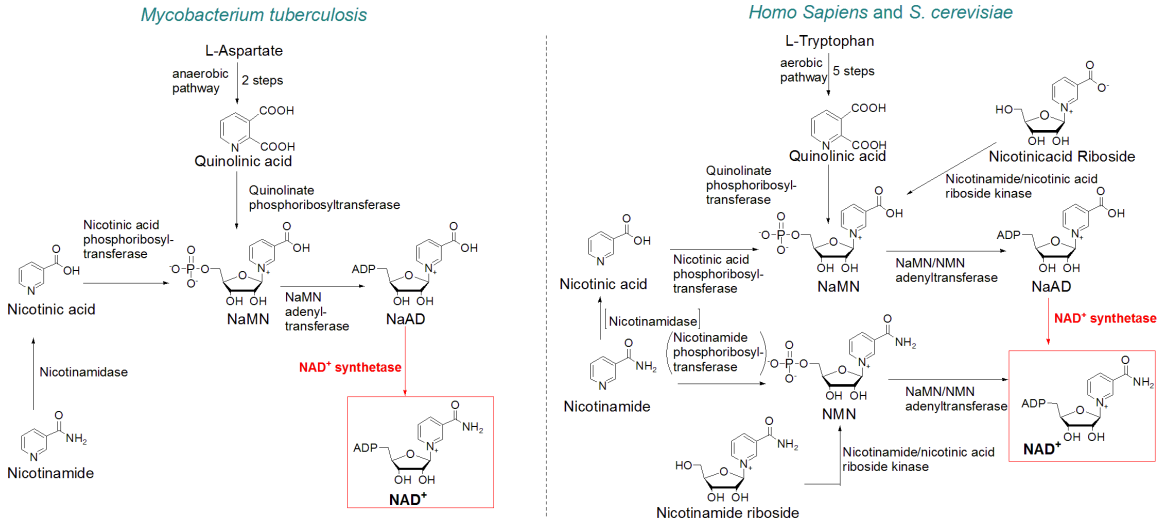

Figure 2.4 The biosynthetic pathways of NAD formation for *Mycobacterium tuberculosis* and Eukaryotic organisms.

The *de novo* NAD biosynthesis pathway for humans starts from L-tryptophan and converges with three recycling pathways at nicotinic acid mononucleotide formation (*85*). Two enzymes catalyze the last step of these pathways, NAD synthetase and nicotinic acid/ nicotinamide mononucleotide adenyltransferase (Figure 2.4) suggesting that NAD synthetase may not be essential for the production of NAD in human cells. Therefore, NAD synthetase is a good candidate as a drug target for M. TB. In addition, the low sequence homology (23%) between the M. TB and human

NAD synthetases may indicate structural and mechanistic differences that may be exploited for M. TB specific inhibitors.

2.4 Goals of Study

The long term goal of this study is to develop inhibitors for NAD synthetase^{TB} that could be developed into drugs for the treatment of M. TB. My project specifically focused on structural and kinetic characterization of NAD synthetase^{TB}. The information here presented is being used by Prof. Gerratana and by our collaborator, Prof. Cynthia Dowd (Dept. of Chemistry, George Washington University) to design mechanistic-based and structural-based inhibitors.

2.5 Cloning and Purification

A previous expression and purification protocol of NAD synthetase^{TB} by the Riccardi group involved the use of fusion glutathione-S-transferase and His_6 tags in order to increase protein solubility (*49*). However, these protocols did not involve the removal of the fusion tags (*49*). Studies in which the fusion tag was removed resulted in low yield of enzyme (approximately 1 mg per 4 L culture) (*99*). It was speculated that the protein was forming inclusion bodies. One construct that utilized a thioredoxin tag to aid in solubility resulted in a yield of 9 mg per 2 L of culture (*99*). However, the fusion tag was removed by thrombin proteolysis at room temperature for 72 hrs. This proteolytic condition is undesirable due to the fact that proteins are often temperature sensitive (*100*). Therefore, I tried several expression systems with the goal of finding a system that will allow expression of soluble protein with

complete removal of the fusion tag under conditions that would result in optimal protein stability (proteolysis at 4 ºC for several hours) and with a reasonable yield.

I cloned the gene for NAD synthetase from the genomic DNA of *M. tuberculosis* into several plasmids allowing the expression of the protein in *E. coli* (Figure 2.5). The pG58 expression vector resulted with the enzyme expressed with proR8FKAM tag (*101*), which is a subtilisin protein tag with a self cleavable tag induced with fluoride. However, the purification resulted in a low yield of 2.3 mg/L culture (0.574 mg/g wet cells) due to inefficient cleavage of the fusion tag. Therefore, other vectors were constructed that allows the expression in *E. coli* of a recombinant protein with an affinity tag either at the C- or N-terminus that could be removed by the TEV protease (*102*). The pET28b vector allowed expression of enzyme with His_6-tag modified with a TEV protease site (Figure 2.5). The enzyme was purified by nickel column and the fusion tag cleaved by TEV protease. However, the proteolysis was not complete; this may have been due to the oligomeric state of the protein preventing the exposure of the TEV protease site. Studies of the yeast NAD synthetase have shown that it is an oligomeric protein suggesting that NAD synthetase^{TB} is also an oligomer and further confirmed by the quaternary structure study as shown below (*103*). A yield of only 4 mg/L culture (1 mg/g wet cells) was obtained. To increase solubility of the enzyme and, therefore, the yield a construct expressing a larger fusion tag was employed (Figure 2.5). The pET32a expressed protein with a thioredoxin tag modified with a TEV protease site (Figure 2.5) resulted in a yield of only 1.4 mg/L culture (0.35 mg/g wet cells). The pET44a expressed the protein with a Nus tag modified with a TEV protease site (Figure 2.5) with a yield of

1.2 mg impure protein/L culture (0.3 mg/g wet cells). Due to the fact that cleavage of the fusion tag appeared to be affecting the yield of the purifications a native protein expression was attempted. A combination of ammonium sulfate and streptomycin sulfate precipitation was performed in combination with anion exchange, hydrophobic and Blue Sepharose affinity column chromatography. None of these techniques resulted in pure protein. The difficulty in the native purification probably arises from the low expression of the protein. The previous expression systems were abandoned in favor of the SUMO expression system (*104*) (Figure 2.5). The presence of the SUMO tag increased the solubility of glutamine-dependent NAD synthetase, but its major advantage was the facile and fast removal of the SUMO tag at 4 °C leaving the recombinant protein with only one additional serine at the N-terminus (*104*). This facile removal of the tag in cases when the protease site is not particularly accessible is likely due to the fact that the surface of interaction between the Ulp1 protease and the SUMO tag is extensive (*104*).

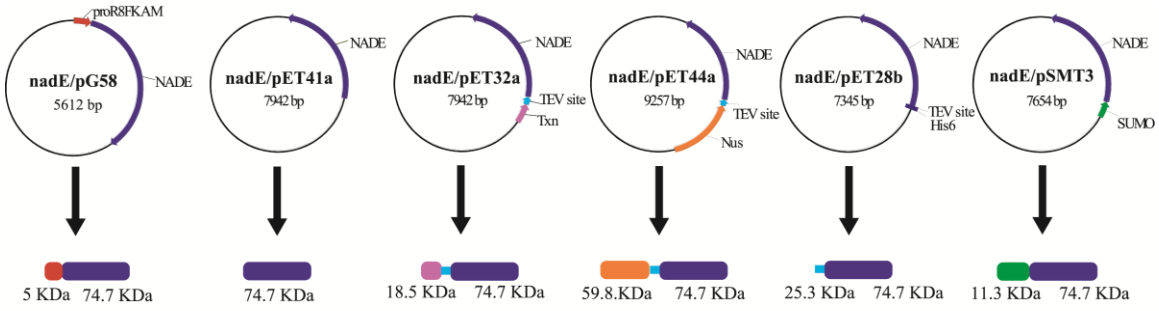

Figure 2.5 The protein expression systems utilized for the expression and purification of NAD synthetase[TB]. Expression plasmids for the vectors *nadE*/pG58, *nadE*/pET41a, *nadE*/pET32a, *nadE*/pET44a, *nadE*/pET28b and *nadE*/pSMT3 and the molecular weights of the expected fusion proteins.

The expression, purification of the SUMO-tagged NAD synthetase^{TB} and removal of the tag were achieved without complications. The enzyme was induced by lactose and expressed for 48 hrs at 20 ºC. The protein was purified by nickel column and the fusion tag removed by Ulp1 proteolysis. The fusion tag and Ulp1 was separated from the protein by a second nickel column followed by gel filtration. The subsequent gel filtration step is absolutely required not necessarily for the removal of impurities but to separate the enzyme from high molecular weight aggregate protein. These aggregate proteins have only 50% of the specific activity of the homogenous enzyme (420 ± 11 mU/mg homogenous enzyme, 216 ± 32 mU/mg aggregate enzyme). The formation of the aggregate protein maybe due to incorrect folding during protein expression because no aggregate peak is observed when the purified and concentrated protein is reloaded on the gel filtration column. This procedure resulted in a yield of approximately 12 mg of protein from 1 L culture (3 mg/ g wet cells) and a purity of over 90% (Figure 2.6).

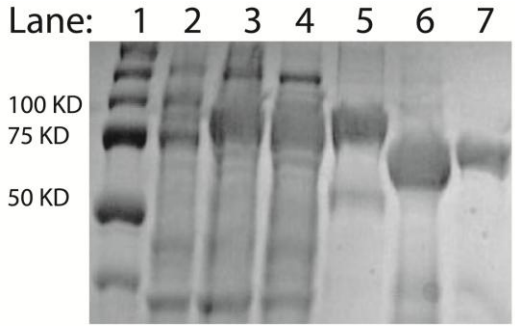

Figure 2.6 The purification gel of NAD synthetase^{TB} (expected molecular weight is 74.682 KDa). Lane 1. Molecular weight ladder. Lane 2. Cells before induction. Lane 3. Cells after induction. Lane 4. After cell lysis. Lane 5. After first nickel column. Lane 6. After proteolysis. Lane 6. After gel filtration.

2.6 Quaternary Structural Characterization

A previous study has shown that NAD synthetase from *Saccharomyces cerevisiae* is an octamer with a total molecular weight of 600 KDa (*103*). This was determined utilizing native polyacrylamide gel electrophoresis (PAGE). Native PAGE is not the most accurate method of determining the molecular weight of a protein (*105*). Proteins will have different charges and shapes as well as molecular weight; therefore, they will run on the native PAGE according to these three factors. The pre-eminent method for the determination of the quaternary structure is ultracentrifugation methods such as sedimentation equilibrium, however, the instability of the protein results in precipitation which does not allow for the use of ultracentrifugation (*105, 106*). Another method for the determination of quaternary structure is light scattering, however, this requires instrumentation that was not easily accessible (*105, 107*). However, a simple method for quaternary structural determination which was utilized is gel filtration which removes the protein charge as a variable and can be performed on available instrumentation (*105*).

The total molecular weight was determined for NAD synthetase^{TB} to be 548 KDa (74.682 KDa per subunit) (Figure 2.7). This would make the protein between an heptamer and an octamer. These data along with the previous characterization data has led to the conclusion that NAD synthetase^{TB} is an octamer, which is confirmed by the structural data discussed in chapter 3.

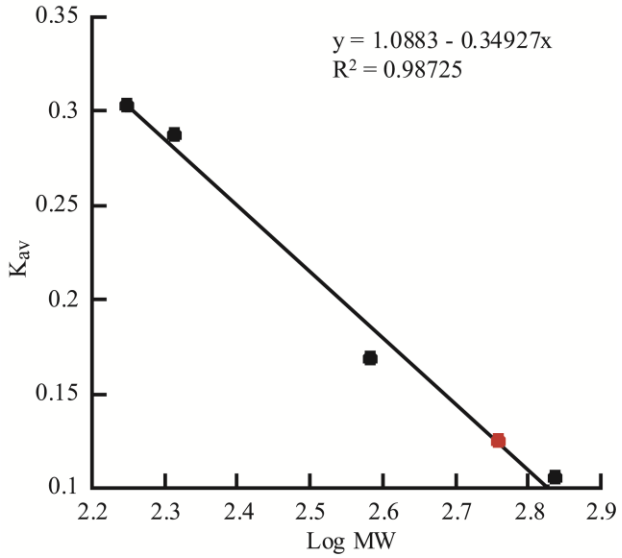

Figure 2.7 The chromatograph of the quaternary structure determination of NAD synthetase^{TB}. The quaternary structure was determined by gel filtration using Sepharose CL-6B resin. Blue Dextran was used to determine the void volume of the column. The molecular weight of Thyroglubin is 689 KDa (K_{av} = 0.10), Ferritin is 382 KDa (K_{av} = 0.17), Catalase is 206 KDa (K_{av} = 0.29), Aldolase is 177 KDa (K_{av} = 0.30). The total molecular weight of NAD Synthetase^{TB} was calculated to be 548 KDa (K_{av} = 0.13 shown in red).

2.7 Assay Development

In order to design drugs against NAD synthetase^{TB} a full characterization of the enzyme needed to be under taken. This required the development of enzymatic assays in order to kinetically characterize the enzyme. There are several different assay methods that can be utilized to monitor the progression of an enzymatic reaction. An assay can be continuous direct in which the product or substrate being monitored has some property that can be directly monitored (UV absorbance,

fluorescence ect.) and quantified. In a continuous indirect assay the disappearance of a substrate or formation of a product can be coupled with another reaction that will produce a product that can be easily detected. The coupled assays can be monitored continuously or discontinuously. In a continuous assay the substrate or product disappearance or formation can be monitored over time. With a discontinuous assay the coupled reaction is not compatible with the reaction conditions of the enzyme and, therefore, the enzymatic reaction of interest must be quenched before the coupled reaction can be performed. The disadvantage of a discontinuous assay is that they can be time consuming and requires more enzyme. Also a proper quench method must be determined.

A method for quenching the reaction of NAD synthetase was devised due to the fact that many of the assays utilized are discontinuous indirect assays. Previous quenching procedures involved boiling the enzyme for 1 min and adding pyrophosphate as an inhibitor (*99*). This procedure takes too much time and incomplete inactivation resulting in a high error and involves addition of one of the products that is to be monitored. Acids such as trichloroacetic acid and HCl were tried as well as coupling the precipitation by the acids with chloroform to remove the enzyme from the solution. In order to determine if the quenches were effective the substrate for the NAD synthetase reaction were combined with the quenching reagent, then enzyme was added. The quenched reaction was then incubated at 37 ºC and product formation monitored by HPLC. It was found that the concentration of acid utilized did not quench the reaction and resulted in degradation of the products. The reaction was effectively quenched with 55 mM metal chelator EDTA in ice as

confirmed by HPLC. Low temperatures decrease the speed of the reaction and the EDTA removes magnesium from the solution stopping the reaction almost instantly.

NAD Assays. NAD formation can be monitored by coupling to the reaction catalyzed by alcohol dehydrogenase after quenching of the NAD synthetase reaction. Alcohol dehydrogenase catalyzes the reversible reaction of ethanol and NAD forming acetaldehyde and NADH (Figure 2.8). The alcohol dehydrogenase assay was performed as a discontinuous assay because it was suspected that NADH would inhibit NAD synthetase activity due the similarity in structure of NADH to NaAD and NAD and could theoretically bind to the NaAD/NAD binding site. This was confirmed by the inhibition studies discussed below. In order to shift the equilibrium toward NADH formation the reaction is performed at pH 8.8 in the presence of an excess of ethanol and semicarbazide (*108*). The semicarbazide traps the acetaldehyde to form a semicarbazone sifting the equilibrium to the formation of NADH (*109*). The formation of NADH is then monitored at 340 nm and the amount of NAD that was present in the reaction can be directly quantified from the amount of NADH. The disadvantage of this assay is that it is a discontinuous assay with a long incubation time (45 mins) for the coupling reaction and the reaction was only sensitive down to the high micromolar range requiring large amounts of enzyme to be utilized (~0.1 μM enzyme per reaction). Therefore, an enzyme cycling assay was adapted (*110*) to overcome the sensitivity issues of the alcohol dehydrogenase assay. The assay couples the formation of NAD with lactate dehydrogenase and diaphorase (Figure 2.8). Lactate dehydrogenase utilizes lactate and NAD to form pyruvate and NADH (*110*). Diaphorase then utilizes NADH to reduce tetrazolium salt to formazan which

is monitored at 450 nm through construction of a calibration curve for NAD concentration (*111*). This allows the amplification of the NAD signal. Therefore, the cycling assay is 200 times more sensitive than the alcohol dehydrogenase assay allowing for less enzyme to be used (~0.5 nM enzyme) and for lower error in the assay. Also the incubation time for the coupled reaction is 10 mins allowing the assays to be faster.

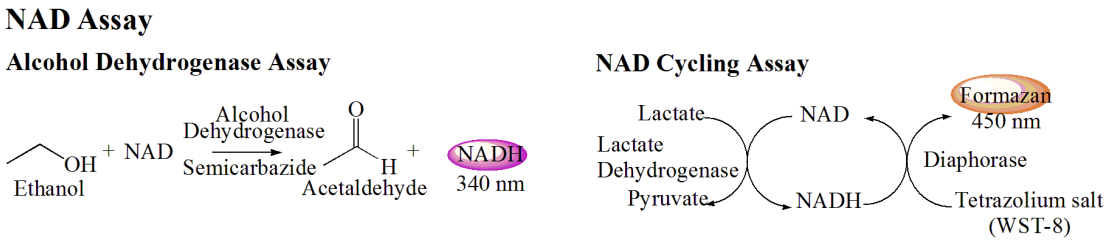

Figure 2.8 The coupling assays for NAD synthetase monitoring NAD formation.

Glutamate Assay. Glutamate formation by NAD synthetase is coupled to the reaction catalyzed by glutamate dehydrogenase. This reaction involves the formation of NADH and α–ketoglutarate from NAD and glutamate (Figure 2.9). NADH formation is favored due to an excess of NAD and hydrazine and is monitored at 340 nm. The quantity of glutamate produced can be determined with the construction of a calibration curve of NADH formation verses glutamate concentration (*112*). One disadvantage of this assay is the high error due to the high background caused by the hydrazine.

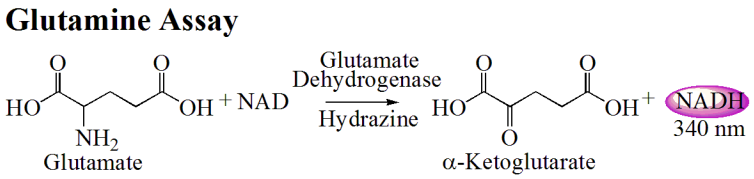

Figure 2.9 The coupling assays for NAD synthetase monitoring glutamine formation.

Pyrophosphate/Inorganic Phosphate Assay. Quantifying the production of the product AMP can be performed by monitoring the formation of pyrophosphate or inorganic phosphate. The formation of inorganic phosphate is assayed with the dye malachite green. Malachite green forms a complex with inorganic phosphate changing the spectral properties of the solution (Figure 2.10). The amount of inorganic phosphate is quantified through the construction of a calibration curve relating the change in absorbance at 630 nm with inorganic phosphate concentration (*113*). Pyrophosphate can be quantified by converting the pyrophosphate to inorganic phosphate through the use of inorganic pyrophosphatase, which hydrolyzes pyrophosphate to inorganic phosphate (*114*). The inorganic phosphate can then be quantified as discussed above. The error for the malachite green assay was high due to the instability of the phosphate/dye complex which changed over time resulting in variations in the absorbance measured. Also with the addition of the inorganic pyrophosphatase the added steps involve increases the error in the assay. A direct assay for inorganic pyrophosphate utilizes Phosphate Sensor (Invitrogen). The phosphate sensor assay involved the use of the mutant *E. coli* phosphate binding protein labeled with fluorophore MDCC (*115*, *116*). The fluorophore allows for an increase in fluorescence when the protein binds inorganic phosphate. The assay has a

sensitivity in the high nanomolar range as oppose to the alcohol dehydrogenase assay, which is sensitive in the micromolar range. The assay can be used as a direct continuous assay for the detection of inorganic phosphate allowing the assay to be faster than the malachite green assay. For the detection of pyrophosphate the assay would be a direct discontinuous assay due the quenching of the NAD synthetase reaction and addition of inorganic pyrophosphates. However, the large amounts of Phosphate Sensor needed for the assay resulted in the assay being too expensive to pursue. For a 450 µl reaction 70 µl (20 µM) of Phosphate Sensor are needed. If five concentrations are necessary to obtain a full calibration curve in triplicate then 1050 µl of Phosphate Sensor would be needed in order to obtain the calibration curve. Since each Phosphate Sensor vial is 200 µl at $1495 one calibration curve would cost $7848.75.

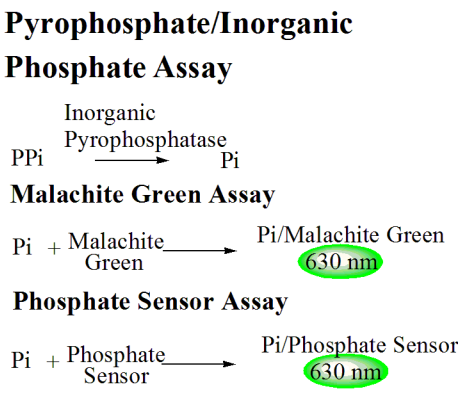

Figure 2.10 The coupling assays for NAD synthetase monitoring pyrophosphate/ inorganic phosphate formation.

HPLC Assay. NAD and AMP can also be quantified through the use of high performance liquid chromatography (HPLC) methods monitoring the nucleotides at

254 nm and quantifying the peaks based on calibration curves performed with an internal standard (Figure 2.11). Two HPLC methods were employed, reverse phase HPLC was used to separate NaAD and NaAD analogs while ion-paired HPLC was utilized for the separation of AMP, ADP and ATP (*117*). However, each time point in the assay requires an HPLC run that is approximately 40 mins. Also the low resolution of the product peaks resulted in high error due to the inaccuracy of the quantitation of the products.

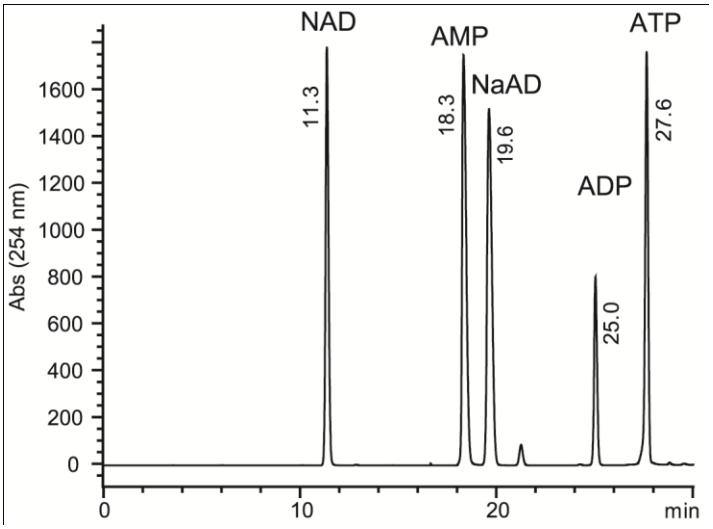

Figure 2.11 The HPLC chromatograph for the substrates and products of NAD synthetase monitored at 254 nm. An ion-paired analytical Alltech Alltima C18 column (5 μm, 4.6 x 250 mm) was utilized. Solvent A is 25 mM KH_2PO_4, pH 6.4, 4 mM tetrabutylammonium bromide, 5% methanol and solvent B is 25 mM KH_2PO_4, pH 6.4, 4 mM tetrabutylammonium bromide, 50% methanol. The various compounds were eluted with a linear gradient from 0-80% in 27 minutes and hold at 80% solvent B for 10 more minutes.

2.8 Order of Substrate Binding: Binding Studies

In order to determine the binding order of the synthetase domain substrates the binding constants were attempted to be determined. The binding constant of NaAD and ATP were determined in the presence and absence of the other substrate. If NaAD binds the enzyme after ATP then a decrease in the NaAD K_d may be observed in the presence of ATP. Two methods were attempted to determine the binding constants of ATP and NaAD, isothermal calorimetry and fluorescent titration.

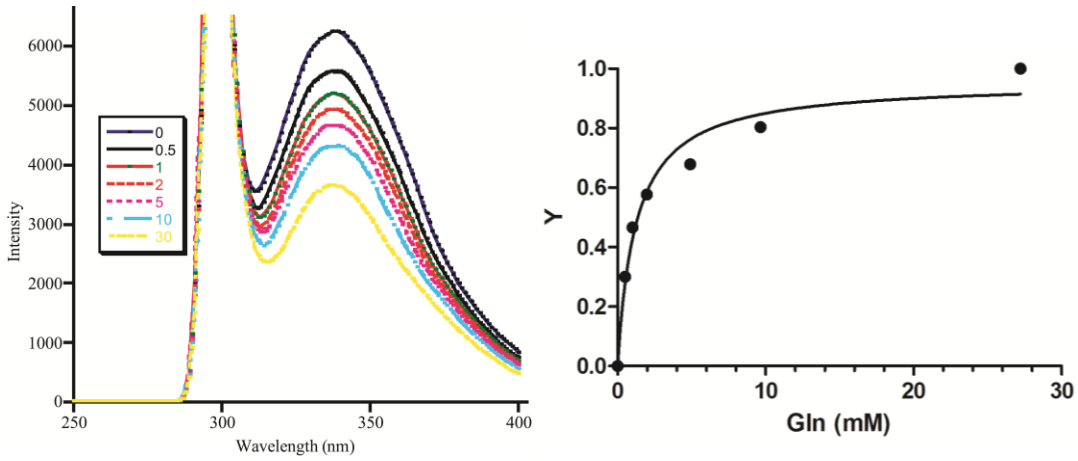

Figure 2.12 The intrinsic fluorescent titration data for glutamine. Y = F_o-F/F_o-F_{max}. Where F_o is the fluorescence with no ligand, F is fluorescence at a particular ligand concentration and F_{max} is fluorescence at the maximum ligand concentration. The tryptophan fluorescence is quenched as glutamine is added over the course of 30 mins at room temperature. The glutamine hydrolysis is negligible under these conditions. Bi-phasic behavior is seen for the binding of the substrates of NAD synthetase M. TB (R^2 is 0.97). The K_d was 1.3 ± 0.4. Curve fitting attempted to Y= [L]/ K_d + [L] with Sigma Plot.

Fluorescent titration studies involve the titration of the ligand into the protein and the fluorescent signal measured is related to the binding of the protein to the ligand. The fluorescence signal can come from a fluorescent ligand or it can be intrinsic fluorescence in which the protein contains a tryptophan that will change fluorescent properties based upon the change in the exposure to solvent. Both methods of obtaining the binding constants through fluorescence were used. For tryptophan fluorescence biphasic behavior was seen for all the ligand binding curves and fitting to a single bind site curve a poor fit to the data (Figure 2.12). This behavior is believed to be due to the presence of 10 tryptophan per monomer in the enzyme, therefore interference from the quenching of other tryptophan in the protein contribute to the fluorescence decrease. This means that the change in fluorescence is not linearly dependent on the binding of the ligand. Instead of relying on the intrinsic fluorescence of the protein we then decided to monitor the fluorescence of the NAD analog, NADH, which was able to bind to the enzyme and act as an inhibitor (see section on inhibition studies). The use of the ligand as the fluorophore has the advantage of avoiding the interference of the 10 tryptophan residues in the enzyme. However, the disadvantage of this is that larger concentrations of proteins are necessary compared to the amount of protein used in intrinsic fluorescence (6 μM versus 0.5 μM enzyme) (*118-120*). Another problem with using the ligand as a fluorophore is concentration quenching (*121, 122*). Above 100 μM NADH fluorescence would cause quenching of the fluorescence signal, therefore, at concentrations above 100 μM the fluorescent signal would not be linear with the concentration of NADH (Figure 2.13). Due to the fact that the K_M of NaAD is 0.1

mM and assuming that the K_M can be utilized as an estimate of the K_d, the concentrations of NADH needed to bind NAD synthetase would be above the linear region of the NADH fluorescence curve.

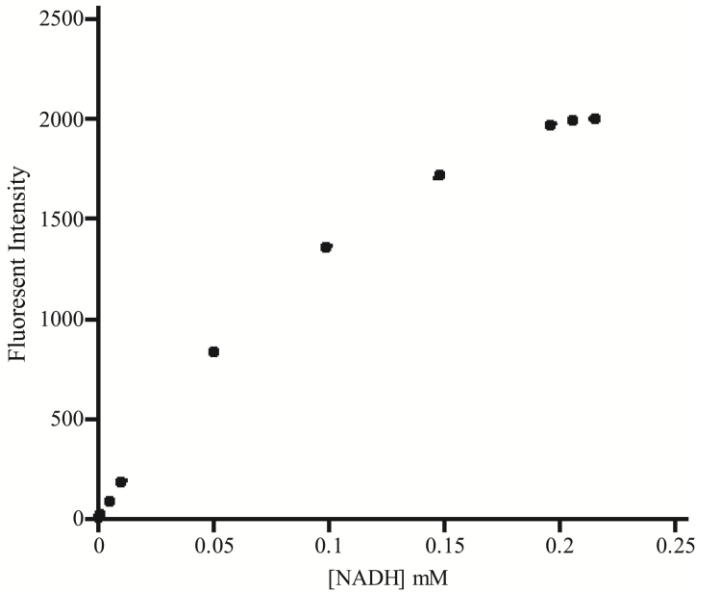

Figure 2.13 NADH concentration based fluorescent intensity. The fluorescence is linear with NADH concentration to 0.1 mM after which NADH self quenches and fluorescence is no longer linear with concentration. The excitation wavelength was 340 nm. The emission spectrum was monitored at 450 nm.

Isothermal calorimetry measures the heat release associated with ligand binding. The heat release is quantified as ligand is titrated into the protein solution. A binding curve is then constructed and the binding constant calculated. This method also proved to be unsuccessful due to the large amounts of protein (40 µM enzyme) needed for a signal to be detected, stirring at room temperature to diffuse the ligand and the removal of glycerol needed for protein stability from the enzyme solution

resulted in the enzyme becoming unstable during the course of the experiment (2 hrs) and precipitating out of solution.

2.9 Ordering of Substrate Binding: Inhibition Studies

Due to the fact that the binding studies proved to be unsuccessful, dead-end inhibition studies were performed. A dead-end inhibitor resembles the substrate and reversibly binds to the enzyme binding pocket but does not turnover preventing product formation (*123, 124*). Dead-end inhibitors are useful in determination of a kinetic mechanism and have the advantage over product inhibitors in that they do not cause partial reversal of the enzymatic reaction, therefore, making analysis of the inhibition patterns less complex (*125*). The inhibition constant (K_I) can be determined for a substrate analog, which is the concentration of inhibitor necessary to obtain half maximum inhibition and is an indicator of how potent the inhibitor is. Inhibition studies can give information on the order of substrate binding. When there are two substrates, A and B, one substrate will be under saturating conditions while the concentration of the other substrate is varied at different inhibitor concentrations. The data are then plotted on a double reciprocal plot. The slope of the double reciprocal plot will be affected if one of two conditions are met: the inhibitor and varied substrate bind to the same form of the enzyme or the inhibitor and varied substrate bind different forms of the enzyme that are reversibly connected and the varied substrate adds after the inhibitor (*123, 125*). The slope is affected in competitive and noncompetitive inhibition plots. The intercept of the double reciprocal plot will be affected by addition of inhibitor if the inhibitor and varied substrate add to different forms of the enzyme (*125*). The intercept is affected in uncompetitive and

noncompetitive inhibition plots. The inhibition patterns can then be predicted for a random mechanism and ordered mechanisms for enzymes with two substrates binding by using two dead-end inhibitors as shown in Figure 2.14 (*126*).

Ordered Mechanism

I vs variable substrate	Fixed substrate	Predicted pattern
I_A vs A	B	Competitive
I_A vs B	A	Noncompetitive
I_B vs A	B	Uncompetitive
I_B vs B	A	Competitive

Example:

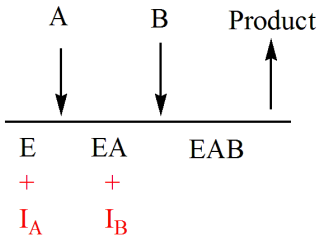

Random Mechanism

I vs variable substrate	Fixed substrate	Predicted pattern
I_A vs A	B	Competitive
I_A vs B	A	Noncompetitive
I_B vs A	B	Noncompetitive
I_B vs B	A	Competitive

Example:

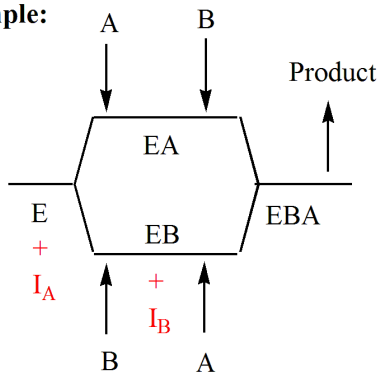

Figure 2.14 The possible inhibition patterns for an enzyme with two substrates, A and B, for an ordered and random mechanism. The dead-end inhibitors are I_A, which is an analog of A, and I_B, which is an analog of B. Below each table is an example of a mechanism of substrate binding. In the example for an ordered mechanism A binds before B. In the example of the random mechanism A and B bind randomly.

The analog of ATP, AMPCPP (Figure 2.15), was used as a dead-end inhibitor versus the ATP binding site and the NaAD binding site. If AMPCPP was noncompetitive versus NaAD then NaAD would bind after ATP. If AMPCPP was

uncompetitive then NaAD would bind before ATP (Figure 2.14). The cycling assay was used to obtain the inhibition plots (Table 2.1). It was determined that under saturating conditions of the other substrate AMPCPP was a competitive inhibitor for both the ATP and NaAD binding sites. This could be due to the inhibitor being able to fit in the NaAD binding site when the ATP binding site is saturated. Therefore, substrate analogs for NaAD, NADH and 3-acetylpyridine adenine dinucleotide (acetyl-NAD) (Figure 2.12) were utilized as dead-end inhibitors to determine the binding order of the synthetase domain substrates. If one of the NAD analogs was noncompetitive versus ATP then ATP would bind after NaAD. If the NAD analog was uncompetitive then ATP would bind before NaAD (Figure 2.14). Both NaAD analogs are incompatible with the cycling assay. NADH is a product of the cycling assay (Figure 2.8). In the absence of NAD synthetase acetyl-NAD causes a high absorbance in the cycling assay due to the fact that it is utilized by lactate dehydrogenase as a substrate. Therefore, HPLC was utilized to monitor the formation of NAD (Table 2.1). However, it was also shown that both NaAD analogs were competitive inhibitors for the NaAD and ATP binding sites. All three substrate analogs contain ADP moieties which can easily fit in the AMP binding pocket of both the ATP and NaAD binding sites. The NaAD analogs are larger than ATP so it was assumed that they would not fit in the ATP binding sit. However, the ADP moiety is able to bind while the rest of the molecule is outside the binding pocket, which was confirmed when the crystal structure was obtained revealing an open ATP/NaAD binding pocket (see Chapter 3). This results in an inability to determine the binding order of ATP and NaAD with the dead-end inhibitors utilized. Attempts were also

made to determine the inhibition constants for glutamine analogs such as glutamic acid 5-methyl ester, ornithine and asparagine and the product glutamate for utilization in crystallographic trials. The inhibition assays contained saturating NaAD and ATP while varying glutamine concentration. No inhibition was observed for the any of the analogs up to 20 mM indicating that the enzyme has very little or no affinity for these glutamine analogs. This behavior is also seen in GMP synthase which, despite a fully formed glutaminase active site, does not bind glutamate (*33*).

Table 2.1 Inhibitor constants for the substrate analogs.

Inhibitor	K_I (mM)
AMPCPP	0.7 ± 0.1
NADH	0.11 ± 0.05
Acetyl-NAD	1 ± 0.7

The enzyme activity was measured in 10 mM $MgCl_2$, 1 mM DTT and 50 mM Tris-HCl, pH 8.3 at 37 °C. The concentrations of ATP and NaAD, 4 and 3 when held constant. The concentrations for AMPCPP, NADH and Acetyl-NAD were 0 - 4 mM, 0.05 - 4 mM and 0 – 2 mM respectively.

2.10 Kinetics Analysis Shows Optimal Kinetics Synergism

We measured the steady-state rate constants for the NAD synthetase^{TB} catalyzed reactions using exogenous ammonia or glutamine (Table 2.2). Each reaction was performed in triplicate and the standard deviation of the error is shown. The turnover number for the reaction using ammonia is at least five- to six-fold faster than for the reaction with glutamine. This does not adjust for the difference in ionic strength which decreases the rate of the glutamine dependent reaction by 10%. A rate-limiting step involved in glutamine hydrolysis and/or ammonia transport could

account for this difference. The steady-state kinetics data support a mechanism of catalysis driven by kinetic synergism. If the K_M values can be considered an approximation of the K_d then decreases in the K_M values of 5- and 12-fold for NaAD and ATP, respectively, when glutamine is the nitrogen source instead of exogenous ammonia suggest that glutamine binding enhances the affinity of the synthetase active site for its substrates. The K_M values for glutamine did not change in the presence or absence of NaAD and ATP. A 179-fold increase in the glutaminase turnover number measured for the reaction in the presence of both synthetase substrates compared to their absence indicates a mechanism of activation of the glutaminase domain triggered by changes occurring at the synthetase domain. The k_{cat} values for glutamine hydrolysis in the presence of only one of the synthetase substrates are identical to the value measured in the absence of synthetase substrates, indicating that both substrates are necessary for glutaminase activation (Table 2.3).

Table 2.2 Steady state kinetic parameters of the wild-type NAD synthetase^{TB} catalyzed reactions[a]

Glutamine-dependent wild-type catalyzed reaction (ionic strength 0.012 M)					
Assay	Variable substrate	Fixed substrates	K_m (mM)[b]	k_{cat} (sec^{-1})	k_{cat}/K_m ($sec^{-1}mM^{-1}$)
NAD	NaAD	Gln, ATP	0.13 ± 0.02	0.50 ± 0.02	3.8 ± 0.6
NAD	ATP	Gln, NaAD	0.12 ± 0.03	0.60 ± 0.03	5.0 ± 1.0
NAD	Gln	NaAD, ATP	1.3 ± 0.1	0.55 ± 0.01	0.42 ± 0.03
Glu	Gln	NaAD, ATP	1.5 ± 0.3	0.68 ± 0.03	0.4 ± 0.1
Glu	Gln	None	1.3 ± 0.4	0.0038 ± 0.0002	0.0029 ± 0.0008
Ammonia-dependent reaction (ionic strength 0.1 M)					
Wild-type NAD synthetase^{TB}					
Assay	Variable substrate	Fixed substrates	K_m (mM)[b]	k_{cat} (sec^{-1})	k_{cat}/K_m ($sec^{-1}mM^{-1}$)
NAD	NaAD	NH_3, ATP	0.7 ± 0.1	2.6 ± 0.1	3.7 ± 0.5
NAD	ATP	NH_3, NaAD	1.4 ± 0.2	2.9 ± 0.1	2.1 ± 0.3
NAD	NH_3	NaAD, ATP	20 ± 2	3.0 ± 0.1	0.15 ± 0.02

[a]The enzyme activity was measured in 10 mM $MgCl_2$, 1 mM DTT and 50 mM Tris-HCl, pH 8.3 at 37 °C. The concentrations of ATP, NaAD, L-glutamine and NH_4Cl were 4, 3, 20 and 100 mM, respectively, when held constant. Each reaction was performed in triplicate. [b]These values are apparent K_m constants at saturating concentrations of the other two substrates.

Full occupancy of the synthetase domain may be necessary and sufficient for the observed activation of the glutaminase domain or it could depend on the formation of the NaAD-AMP intermediate or the NaAD-AMP/PPi intermediate complex. To distinguish between these possible mechanisms, we tested the ability of AMPCPP, a competitive inhibitor of ATP (Table 2.3) (Figure 2.15), to activate the glutaminase domain in the presence of NaAD. We did not detect any activation (Table 2.3). However, we found that NAD synthetase^{TB} does not catalyze NAD formation in the presence of the ATP substrate analog AMPPCP, which contains the phosphodiester bond cleaved in the NAD synthetase–catalyzed reaction. The lack of AMPPCP activity can be attributed to a nonproductive binding mode of AMPPCP. Similarly, the absence of activation by AMPCPP could be the result of a binding

mode that inhibits conformational changes required for glutaminase activity. Therefore, we tested the ability of product NAD and analog acetyl-NAD (Figure 2.15) to activate the glutaminase domain in the presence of ATP, but, again, we observed no appreciable increase in activity (Table 2.2). This indicated that binding of substrates was not sufficient for activation of the glutaminase domain. Therefore, glutaminase activation was triggered by the formation of the acyladenylate intermediate or the formation of the acyladenylate/pyrophosphate intermediate complex. A non-hydrolyzable acyladenylate intermediate analog was synthesized by our collaborator Dr. Clifton E Barry (National Institute of Health, National Institute of Allergy and Infectious Diseases, Bethesda, Maryland) in order to mimic the intermediate complex (Figure 2.15). The GAT activation of the intermediate complex was tested in the presence and absence of 2.5 mM pyrophosphate/Mg^{2+}. The intermediate analog 1/pyrophosphate/ Mg^{2+} complex showed a 16 fold activation of the glutaminase domain (Table 2.3) of the GAT domain. However, intermediate analog 1 did not show any inhibition against the enzyme up to 5 mM when ATP or NaAD was varied due to the fact that inhibition assays could not be performed in the presence of pyrophosphate, which itself is clearly required for binding of inhibitor 1 based on the inactivation experiment. The moderate activation of the GAT domain (16 fold versus 179 fold, Table 2.3) by intermediate analog 1 may be due to the fact that limited amount of intermediate analog did not allow saturation to be reached. Saturating concentrations of NaAD, AMP, pyrophosphate/Mg^{2+} were utilized as a more accurate mimic of the intermediate complex and an activation of 44 fold was observed (Table 2.3). The presence of pyrophosphate and Mg^{2+} in all cases was

absolutely required for GAT activation. Taken together, these results indicate that the activation of the glutaminase domain is dependent on the formation of the NaAD-AMP/ pyrophosphate/Mg^{2+} intermediate complex.

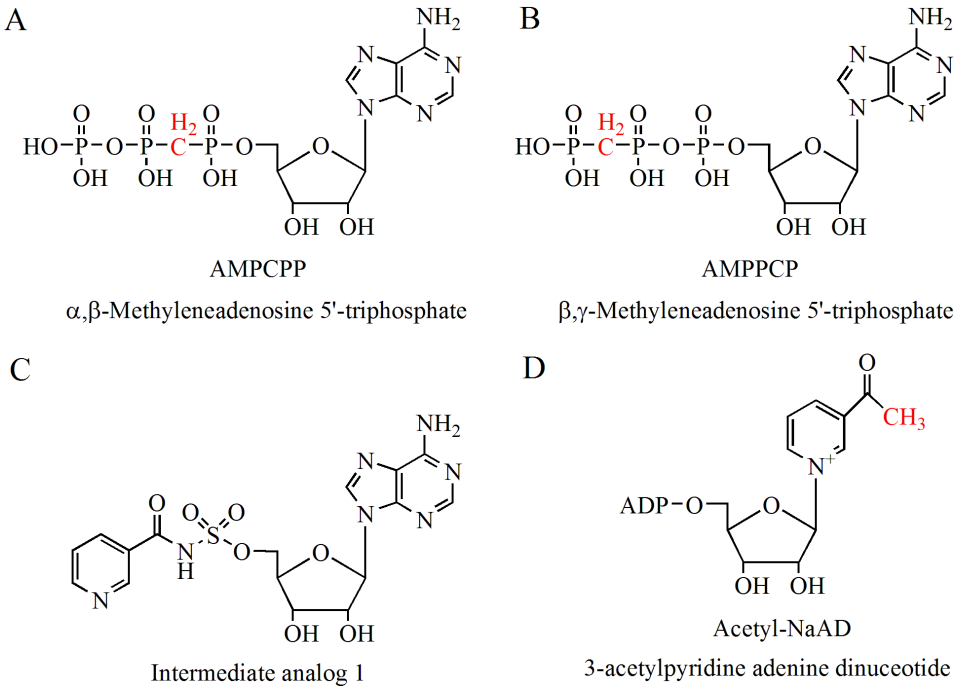

Figure 2.15 The effectors of GAT activation. A and B are the analogs of ATP, D is the analog of the acyladenylate intermediate and E is the analog of NAD.

Table 2.3 Activation of the glutaminase domain of NAD synthetase$^{TB\ a}$

Effectors	Sample Reactions	k_{cat} (sec^{-1})	Fold activation
none	L-glutamine	0.0038 ± 0.0002	---
ATP/Mg^{2+}, NaAD	L-glutamine	0.68 ± 0.03	179
AMPCPP/ Mg^{2+}	L-glutamine, NaAD	0.013 ± 0.002	3.4
NAD	L-glutamine, ATP/Mg^{2+}	0.005 ± 0.001	1.3
Acetyl-NAD	L-glutamine, ATP/Mg^{2+}	0.0003 ± 6E-5	No activation
NaAD, AMP, PPi/Mg^{2+}	L-glutamine	0.167 ± 0.007	44
PPi/Mg^{2+}	L-glutamine	0.002 ± 0.001	No activation
NaAD, AMP/Mg^{2+}	L-glutamine	0.003 ± 0.001	No activation
Intermediate analog 1	L-glutamine	0.0021 ± 0.0002	No activation
Intermediate analog 1, PPi/Mg^{2+}	L-glutamine	0.061 ± 0.004	16

[a]Glutaminase activity was measured in 10 mM $MgCl_2$, 1 mM DTT, 50 mM Tris-HCl, pH 8.3 at 37 ^oC, and with 20 mM L-glutamine. The concentrations of ATP, NaAD, AMPCPP, AMPPCP, Acetyl-NAD, NAD, Intermediate analog 1 and PPi were 4, 3, 10, 10, 6, 6, 5 and 2.5 mM, respectively. The lower limit of detection is 0.0006 sec^{-1} under the conditions of these glutamate assays.

As discussed in Chapter 1, glutamine-dependent NAD synthetase is a member of the GAT family of enzymes. It had been determined that some GAT enzyme transport ammonia from one active site to another within the enzyme. A classic experiment for the determination of ammonia transport within an enzyme is the isotope exchange experiment outlined in Chapter 1. However, a stoichiometric ratio of 1:1 = NAD:glutamate produced (Table 2.4) is also indicative of ammonia transport within the enzyme due to the fact that a perfect stoichiometric ratio could not be achieved if ammonia were released into solvent (see Chapter 1). These data show that NAD synthetase^{TB} achieves maximum efficiency at or below physiologically relevant concentration of glutamine (4.5 mM) (*127*) and that the synthetase and glutaminase activities are highly synchronized (Figure 2.16). As the glutamine concentration increases to 20 mM, the activities of the active sites become partially uncoupled and channeling efficiency is reduced to 73%.

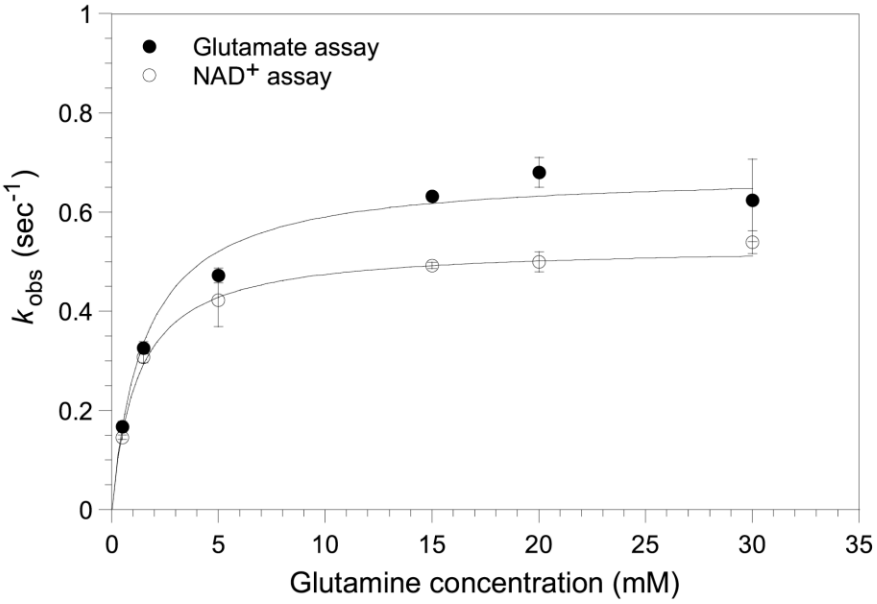

Figure 2.16 The formation of glutamate or NAD production versus glutamine concentration. At cellular concentrations of glutamine (~4.5 mM) the channeling efficiency is ~100%, as the glutamine concentration increase uncoupling of the activities are seen. Curves fitted to $k_{obs} = k_{cat}$ [S] / K_M + [S].

Table 2.4 Stoichiometry analysis for NAD synthetase^{TB} catalyzed reaction[a]

Gln concentration	AMP/NAD	Glu/ NAD	% Channel Efficiency
1.5 mM	n.d	1.05 ± 0.05	95 ± 5
5.0 mM	n.d.	1.12 ± 0.13	89 ± 12
20.0 mM	0.9 ± 0.2	1.36 ± 0.13	73 ± 10

[a]All reactions were carried out in 10 mM $MgCl_2$, 1 mM DTT and 50 mM Tris-HCl, pH 8.3, at 37 °C and 0.23 μM NAD^+ synthetase. The concentration of ATP and $NaAD^+$ were 4 and 3 mM, respectively.

2.11 Affect of Glutaminase on Synthetase Domain

To determine whether the glutaminase domain acts reciprocally to control the ammonia-dependent NAD synthesis, we measured the catalytic properties of the 6-

diazo-5-oxo-L-norleucine (DON)-modified enzyme and of the C176A variant. DON is an analog of glutamine that reacts with nucleophilic cysteine residues. Modifying NAD synthetase with DON traps the GAT domain in the γ-glutamylthioester intermediate state. The inactivation of NAD synthetase^{TB} by DON was first characterized (Figure 2.17). The progress curve was determined by monitoring NAD formation in the presence of various concentrations of DON. The assay was an indirect continuous assay coupling the formation of NAD with the activity of alcohol dehydrogenase. The alcohol dehydrogenase assay can be used continuously because the substrates were under saturating conditions, therefore, there would be no competitive inhibition due to NADH formation. DON binds to the enzyme with a k_{inact} of 0.21 ± 0.02 sec^{-1} and a K_I of 0.35 ± 0.06 mM. The k_{inact}/K_I for DON (0.6 ± 0.1 sec^{-1} mM^{-1}) and k_{cat}/K_m values for glutamine (0.42 ± 0.03 sec^{-1} mM^{-1}) were similar indicating equal specificity for both glutamine and the irreversible inhibitor. As reported in Chapter 1 C176 is a member of the catalytic triad and acts as a nucleophile involved in the hydrolysis of glutamine (Figure 1.1). If this assignment is correct mutation of C176 to an alanine residue would result in loss of glutaminase activity. The C176A variant lacked glutamine-dependent activity but retained ammonia-dependent activity (Table 2.5). However, the DON-modified enzyme showed only 18% (k_{cat} = 0.48 ± 0.01 s^{-1}) of the ammonia-dependent activity of the wild type. This decrease in the activity could be attributed to the inhibition of conformational changes required for the synthetase activity due to the increased rigidity of the DON-modified enzyme and/or to a limited access to the synthetase active site through the glutaminase domain arising from the presence of DON.

Table 2.5 Steady state kinetic parameters of the C176A NAD

C176A NAD synthetase[TB] (ionic strength 0.1 M)					
Assay	Variable substrate	Fixed substrates	K_m (mM)[b]	k_{cat} (sec^{-1})	k_{cat}/K_m ($sec^{-1}mM^{-1}$)
NAD	NaAD	NH_3, ATP	0.65 ± 0.08	3.7 ± 0.1	5.7 ± 0.7
NAD	ATP	NH_3, NaAD	0.60 ± 0.09	3.0 ± 0.1	5.0 ± 0.8
NAD	NH_3	NaAD, ATP	15 ± 2	3.3 ± 0.1	0.22 ± 0.03

[a]The enzyme activity was measured in 10 mM $MgCl_2$, 1 mM DTT and 50 mM Tris-HCl, pH 8.3 at 37 °C. The concentrations of ATP, $NaAD^+$, L-glutamine and NH_3 were 4, 3, 20 and 100 mM, respectively, when held constant. [b]These values are apparent K_m constants at saturating concentrations of the other two substrates.

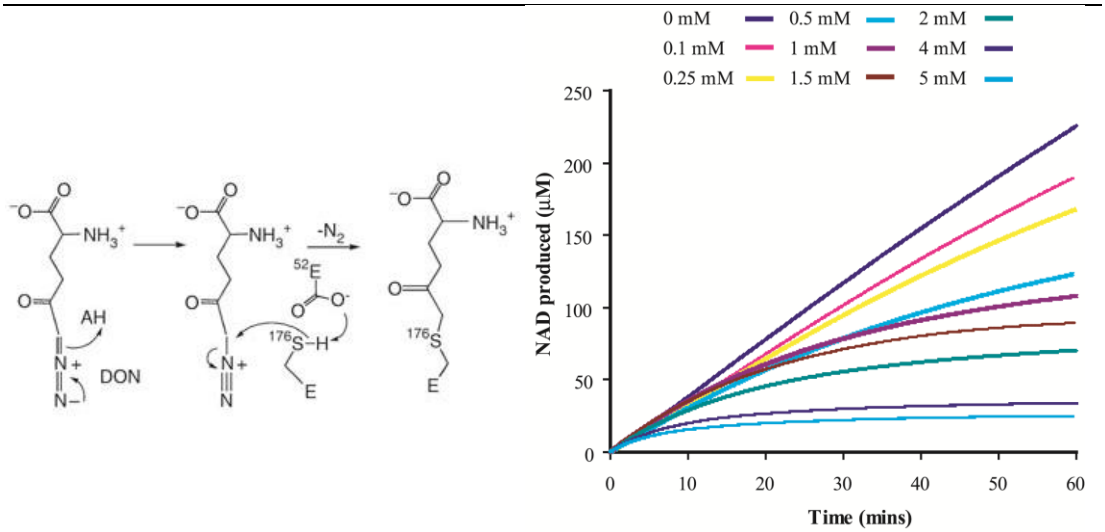

Figure 2.17 The inactivation of NAD synthetase[TB] by DON. Left: The mechanism of DON inactivation. Right: The data for the progress curve for DON inactivation and the inactivation constants obtained. The progress curves were fitted to the equations $[P] = [P]_\infty (1\text{-}e^{(-kt)})$ and $k = k_{inact}\,[I]/\,K_I\,(1 + [S]/K_m + [I]/K_I)$ (*128*, *129*) with Sigma Plot. Where [P] is the concentration of the product, t is the time, k is the rate of the progress curve, [I] is the concentration of DON, [S] is the concentration of glutamine. The k_{inact} is 0.21 ± 0.02 sec^{-1} and K_I is 0.35 ± 0.06 mM.

2.12Kinetic Mechanism of NAD Synthetase[TB]

A kinetic mechanism for the enzymatic reaction is proposed based on the kinetic data available (Figure 2.18). The decrease in the K_M values for the synthetase substrates in the glutamine dependent reaction versus the ammonia dependent reaction and the fact that the K_M for glutamine does not change in the presence of NaAD and ATP suggests that glutamine binds the GAT domain first causing an increase in the binding affinity toward the substrates of the synthetase domain. It is unknown whether NaAD or ATP binds randomly or sequentially. The activation studies have shown that formation of the acyladenylate intermediate and pyrophosphate in the synthetase domain triggers a conformational change, which causes activation of the glutaminase active site resulting in a 179 fold increase in activity. The glutamine is hydrolyzed and the DON modification studies suggest that the γ-glutamylthioester formation may have some effect on the synthetase domains activity. The ammonia produced from the glutamine hydrolysis travels within the enzyme through a proposed ammonia tunnel and reacts with the acyladenylate intermediate forming the products NAD and AMP.

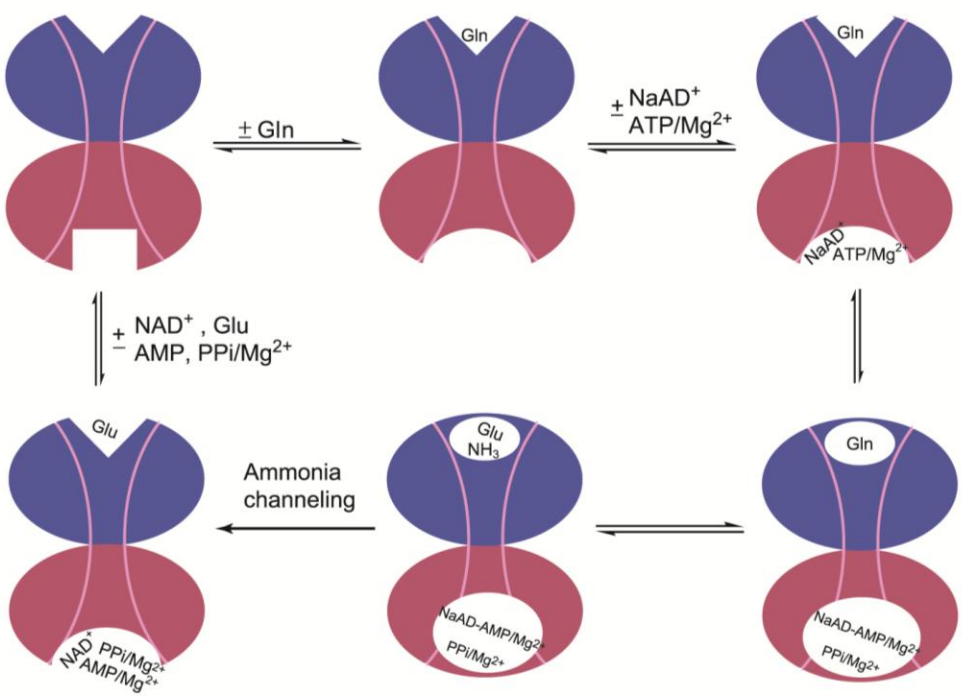

Figure 2.18 The kinetic mechanism of NAD synthetase[TB]. The mechanism, based on the kinetic data, shows binding of glutamine causing increased affinity for NaAD and ATP, acyladenylate intermediate formation causing activation of the GAT domain, then ammonia channeling and NAD formation.

Chapter 3: Structural and Mutagenesis Studies of NAD Synthetase^{TB}

3.1 Structure of NAD Synthetase^{TB}

The coordination between the synthetase and glutaminase active sites of NAD synthetase^{TB} reported in Chapter 2 indicates a high level of communication between the two domains. No crystal structure of a glutamine-dependent NAD synthetase was available; therefore, the crystal structure of NAD synthetase^{TB} was determined to elucidate the interactions that may be involved in active site coupling and determine the mode of ammonia transport through the enzyme.

My contribution to this chapter included the expression and purification of the enzyme for the crystallization trials. The remaining aspects of the structural determination were performed by Dr. Gerratana and Dr. LaRonde-LeBlanc. I also carried out the cloning, expression, purification and kinetic characterization of the variants with the assistance of Andrew Chang (a biochemistry undergraduate student).

3.2 The Quaternary Structure of NAD synthetase^{TB}

The crystal structure of DON-modified NAD synthetase^{TB} was determined at 2.35 Å resolution bound to 3 mM NaAD. The crystallization conditions were 1.8 M ammonium citrate tribasic dihydrate, pH 7.0, 5% glycerol. The crystals contained four subunits per asymmetric unit, and the expected biological homooctamer is

generated by interaction with an adjacent asymmetric unit related by two-fold crystallographic symmetry (Figure 3.1). The crystal structure revealed the enzyme to be a 600 KDa homooctamer as proposed in Chapter 2. The overall structure of the enzyme consists of the core consisting of the glutaminase domains and the synthetase domains pointing outward toward the solvent (Figure 3.1). The glutaminase core is formed by two stacked rings rotated roughly 50º relative to each other composed of four domains. The two rings are held to together by extensive contacts over 1,687 $Å^2$; however, the glutaminase domains in the same ring have limited interactions with only 709 $Å^2$ buried surface area per interface per subunit. Each glutaminase domain also has extensive contacts with the synthetase domains of two adjacent subunits burying 2,002 $Å^2$ of surface area per glutaminase domain (Figure 3.1b). However, limited contacts occur between the glutaminase and synthetase domains in the same monomer resulting in only 918 $Å^2$ buried surface area per domain per subunit. The glutaminase domains of subunits whose synthetase domains interact do not directly interact. The synthetase domains are arranged in four dimers situated around the glutaminase core at the corners of a square (Figure 3.1a). The synthetase dimers are similar in structure to the dimers of the ammonia-dependent NAD synthetase (Figure 3.2) (*48*). There are extensive contacts between the dimers of NAD synthetase^{TB} burying 1,841 $Å^2$ which is comparable to the 2,678 $Å^2$ of surface area buried in the ammonia-dependent NAD synthetase from *Bacillus subtilis* (*48*). A superposition of the synthetase dimer of NAD synthetase^{TB} and several NAD synthetase^{NH3} reveals a high degree of similarity in the structures around the active site (Figure 3.2a and b). In the synthetase active site the orientation of the ADP moiety of the NaAD ligand is

the same for each NAD synthetase^{TB} subunit as well as in the ammonia-dependent enzyme. However, the nicotinic acid ring is conformationally flexible (Figure 3.2c). The synthetase domains are inclined toward the plane between two rings, and dimers are formed from synthetase domains of subunits from separate rings (Figure 3.1a). Thus, the synthetase domains interlock the rings formed by the glutaminase domains. As a result of the complex architecture, one subunit contacts five other subunits in the octamer (Figure 3.1).

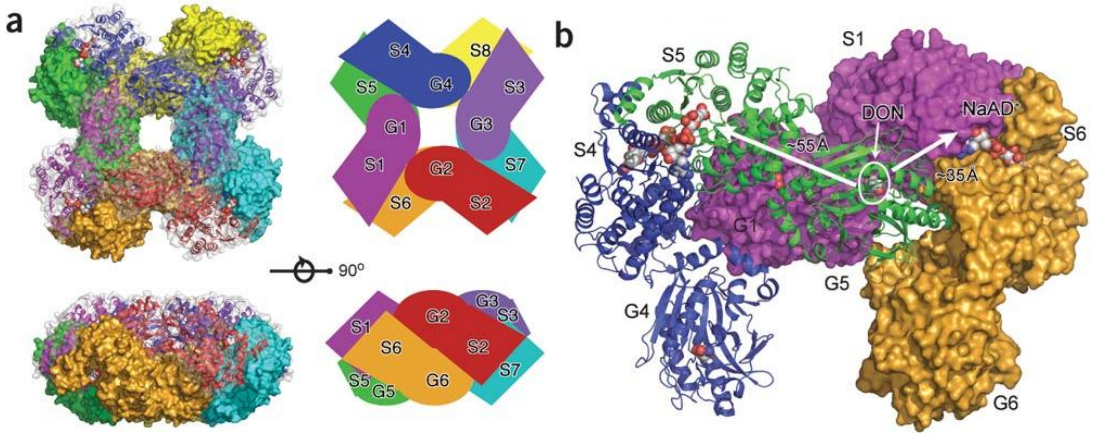

Figure 3.1 Oligomeric assembly of NAD synthetase^{TB}. (a) Quaternary structure of NAD synthetase^{Gln}. Glutaminase domains (G1 to G8) line the central cavity, whereas synthetase domains (S1 to S8) are on the outside. Glutaminase domains in the top ring are illustrated in ribbon with a transparent surface representation. The subunits are color coded as indicated in the model shown to the right. NaAD bound in the synthetase active site is shown in CPK. A 90º rotation about the x axis is shown below. (b) Surface and ribbon representation of the four subunits in the asymmetric unit. The synthetase and glutaminase active sites are indicated by NaAD and DON in CPK, respectively. The white arrows indicate the distances of the active site in G5 to the active sites in S5 and in S1.

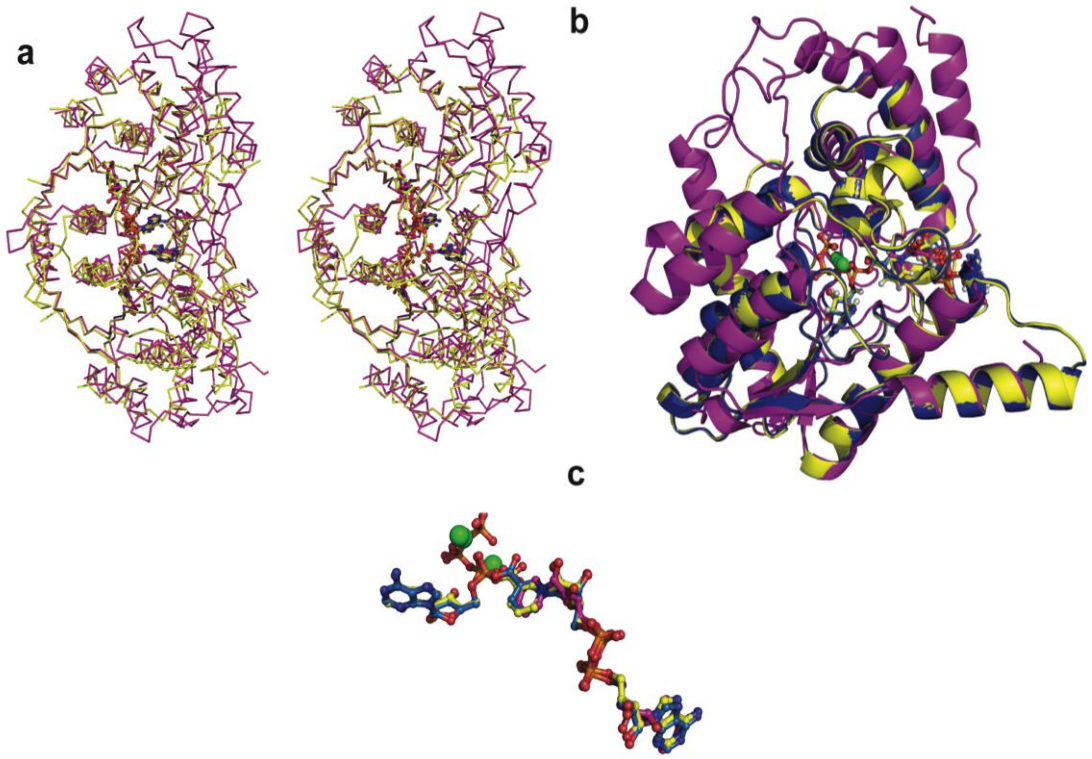

Figure 3.2 Superposition of the synthetase domain (residues 320-679) with NAD synthetase^{NH3} with different ligands. (a) Stereo view of a ribbon representation of backbone superposition (r.m.s.d. 1.78 Å for 206 matched residues) of the S1 and S6 synthetase domain in magenta on the NAD synthetase^{NH3} (PDB code 1IFX) both with NaAD bound shown in sticks. Two NaAD molecules bind each dimer of synthetase domains, with the binding site located across the dimer interface as in NAD synthetase^{NH3}. (b) Cartoon representation of the backbone superposition of S1 in yellow with NaAD in sticks on the NAD synthetase^{NH3} with NaAD and ATP/Mg^{2+} (PDB code 1EE1) in blue (r.m.s.d. 1.88 Å for 207 matched residues), and with NaAD-AMP and PPi/Mg^{2+} (PDB code 1KQP) in magenta (r.m.s.d. 1.80 Å for 202 matched residues). (c) Shows the ligands of panel b in the absence of the proteins. Ligands are color coded according to the proteins to which they are bound in b. Mg^{2+} ions are shown in green spheres.

3.3 The Glutaminase Domain and the Glutamine Tunnel

The glutaminase domain of NAD synthetase^{TB} is similar in structure to PH0642 (PDB 1J31) (*130*) a nitrilase from *Pyrococcus horikoshii* according to a secondary-structure matching (SSM) database search (Figure 3.3). The SSM database compares the three dimensional structure of proteins by matching secondary structures and aligning the protein backbone (*131*). As with the nitrilase the glutaminase domain consists of a β-sandwich surrounded by α-helices. Due to the fact that the core of NAD synthetase^{TB} is composed of the glutaminase domains surrounded by the synthetase domains the glutaminase active site is not exposed to solvent as it would be in a monomer. This leads to the question of how the glutamine enters the glutaminase active site. Utilizing CAVER analysis and visual inspection a 33 Å tunnel was identified and proposed to allow the passage of glutamine into the glutaminase active site (Figure 3.4). This glutamine tunnel is formed from two subunits. The tunnel leading to the glutaminase active site in subunit 5 (G5) is formed by non-conserved residues (Figure 3.4) from the glutaminase and synthetase domains of subunit 1 (G1 and S1) as well as mostly conserved residues from G5 which make up the third of the tunnel near the glutaminase active site. The average radius of the glutamine tunnel is 2.7 Å.

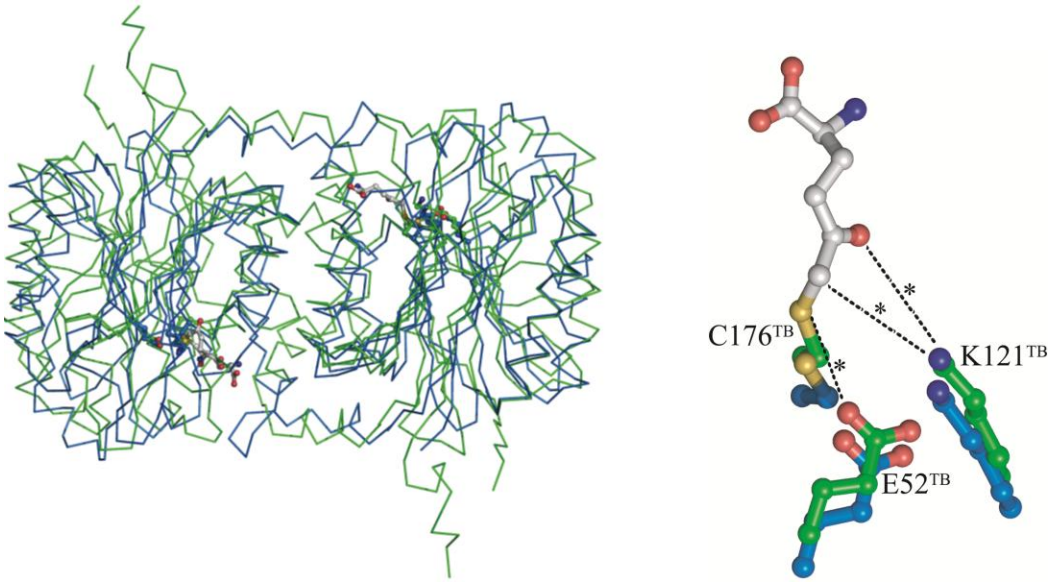

Figure 3.3 Right: Backbone superposition of G5 and G1 (1-320 residues) in green on PH0642 (PDB code 1J31) in blue slate with r.m.s.d. of 1.66 Å for 230 matched residues per subunit. The proposed catalytic triad (E52-K121-C176) and DON are shown in sticks. Left: The superposition of the atoms of the glutaminase active sites. The residues of the active site are in different positions in NAD synthetase^{TB} then the nitrilase PH0642. *The distance between E52^{TB} and the sulfur of C176^{TB} ranges from 4.1 to 3.6 Å. The distance between the K121^{TB} amine nitrogen and the methylene carbon ranges from 5.4 to 4.4 Å and the carbonyl oxygen is 5.1 to 3.8 Å.

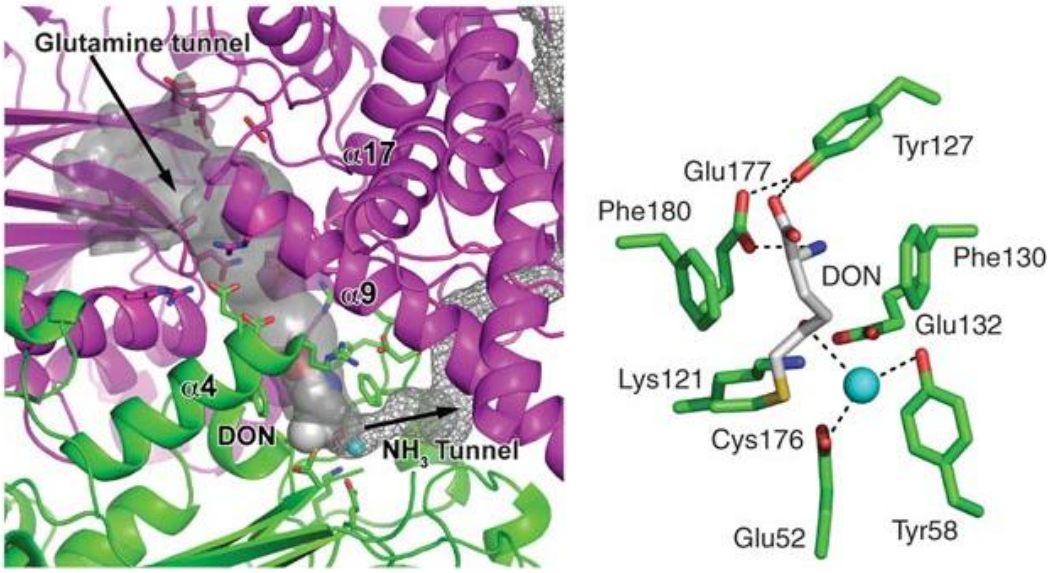

Figure 3.4 DON inhibition of the glutaminase domain. Left: Solid surface representation of the 33-Å glutamine tunnel. Subunits 1 and 5 are in magenta and green, respectively. DON is shown in CPK. The ammonia tunnel is shown in mesh, with the first solvent molecule identified in it shown in cyan sphere. Right: Close-up view of the glutaminase active site (green sticks) with C176 covalently modified by DON (white sticks). In all eight glutaminase domains a $C176^{TB}$-DON adduct was observed, confirming the assignment of C176 as the residue that acts as the nucleophile in the glutaminase reaction. The first solvent molecule identified in the ammonia tunnel is shown in cyan sphere. Because the crystals were grown in 1.8 M ammonium citrate, some of the density modeled as water could be ammonia.

A.

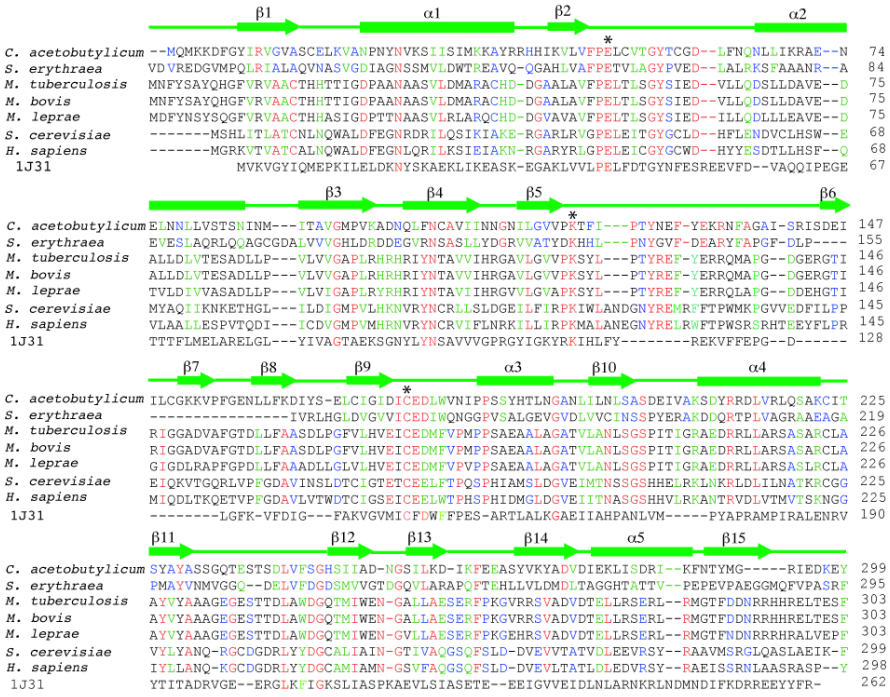
β1 α1 β2 α2
C. acetobutylicum --MQMKKDFGYIRVGVASCELKVANPNYNVKSIISIMKKAYRRHHIKVLVFPELCVTGYTCGD--LFNQNLLIKRAE--N 74
S. erythraea VDVREDGVMPQLRIALAQVNASVGDIAGNSSMVLDWTREAVQ-QGAHLVAFPETVLAGYPVED--LALRKSFAAANR--A 84
M. tuberculosis MNFYSAYQHGFVRVAACTHHTTIGDPAANAASVLDMARACHD-DGAALAVFPELTLSGYSIED--VLLQDSLLDAVE--D 75
M. bovis MNFYSAYQHGFVRVAACTHHTTIGDPAANAASVLDMARACHD-DGAALAVFPELTLSGYSIED--VLLQDSLLDAVE--D 75
M. leprae MDFYNSYSQGFVRVAACTHHASIGDPTTNAASVLRLARQCHD-DGVAVAVFPELTLSGYSIED--ILLQDLLLEAVE--D 75
S. cerevisiae --------MSHLITLATCNLNQWALDFEGNRDRILQSIKIAKE-RGARLRVGPELEITGYGCLD--HFLENDVCLHSW--E 68
H. sapiens -------MGRKVTVATCALNQWALDFEGNLQRILKSIEIAKN-RGARYRLGPELEICGYGCWD--HYYESDTLLHSF--Q 68
1J31 MVKVGYIQMEPKILELDKNYSKAEKLIKEASK-EGAKLVVLPELFDTGYNFESREEVFD--VAQQIPEGE 67
β3 β4 β5 β6
C. acetobutylicum ELNNLLVSTSNINM---ITAVGMPVKADNQLFNCAVIINNGNILGVVPKTFI---PTYNEF-YEKRNFAGAI-SRISDEI 147
S. erythraea EVESLAQRLQQAGCGDALVVVGHLDRDDEGVRNSASLLYDGRVVATYDKHHL---PNYGVF-DEARYFAPGF-DLP---- 155
M. tuberculosis ALLDLVTESADLLP---VLVVGAPLRHRHRIYNTAVVIHRGAVLGVVPKSYL---PTYREF-YERRQMAPG--DGERGTI 146
M. bovis ALLDLVTESADLLP---VLVVGAPLRHRHRIYNTAVVIHRGAVLGVVPKSYL---PTYREF-YERRQMAPG--DGERGTI 146
M. leprae TVLDIVVASADLLP---VLVIGAPLRYRHRIYNTAVIIHRGVVLGVAPKSYL---PTYREF-YERRQLAPG--DDEHGTI 146
S. cerevisiae MYAQIIKNKETHGL---ILDIGMPVLHKNVRYNCRLLSLDGEILFIRPKIWLANDGNYREMRFFTPWMKPGVVEDFILPP 145
H. sapiens VLAALLESPVTQDI---ICDVGMPVMHRNVRYNCRVIFLNRKILLIRPKMALANEGNYRELRWFTPWSRSRHTEEYFLPR 145
1J31 TTTFLMELARELGL---YIVAGTAEKSGNYLYNSAVVVGPRGYIGKYRKIHLFY--------REKVFFEPG--D------ 128
β7 β8 β9 α3 β10 α4
C. acetobutylicum ILCGKKVPFGENLLFKDIYS-ELCIGIDICEDLWVNIPPSSYHTLNGANLILNLSASDEIVAKSDYRRDLVRLQSAKCIT 225
S. erythraea ----------------IVRLHGLDVGVVICEDIWQNGGPVSALGEVGVDLVVCINSSPYERAKDDQRTPLVAGRAAEAGA 219
M. tuberculosis RIGGADVAFGTDLLFAASDLPGFVLHVEICEDMFVPMPPSAEAALAGATVLANLSGSPITIGRAEDRRLLARSASARCLA 226
M. bovis RIGGADVAFGTDLLFAASDLPGFVLHVEICEDMFVPMPPSAEAALAGATVLANLSGSPITIGRAEDRRLLARSASARCLA 226
M. leprae GIGDLRAPFGPDLLFAAADLLGLVLHVEICEDMFVPVPPSAEAALAGATVLANLSGSPITIGRAEDRRLLARSASLRCLA 226
S. cerevisiae EIQKVTGQRLVPFGDAVINSLDTCIGTETCEELFTPQSPHIAMSLDGVEIMTNSSGSHHELRKLNKRLDLILNATKRCGG 225
H. sapiens MIQDLTKQETVPFGDAVLVTWDTCIGSEICEELWTPHSPHIDMGLDGVEIITNASGSHHVLRKANTRVDLVTMVTSKNGG 225
1J31 --------LGFK-VFDIG---FAKVGVMICFDWFFPES-ARTLALKGAEIIAHPANLVM-----PYAPRAMPIRALENRV 190
β11 β12 β13 β14 α5 β15
C. acetobutylicum SYAYASSGQTESTSDLVFSGHSIIAD-NGSILKD-IKFEEASYVKYADVDIEKLISDRI--KFNTYMG-----RIEDKEY 299
S. erythraea PMAYVNMVGGQ--DELVFDGDSMVVGTDGQVLARAPQFTEHLLVLDMDLTAGGHTATTV--PEPEVPAEGGMQFVPASRF 295
M. tuberculosis AYVYAAAGEGESTTDLAWDGQTMIWEN-GALLAESERFPKGVRRSVADVDTELLRSERL--RMGTFDDNRRHHRELTESF 303
M. bovis AYVYAAAGEGESTTDLAWDGQTMIWEN-GALLAESERFPKGVRRSVADVDTELLRSERL--RMGTFDDNRRHHRELTESF 303
M. leprae AYVYAAAGEGESTTDLAWDGQTMIWEN-GVLLAESERFPKGEHRSVADVDTELLRSERL--RMGTFNDNRRRHRALVEPF 303
S. cerevisiae VYLYANQ-RGCDGDRLYYDGCALIAIN-GTIVAQGSQFSLD-DVEVVTATVDLEEVRSY--RAAVMSRGLQASLAEIK-F 299
H. sapiens IYLLANQ-KGCDGDRLYYDGCAMIAMN-GSVFAQGSQFSLD-DVEVLTATLDLEDVRSY--RAEISSRNLAASRASP--Y 298
1J31 YTITADRVGE--ERGLKFIGKSLIASPKAEVLSIASETE--EEIGVVEIDLNLARNKRLNDMNDIFKDRREEYYFR- 262

B.

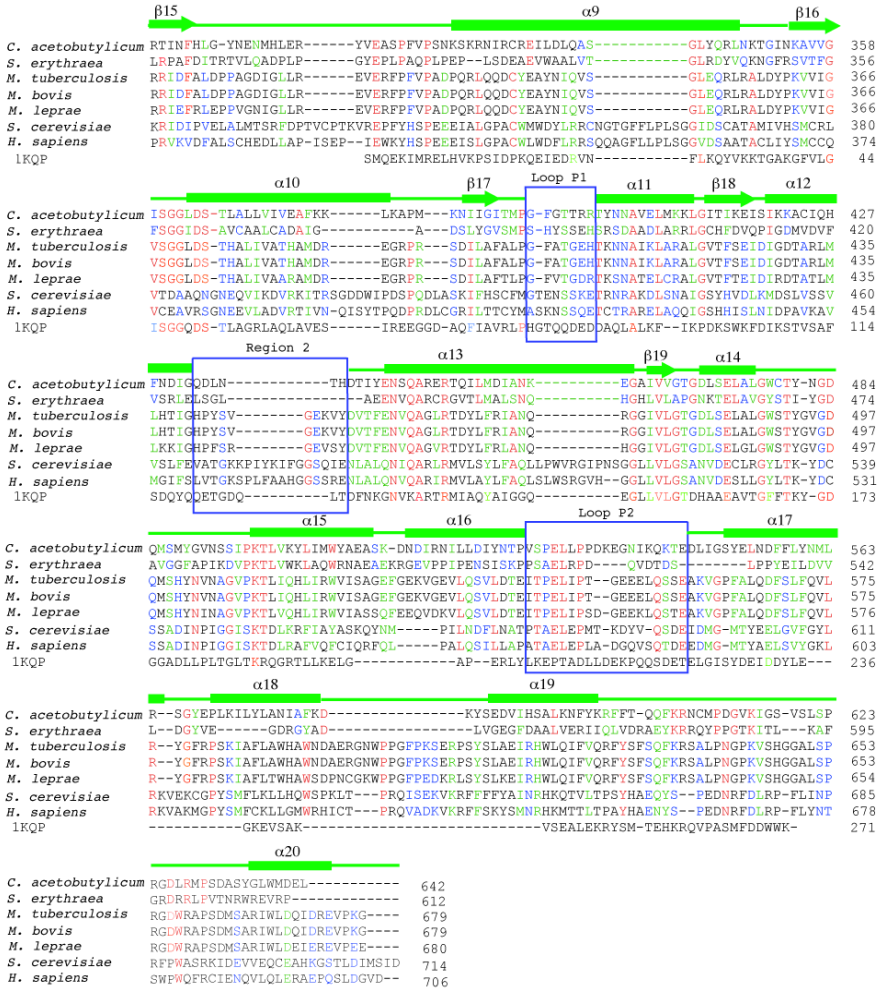

Figure 3.5 Sequence alignments by ClustalW of the glutaminase A. and synthetase B. domains of NAD synthetase^{TB} with prokaryotic and eukaryotic NAD synthetases. Sequence alignments of NAD synthetase^{TB} with the N-terminal domain of the putative nitrilase from *P. horikoshii* (PDB code 1J31) and with *B. subtilisis* NAD synthetase^{NH3} (PDB code IKQP) was obtained by structural alignment using Swiss PDB Viewer. Regions lacking electron density in the synthetase domain are shown in blue boxes. Amino acid residues are colored according to conservation with *M. tuberculosis* YP_001283796. The *S. erythraea* CAM00930 and *C.*

acetobutylicum NP_348407 amino acid sequences are colored coded according to conservation to each other and to the *M. tuberculosis* enzyme. The *M. tuberculosis*, *M. leprae* NP_302028, *M. bovis* NP_856111, *H. sapiens* BAC65148 and *S. cerevisiae* NP_001283796 amino acid sequences are colored according to conservation with each other. Red identical, green high similar and blue weak similar. The catalytic triad residues are indicated with a *.

NAD synthetase^{TB} was covalently modified with DON, which mimics the γ-glutamylthioester intermediate (Figure 2.17). The glutaminase domain of NAD synthetase is a member of the nitrilase superfamily and contains a catalytic triad consisting of Glu-Lys-Cys as discussed in Chapter 1. The DON modification occurred at C176^{TB} confirming the cysteine as the nucleophile. The C176^{TB} is located in loop rich region of the protein. In the glutaminase active site the C176^{TB}-DON adduct has a high degree of conformational flexibility as indicated by the multiple conformations observed by comparison of the four C176^{TB}-DON adducts and the high B factor (Figure 3.6). The B factor (temperature factor) describes the mobility of an atom around the position specified in the model. Therefore, it can provide information on conformational flexibility of a molecule. The α-carboxylate and α-amino groups of the DON adduct interacts with Y127^{TB} and E177^{TB}. The other two members of the catalytic triad are K121^{TB} and E52^{TB}. Lys121^{TB} is positioned to stabilize the negative charge on the γ-glutamylthioester intermediate transition state (Figure 3.4 and 3.7) (*132*). The position of E52^{TB} allows it to abstract a proton from C176^{TB} and donate it to the departing ammonia (Figure 3.7). An ordered solvent

molecule is found within 3 Å of all the $C176^{TB}$-DON adducts and the hydroxyl of $E52^{TB}$ and, therefore, may interact with these molecules. In comparison of the glutaminase active sites of NAD synthetase^{TB} to the active site of PH0642 there is a discrepancy in the positions of $C176^{TB}$, $E52^{TB}$ and $K121^{TB}$ (Figure 3.3). The distance between the $K121^{TB}$ amine nitrogen and the methylene carbon and carbonyl oxygen of the DON molecule ranges from 5.4 to 4.4 Å and 5.1 to 3.8 Å, respectively (Figure 3.3). This is outside the range expected for an interaction (~ 3 Å) to occur between K121TB and the negative charge on the γ-glutamylthioester intermediate (Figure 3.7). PH0642 was not crystallized in the presence of DON. Therefore, it cannot be determined what the distance would be between the Lys residue and the DON molecule. The distance between $E52^{TB}$ and the sulfur of $C176^{TB}$ ranges from 4.1 to 3.6 Å (Figure 3.3) while the distance between the corresponding residues in PH0642 ranges from 3.4 to 3.2 Å. Therefore, the Glu of PH0642 is positioned in the active site such that the Glu could abstract a hydrogen from Cys. In the PH0642 enzyme no glutaminase activation is necessary; therefore, the conformation of the active site is in a conformation optimum for catalysis, the active conformation. It can be proposed that glutaminase activation in NAD synthetase^{TB} (Chapter 2) occurs due to a small conformational change in $E52^{TB}$ and $K121^{TB}$ that positions the residues in an active confirmation.

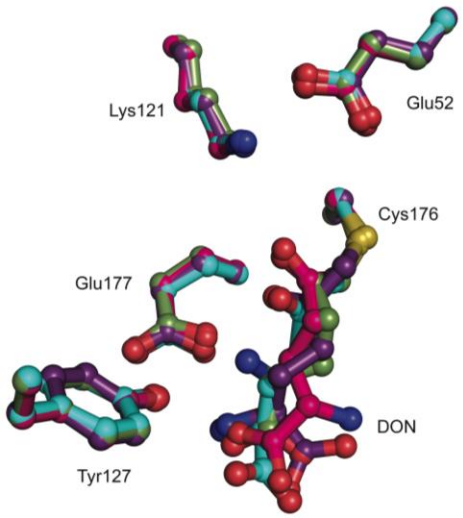

Figure 3.6 Superposition of the proposed catalytic triad (Glu52-Lys121-Cys176), of the side chain of the DON adduct and of Glu177-Tyr127 residues of the four glutaminase domains in the asymmetric unit. Glu177 and Tyr127 side chains interact with the DON adduct side chain. The side chain of the DON adduct has slightly different conformation in each subunit and above average B factors. The four glutaminase domains superimpose with an average r.m.s.d. of 0.17Å for 319 Cα's.

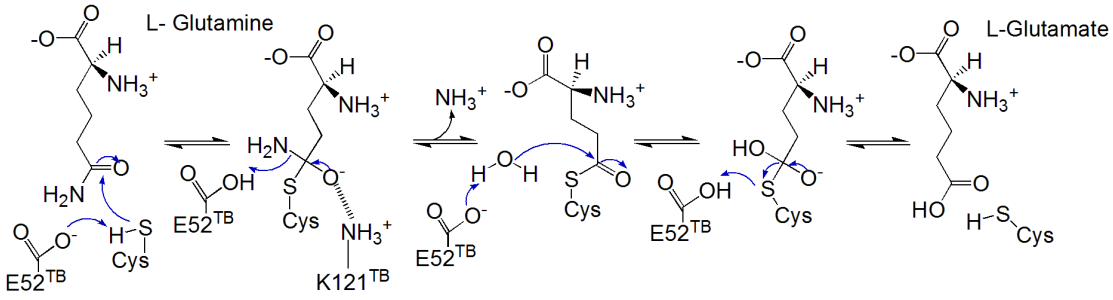

Figure 3.7 The mechanism of glutamine hydrolysis. A base, proposed to be $E52^{TB}$, abstracts a proton from the Cys nucleophile and donates it to the ammonia leaving group.

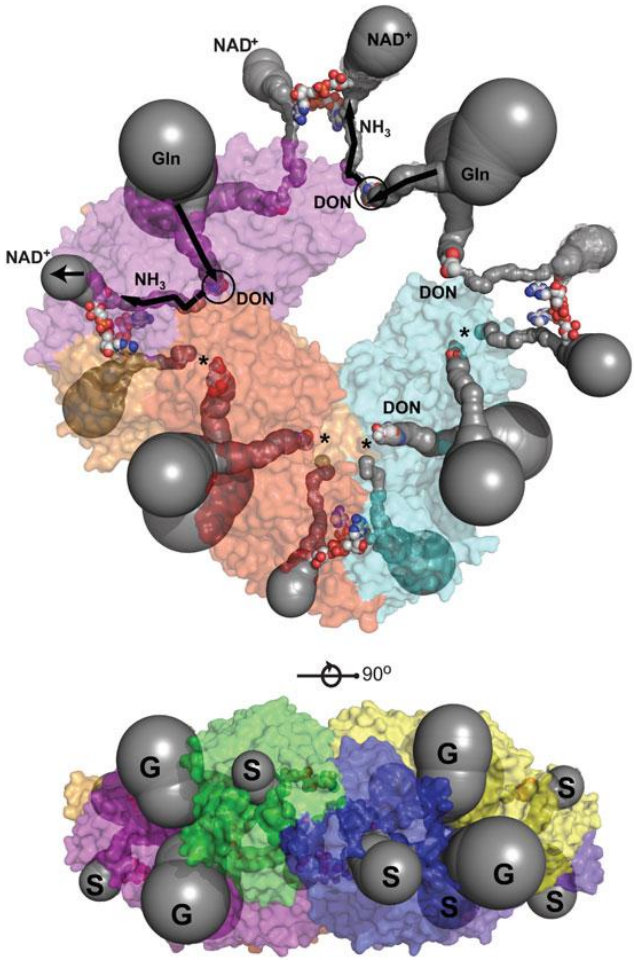

Figure 3.8 The homooctameric structure of NAD synthetase^{TB} with all eight intersubunit tunnels. Half of the subunits are shown in transparent surface and are color coded as in Figure 2.11a. The remaining subunits (3, 4, 5 and 8) are not shown for clarity. The tunnels identified by CAVER were not continuous between the glutaminase and synthetase active sites in all subunits and the gap is indicated by *. NaAD and DON are shown in CPK. DON (indicated by a wide circle) is buried in the glutaminase domain. The black arrows track the CAVER-identified tunnels with glutamine reaching the glutaminase active site and ammonia departing from this site to the synthetase active site where NAD is formed. G and S indicate the entrance of

glutamine and the exit of NAD, respectively, in the representation shown below obtained by a 90º rotation.

As discussed in Chapter 1 some members of the GAT family transport ammonia through ~ 18 -40 Å molecular tunnels that connect the active sites. The glutaminase and synthetase active sites of a single subunit of NAD synthetase^{TB} are ~55 Å from each other (Figure 3.1) while the closest active sites are ~35 Å apart. Utilizing CAVER a second tunnel was identified that extends for 40 Å from the closest synthetase and glutaminase active site (Figure 3.8). The two tunnels join together to form a 73-Å U-shaped tunnel (Figure 3.8). Focusing on only subunits G5 and S1 the intersubunit ammonia tunnel extends 40 Å from ^{G5}C176^{TB} in the glutaminase domain to the carboxyl group of NaAD in the synthetase domain and has an average radius of 2.0 Å, wide enough for an ammonia molecule (*133*). The first third from the glutaminase active site of this intersubunit ammonia tunnel is lined with residues from the glutaminase domain (G5), and the remaining two-thirds is lined with residues of the synthetase domain (S1) (Figure 3.8 and Figure 3.6). Ammonia could be transferred through a hydrogen-bonding network starting at ^{G5}Y58 and ending at ^{G5}D241^{TB} at the G5-S1 interface of the ammonia tunnel (Figure 3.8). The residue Y58^{TB} was mutated to an alanine residue. However, the Y58A mutant was unstable under optimized storage conditions of 15% glycerol at -80 ºC. This was indicated by the complete loss of activity three days after purification (initial k_{obs} of 0.0210 ± 0.0001 sec^{-1} a day after purification). Attempts to fully characterize the mutant can be made in the future if it is determined that there is a period where the

activity of the mutant is stable to allow characterization. $Y58^{TB}$ is located in the glutaminase active site and the hydroxyl group interacts with the solvent molecule positioned there (Figure 3.4). The solvent molecule interacts with $E52^{TB}$ and the DON molecule. The hydroxyl group of $Y58^{TB}$ also hydrogen bonds to $E132^{TB}$ (Figure 3.8). The removal of the tyrosine side chain also results in the removal of possible hydrophobic interactions with $F130^{TB}$ and other hydrophobic residues lining the tunnel. An $Y58F^{TB}$ mutant can be attempted in order to retain hydrophobic interactions and conserve the size of the residue (Van der Waals volume of Tyr is 141 $Å^3$ and Phe is 135 $Å^3$) resulting in only removal of hydroxyl group interactions.

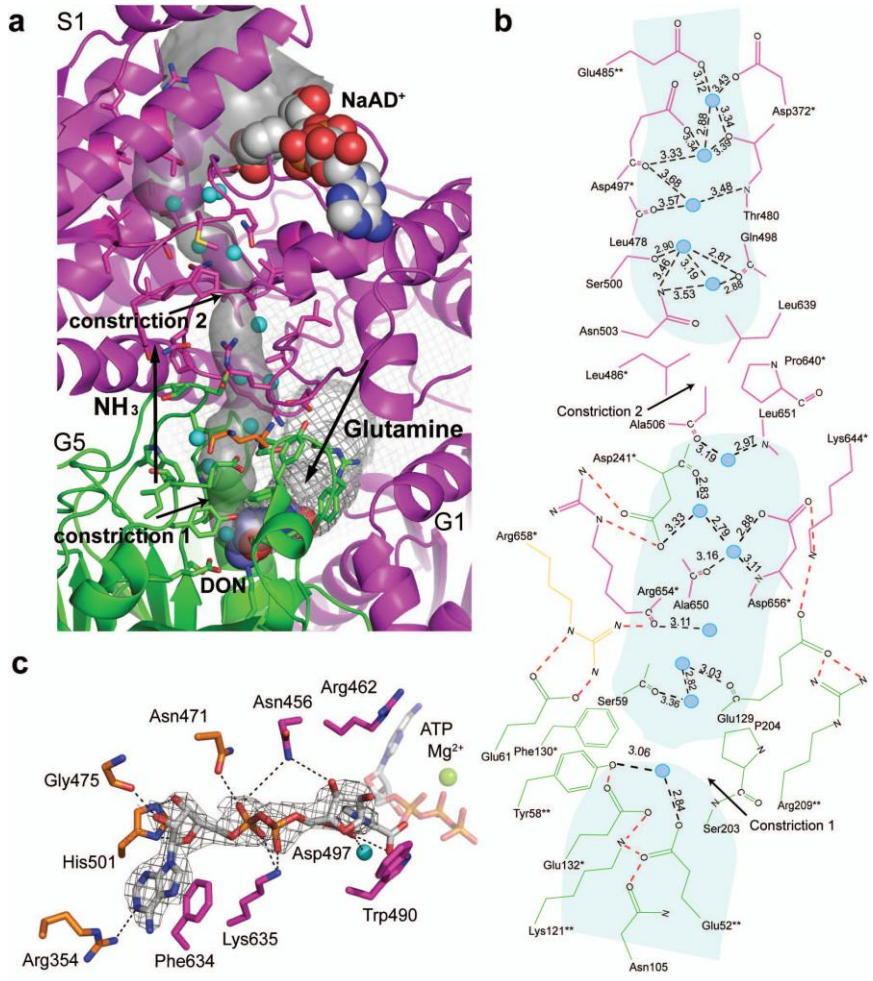

Figure 3.9 The ammonia tunnel and the synthetase active site. Subunits 1, 5 and 6 are in magenta, green and orange, respectively. (a) Solid surface representation of the G5-S1 ammonia tunnel. Large black arrows indicate the direction of ammonia transfer in this tunnel and the entrance of glutamine in the glutaminase active site through the glutamine tunnel (mesh). DON and NaAD are shown in CPK while ordered solvent molecules identified are shown in cyan spheres. The two small black arrows indicate the hydrophobic constrictions identified in the ammonia tunnel. (b) A schematic of the interactions with solvent molecules (cyan spheres) identified in the ammonia tunnel. Residues are colored according to the subunit to which they belong.

Residues invariant among the prokaryotic glutamine-dependent enzymes are indicated by * and those conserved also in the eukaryotic enzymes by **. (c) Fo-Fc map contoured at 1.0 σ of NaAD in a close-up of the synthetase active site. Active site residues shown in sticks are colored according to the subunit to which they belong. The location of the ATP molecule (transparent sticks) was assigned by superposition with the NAD synthetase^{NH3} structure with NaAD and ATP/Mg^{2+} bound (PDB code 1EE1). Mg^{2+} and an ordered solvent molecule are shown as a transparent green sphere and a cyan sphere, respectively.

As a result of the tunnel's convoluted U shape, one short loop (residues 127–131, the YRE loop) conserved in mycobacterium and eukaryotes (Figure 3.5 and 3.9) contacts the DON molecule (^{G5}Y127^{TB}) and three different sections of the tunnel (Figure 3.8). Near the glutaminase active site, ^{G5}F130^{TB} forms with two other hydrophobic residues the first constriction (0.8 Å) of the ammonia tunnel (Figures 3.8b and 3.10). ^{G5}R128^{TB} interacts at the S1-G5 interface in the glutamine tunnel, whereas ^{G5}E129^{TB} and ^{G5}Y131^{TB} are located at the S1-G5 interface in the ammonia tunnel (Figures 3.8b and 3.9). Interactions among ^{G5}E129^{TB}, ^{S1}K644^{TB} and ^{S1}D656^{TB}, conserved residues in prokaryotic enzymes, mediate the transition from the G5 to the S1 section of the ammonia tunnel (Figures 3.8b and 3.9). Mutation of ^{S1}D656^{TB} to alanine (^{S1}D656A^{TB}) inhibits activation of the glutaminase domain in the reaction with the synthetase substrates, as evidence by the only 9-fold activation of this variant compared to the 179-fold activation measured for the wild type (Table 3.1 and 2.3). The basal glutaminase turnover was essentially the same for the ^{S1}D656A^{TB} and wild-type reactions. In addition, ammonia transfer from one active site to the other in the

reaction catalyzed by $^{S1}D656A^{TB}$ was significantly compromised, as evidenced by the only ~30% maximum channel efficiency of this variant compared to the 100% maximum channel efficiency measured in the wild-type catalyzed reaction (Table 3.2). The $D656A^{TB}$ substitution could have caused a large disruption of the enzyme structure resulting in a lower channeling efficiency or the mutation could have resulted in small conformational changes disrupting key interactions. In order to assure that the structure of the protein was not compromised by the D656A mutation the circular dichroism (CD) spectra were obtained for wild type and mutant NAD synthetase^{TB}. The CD spectra show that there are no large scale differences between the structure of wild type enzyme and the D656A mutant (Figure 3.11). It is possible that disruption of the interactions at the S1-G5 interface and loop YRE yields an enzyme that is markedly wasteful of glutamine and with a substantially compromised ability to transfer ammonia between active sites. It would be beneficial to obtain a crystal structure of the D656A mutant in order to determine the cause of the compromise in channeling efficiency.

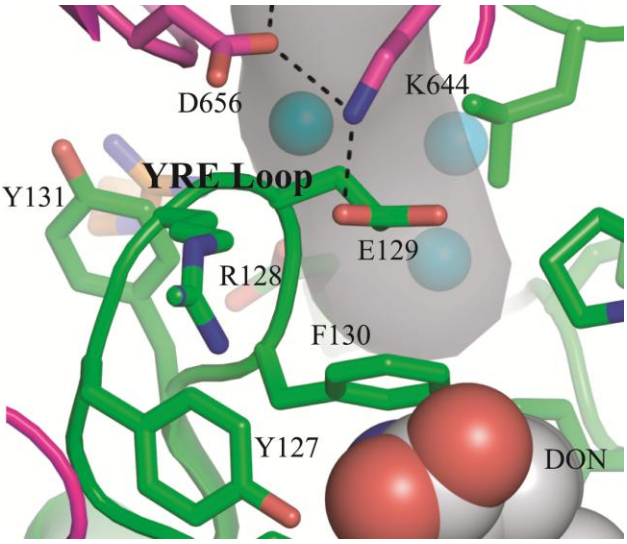

Figure 3.10 The YRE loop in of the glutaminase domain (G5) of NAD synthetase[TB]. The interactions of the YRE loop with K644 and D656 are shown.

Table 3.1 Steady state kinetic parameters of the D656A NAD synthetase[TM] catalyzed reactions

Assay	Variable substrate	Fixed substrates	K_m (mM)	k_{cat} (sec^{-1})	k_{cat}/K_m ($sec^{-1}mM^{-1}$)
NAD	NH_3	NaAD, ATP	0.089 ± 0.005	0.0045 ± 0.0001	0.051 ± 0.003
NAD	Gln	NaAD, ATP	7.8 ± 1.4	0.012 ± 0.0007	0.0015 ± 0.0003
Glu	Gln	NaAD, ATP	9.3 ± 1.5	0.048 ± 0.003	0.051 ± 0.0009
Glu	Gln	None	0.1 ± 0.05	0.006 ± 0.0003	0.053 ± 0.02

[a]The enzyme assays were performed in 10 mM $MgCl_2$, 1 mM DTT and 50 mM Tris-HCl, pH 8.3, at 37°C.
[b]These values are apparent K_M constants at saturating concentration of the other two substrates.

Table 3.2 Stoichiometry analysis for wild type and D656A NAD synthetase^{TB} catalyzed reaction[a]

Wild-type NAD synthetase^{TB}			
Gln concentration	AMP/NAD	Glu/ NAD	% Channel Efficiency
1.5 mM	n.d	1.05 ± 0.05	95 ± 5
5.0 mM	n.d.	1.12 ± 0.13	89 ± 12
20.0 mM	0.9 ± 0.2	1.36 ± 0.13	73 ± 10
D656A NAD synthetase^{TB}			
1.5 mM	n.d	3.1 ± 0.5	32 ± 5
5.0 mM	n.d.	3.5 ± 0.4	28 ± 3
20.0 mM	n.d.	3.5 ± 0.3	29 ± 3

[a]All reactions were carried out in 10 mM $MgCl_2$, 1 mM DTT and 50 mM Tris-HCl, pH 8.3, at 37 °C and 0.23 μM NAD^+ synthetase. The concentration of ATP and $NaAD^+$ were 4 and 3 mM, respectively.

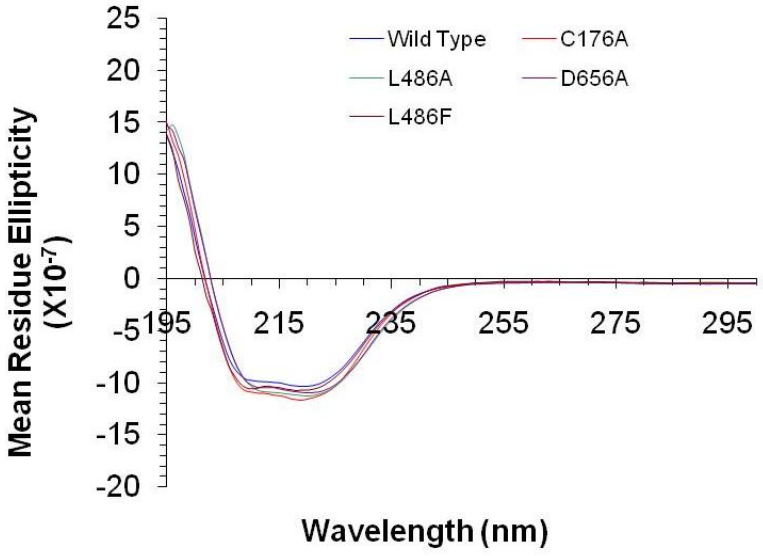

Figure 3.11 The CD spectra of wild type and mutant NAD synthetase^{TB}. The UV CD spectra of C176A, D656A, L486A, L486F and wild type NAD synthetase^{TB} was acquired from a range of 300 nm to 185 nm at 37 ºC in Na_2HPO_4/NaH_2PO_4, pH 8.5. The A_{280} of all the samples were 0.4. The mutant enzymes have similar spectra to the wild type.

A second set of contacts between the side chain of ^{S6}R658^{TB} with the side chain of ^{G5}E61^{TB} and the backbone carbonyl of ^{S1}R654^{TB} mediates the transition from the G5 to the S1 section of the ammonia tunnel (Figure 3.9a, b). Thus, a residue from a third subunit, S6, is part of the G5-S1 ammonia tunnel. The R658L mutant was unstable and lost all catalytic activity one week after purification (initial k_{obs} one day after purification 0.0034 ± 0.0004 sec^{-1}). This may have been the result of the loss of hydrogen bonding interactions or due to the Leu taking on a different conformation then the Arg. The S1 section of the tunnel closer to the glutaminase domain is lined with polar residues and contains ordered solvent molecules. The tunnel narrows to 1.0 Å in a second hydrophobic patch, composed of ^{S1}L486^{TB}, ^{S1}L639^{TB}, ^{S1}A506^{TB} and ^{S1}P640^{TB} and void of solvent molecules (Figure 3.9a, b), to resume its hydrophilic character near the synthetase active site. The importance of the second hydrophobic patch was demonstrated by the mutation of L486^{TB}. The L486A variant removed the leucine side chain in an attempt to open the hydrophobic constriction (Van der Waals volume of Leu is 124 $Å^3$ and Ala is 67 $Å^3$) (Figure 3.11). The mutant was found to have no change in channeling efficiency from wild type (Table 3.5); however, there is only a 16-fold activation of the glutaminase domain (Table 3.3). The L486F variant was constructed in an attempt to partially block the ammonia tunnel due to the increase in Van der Waals volume of Phe (Van der Waals volume of Phe is 135 $Å^3$) (Figure 3.11). This variant resulted in an enzyme with a slight compromise in channeling efficiency (Table 3.5, 73.7% channeling efficiency versus 95%). The activation of the glutaminase activity was 24-fold (Table 3.4). These data indicate that the second hydrophobic constriction may be important for communicating to the

glutaminase domain the formation of the NaAD-AMP/pyrophosphate intermediate complex formation, causing glutaminase activation. The second constriction site may also be involved in the regulation of ammonia transport through the tunnel. Slight changes in the conformation of the enzyme may occur during catalysis or due to breathing of the protein allowing ammonia to pass the second constriction site. If this is the case then the introduction of a smaller side chain (L486A) would not affect the passage of ammonia, however, the introduction of a larger side chain (L486F) would result in a partial blockage of the tunnel and a decrease in channeling efficiency. Construction of a L486W mutant may result in a larger blockage of the ammonia tunnel (Van der Waals volume of Trp is 163 $Å^3$) and would be predicted to cause a larger compromise in channeling efficiency. Construction of the L486W mutant is under way. This combination of hydrophobic and hydrophilic surfaces of the tunnel differs from the ammonia tunnels in all other GAT enzymes, which are either uniformly hydrophobic (*10, 14, 134, 135*) or hydrophilic (*133, 134*).

Table 3.3 Steady state kinetic parameters of the L486A NAD synthetase™ catalyzed reactions

Assay	Variable substrate	Fixed substrates	K_m (mM)	k_{cat} (sec^{-1})	k_{cat}/K_m ($sec^{-1}mM^{-1}$)
NAD	NH_3	NaAD, ATP	14 ± 3	1.8 ± 0.1	0.13 ± 0.03
NAD	Gln	NaAD, ATP	1.15 ± 0.08	0.67 ± 0.01	0.58 ± 0.05
Glu	Gln	NaAD, ATP	2 ± 0.1	0.94 ± 0.02	0.47 ± 0.03
Glu	Gln	None	0.3 ± 0.1	0.058 ± 0.001	0.20 ± 0.06

[a]The enzyme assays were performed in 10 mM $MgCl_2$, 1 mM DTT and 50 mM Tris-HCl, pH 8.3, at 37°C.
[b]These values are apparent *Km* constants at saturating concentration of the other two substrates.

Table 3.4 Steady state kinetic parameters of the L486F NAD synthetase^{TM} catalyzed reactions

Assay	Variable substrate	Fixed substrates	K_m (mM)	k_{cat} (sec^{-1})	k_{cat}/K_m ($sec^{-1}mM^{-1}$)
NAD	NH_3	NaAD, ATP	21 ± 3	0.77 ± 0.04	0.036 ± 0.005
NAD	Gln	NaAD, ATP	1.13 ± 0.05	0.311 ± 0.003	0.27 ± 0.01
Glu	Gln	NaAD, ATP	2.2 ± 0.3	0.55 ± 0.02	0.25 ± 0.04
Glu	Gln	None	0.5 ± 0.2	0.023 ± 0.002	0.05 ± 0.02

[a]The enzyme assays were performed in 10 mM $MgCl_2$, 1 mM DTT and 50 mM Tris-HCl, pH 8.3, at 37°C.
[b]These values are apparent *Km* constants at saturating concentration of the other two substrates.

Table 3.5 Stoichiometry analysis for NAD synthetase^{TB} catalyzed

Gln concentration	AMP/NAD	Glu/ NAD	% Channel Efficiency
Wild-type NAD synthetase^{TB}			
1.5 mM	n.d	1.05 ± 0.05	95 ± 5
5.0 mM	n.d.	1.12 ± 0.13	89 ± 12
20.0 mM	0.9 ± 0.2	1.36 ± 0.13	73 ± 10
L486A NAD synthetase^{TB}			
1.5 mM	n.d	1.08 ± 0.04	92.8 ± 0.03
5.0 mM	n.d.	1.19 ± 0.05	84 ± 3
20.0 mM	n.d.	1.36 ± 0.10	74 ± 5
L486F NAD synthetase^{TB}			
1.5 mM	n.d	1.36 ± 0.01	73.7 ± 0.01
5.0 mM	n.d.	1.37 ± 0.01	72.8 ± 06
20.0 mM	n.d.	1.70 ± 0.04	58.8 ± 0.2

[a]All reactions were carried out in 10 mM $MgCl_2$, 1 mM DTT and 50 mM Tris-HCl, pH 8.3, at 37 °C and 0.23 μM NAD^+ synthetase. The concentration of ATP and $NaAD^+$ were 4 and 3 mM, respectively.

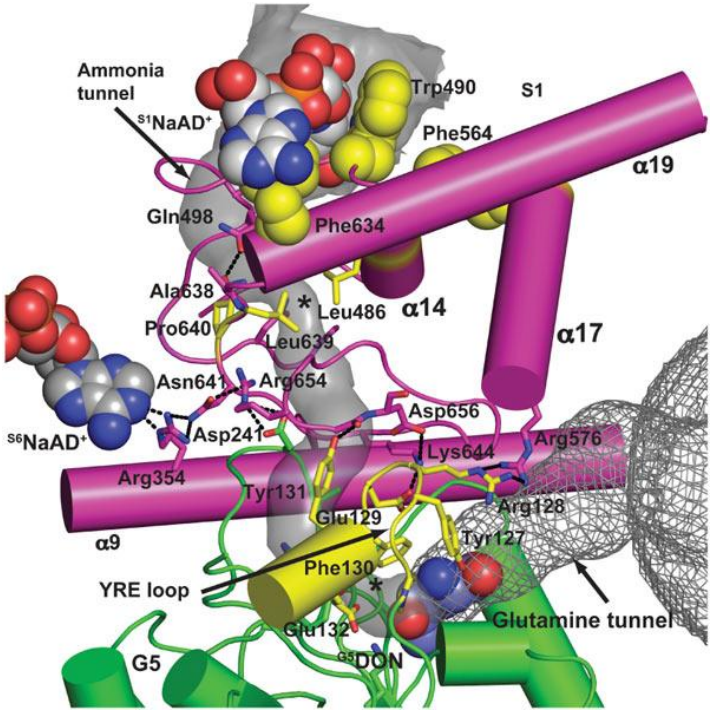

Figure 3.12 Connecting elements between glutaminase and synthetase active sites. Cartoon representation of α-helices that connect the synthetase active site to the glutaminase active site and the tunnel. Residues involved in interactions between elements are labeled. Synthetase domain residues, which form constriction 2 (indicated by *), and glutaminase domain residues of the YRE loop, which form constriction 1 (indicated by *), are shown in yellow sticks. Yellow spheres indicate the positions of key hydrophobic residues that bind to NaAD or may sense interaction at the end of α17. DON and NaAD are shown in CPK. Ammonia and glutamine tunnels are shown in grey solid surface and mesh, respectively.

At the end of the ammonia tunnel in the synthetase active site the conserved residue ^{S1}D497^{TB}, close to NaAD, is positioned to act as a general base for activation of an ammonium ion to ammonia, if an ammonium ion is transferred, or as the last

site for the hydrogen-bonding interaction if ammonia is transferred (Figure 3.9a, b). This role was assigned to the $D173^{Bac}$ in NAD $synthetases^{NH3}$ (*56*).

An ammonia tunnel was previously identified in a homology model of NAD $synthetase^{yeast}$ generated by threading (*136*). The suggested ammonia tunnel is inconsistent with the structure presented here. Using sequence alignment, we identified the corresponding residues in the three-dimensional structure of NAD $synthetase^{TB}$ to those reported in NAD $synthetase^{yeast}$ (Figure 3.5). Most of the residues proposed to line the tunnel for the yeast enzyme are scattered in the crystal structure and are located far from active sites and from the ammonia tunnel identified by CAVER (Figure 3.13). The only exceptions are $Y532^{yeast}$ (corresponding to $W490^{TB}$ and $F167^{Bac}$), which was shown in this structure and in the NAD $synthetase^{NH3}$ (*56*) to be involved in NaAD binding, $Glu177^{yeast}$ ($D178^{TB}$), which is located on the same loop as $C176^{TB}$ but faces in the opposite direction from the glutaminase active site, and $Y601^{yeast}$ ($L566^{TB}$), which lies at the end of α17 helix near the synthetase active site.

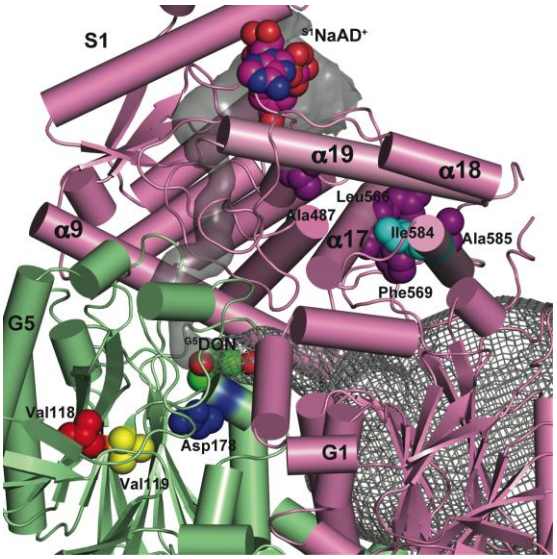

Figure 3.13 Mapping of the mutations of yeast NAD synthetase reported in Brenner *et al*.(*137*) on S1 and G5 of NAD synthetase^{TB}. Residues corresponding to those mutated are shown in spheres and colored red (class I), blue (class II), yellow (class III), cyan (class IV), and purple (class V) (*137*). Ammonia and glutamine tunnels are shown in grey solid surface and mesh, respectively.

3.5 The Synthetase Domain of NAD Synthetase^{TB}

The synthetase domain of NAD synthetase^{TB} belongs to the N-type ATP pyrophosphatase family present in two other GAT enzymes, GMP and asparagine synthetases (*27*, *33*). However, the similarity is limited to the ATP binding site, and the remaining structural elements among these synthetase domains are substantially different (Figure 3.14). The complete active unit consists of a dimer of two synthetase domains. Whereas the secondary-structural elements in the NAD synthetase^{NH3}, including the dimerization interface, are conserved in the synthetase domain, NAD synthetase^{Gln} contains two unique additional helices, α18 and α20, which are required

for oligomeric assembly (Figure 3.15). Many of the conserved α-helices, most notably α9, are offset and/or longer in the synthetase domain of NAD synthetase^{TB} compared to that of the ammonia-dependent enzyme. The extended N-terminal helical segment of α9 (residues 333–339^{S1}), which is absent in the NAD synthetases^{NH3} (Figure 3.12 and Figure 3.2), contacts the glutamine tunnel. The C terminus of α9 is located at the binding site of the ^{S6}NaAD molecule in the synthetase dimer and contacts the ammonia tunnel through ^{S1}R354^{TB} and ^{S1}G350^{TB}, which are conserved in the prokaryotic NAD synthetases^{Gln} (Figure 3.12 and Figure 3.5). These residues form hydrogen bonds with the side chain of ^{S1}N641^{TB}, whose backbone atoms line the ammonia tunnel. Notably, ^{S1}N641^{TB} is located on a loop lining the tunnel that contains two of the residues that contribute to the constriction (constriction 2) in the ammonia tunnel near the synthetase active site (Figure 3.12). α9 is a connecting structural element that is likely to contribute to regulation of the reactions at the synthetase and glutaminase active site.

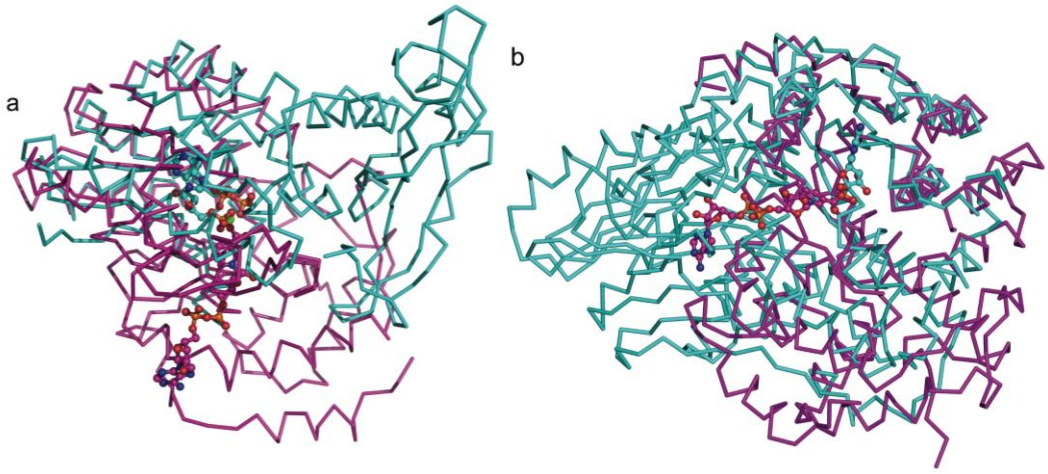

Figure 3.14 Superposition of the synthetase domains of NAD synthetase^{TB} with GMP synthetase and with asparagine synthetase. (a) Backbone superposition

(r.m.s.d. 3.04 Å for 175 matched residues) of S1 (residues 320-679) in magenta with NaAD in sticks on GMP synthetase in cyan with AMP and PPi/Mg^{2+} in sticks (PDB code 1GPM). (b) Backbone superposition (r.m.s.d. 3.00 Å for 153 matched residues) of S1 (residues 320-679) in magenta with NaAD in sticks on asparagine synthetase in cyan with AMP in sticks (PDB code 1CT9).

The synthetase domain contains three regions for which we observed no electron density. Region 1 (residues 402–407, equivalent to loop P1 in the ammonia-dependent enzymes[10]) acts as a lid when ATP is bound in the ATP binding site and is disordered in the absence of ATP. A similar role for loop P1 in the synthetase domain of NAD^+ synthetases^{Gln} is likely, given the structural similarity of the ATP binding sites among NAD synthetases. Region 2 residues 442–450 on the surface of the synthetase domain is disordered in half of the synthetase domains in the octamer. Ordering in the other subunits is probably due to crystal packing. Region 3 residues 542–558, corresponding to loop P2 in NAD synthetase^{NH3} is also always disordered when the ATP binding site is empty. Loop P2 ordering is probably required to protect the NaAD-AMP intermediate from hydrolysis (*52*). The N terminus of α17 is connected to loop P2 in the NAD synthetases^{NH3} and contacts the NaAD biding site by hydrophobic interaction between ^{S1}F564^{TB} and ^{S1}W490^{TB} (Figure 3.12). At the C terminus of α17, the conserved ^{S1}R576^{TB} interacts with ^{G5}R128^{TB} from the YRE loop in the glutamine tunnel (Figure 3.12). Therefore, α17 is another structural element that is likely to contribute to the regulation of catalysis in NAD synthetases^{TB}. The N terminus of α17 is connected to loop P2 in the NAD synthetases^{NH3}, which should become ordered in the presence of the NaAD-AMP intermediate, confirming the link

between NaAD-AMP/pyrophosphate formation and ammonia formation and/or access to the tunnel by contacting the YRE loop. Notably, an alanine variant of Tyr601^{yeast}, which corresponds to Leu566^{TB} near the end of α17 (Figure 3.13), shows poor ammonia-dependent synthetase–specific activity (*137*), probably because of an impaired movement of loop P2 in formation of the intermediate. If α17 indeed acts as a communication wire between conformational changes at loop P2 and ammonia formation, this variant should have a decreased activation of the glutaminase domain in the presence of synthetase substrates. Accordingly, the turnover number for the glutaminase activity in the presence of the saturating synthetase substrate decreased by 40-fold for this variant, whereas the decrease in the basal glutaminase activity was only four-fold (*137*), supporting a compromised glutaminase-activation mechanism. Two other elements, α14 and α9, are positioned to transmit information about the NaAD binding state, and α14 may also respond to intermediate formation (Figure 3.12). As a result of its close connection to constriction 2, it induces widening of the constriction to allow ammonia to move into the synthetase active site.

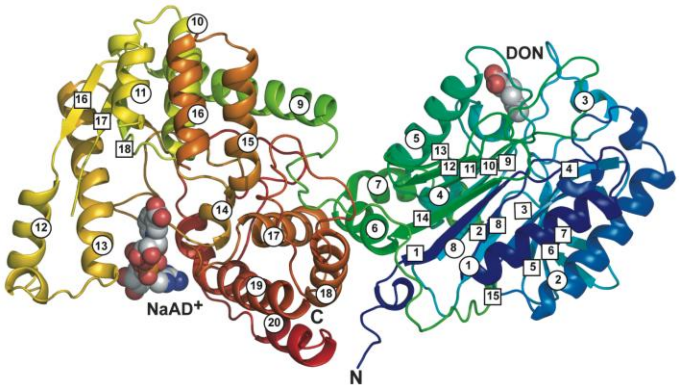

Figure 3.15 Cartoon representation of one subunit of NAD synthetase^{TB} shows the relative orientations of the glutaminase (bound to DON) and synthetase

(bound to NaAD), and little intrasubunit domain interaction. The α-helices (circles) and β-strands (squares) are numbered and colored from blue to red from the N- to the C-terminii.

Chapter 4: Comparative Study of Glutamine Dependent NAD Synthetases

4.1 Thermophilic Proteins and Structural Stability

Life occurs in all regions of the globe including many extreme environments. In order to survive cells must adapt to high salt concentrations, extreme pH conditions, high pressure and extreme high or low temperatures. Thermophilic organisms are capable of optimum growth at high temperatures. Extreme thermophiles grow optimally at temperatures above 60 ºC while hyperthermophiles grow at temperatures of over 80 ºC (*138*). Extreme thermophilic organisms belong to the domains Archaea and Bacteria while the majority of hyperthermophiles tend to be uniquely from the Archaea. Organisms that grow at temperatures of 100-110 ºC are exclusively Archaea (*139, 140*). Thermophilic organisms are often studied because the proteins of a thermophilic organism must be thermostable and can be utilized for industrial purposes (*141*). Thermophilic enzymes are the most investigated of the extremophilic proteins (*139*). The most famous example of this type of application is Taq polymerase from the extreme thermophile *Thermus aquaticus* utilized for PCR (*142*). Thermophilic enzymes can be utilized in industrial reactions that need to be performed at high temperatures (*139*). The study of thermophilic enzymes can also give insight into the understanding of protein folding and stability (*139*). Decreasing the flexibility of the enzyme at low temperatures can aid in increasing stability (*143*). This can be achieved by shortening surface loops, increasing the number of prolines and the number of ion pairs and hydrogen-bonds (*138, 141, 144*). Individual

hydrogen bonds have been shown to contribute 1.3 kcal/mol to protein stabilization (*145*). Increase in hydrogen bonds is seen in the crystal structures of glyceraldehyde-3-phosphate dehydrogenase from *Thermus aquaticus* that showed a higher number of hydrogen bonds then the mesophilic homologs (*144*). Increase in ion pairs compared to their mesophilic homologs has been seen almost in every hyperthermophilic enzyme including O^6-methylguanine-DNA methyltransferase from *Thermococcus kodakara*, which has four more ion pairs then the homolog form *E. coli* (*144*). Increasing ion pairs confers thermal stability because of a reduced desolvation penalty for the formation of ion pairs at higher temperatures (*143*). High packing density or decreasing solvent exposed surface areas was shown to increase the stability of hyperthermophilic aldehyde ferredoxin oxidoreductase compared to the mesophilic enzyme by decreasing entropy (*144*). This is also true for increasing subunit contacts that is shown, for example, to increase the thermostability of citrate synthases from various thermophilic organisms compared to mesophilic enzymes (*143*). Different thermophilic proteins will utilize several different methods to increase thermostability. These structural stabilizing factors are incorporated into thermophilic proteins through manipulation of the protein sequence (*141*). However, there is a balance between stability and function because conformational flexibility is necessary for catalysis (*143*). With an increase in stability, function can be compromised and an increase in function may decrease structural stability (*146*). As seen with hyperthermophilic RNase from *T. kodakaraensis*, the enzyme was less active when the active site was mutated to increase thermostability. The local instability of the active site was necessary for the activity of the enzyme (*146*).

4.2 Thermotoga maritima

The organisms of the *Thermotogae* phylum are rod-shaped, non-spore forming bacteria with an outer sheath that envelope the cells referred to as 'toga' (*147*). These bacteria are isolated from a wide range of environments. The most remarkable characteristic of these bacteria is that they are thermophiles with one of the highest growing temperatures of bacteria (65-90 ºC) (*147*). The first bacterium from this phylum to undergo extensive study when the genome was sequenced (*148*) was *Thermotoga maritima* (*T. maritima*), which was isolated from a geothermal feature off Volcano Island, Italy (*147*). *T. maritima* has an optimum growing temperature of 80 ºC making it a rare bacterial hyperthermophile (*140, 148*). Another interesting aspect of *T. maritima* is that it is possibly one of the deepest branching lineages of Bacteria (*148, 149*). The genome of *T. maritima* shows many genes that resemble archaeal genes. It was found that 24% of the open reading frames were similar to gene from Archaea (*148*). This is believed to be due to lateral gene transfer between the *T. maritima* and archaeal species (*148, 149*).

The work that I contributed to this chapter was the cloning, expression and purification of NAD synthetase from *T. maritima* and the phylogentic analysis. The kinetic experiments were performed by myself and Jason Yaffe (a undergraduate biochemistry student).

4.3 Phylogentic Analysis of Glutamine-Dependent NAD Synthetases

As discussed in Chapter 2 steady-state kinetic analysis of NAD synthetase^{TB} and NAD synthetase^{Yeast} (*137*) have been performed and revealed significant differences in the kinetic mechanism. NAD synthetase^{TB} was shown to undergo

catalysis with a 95% channeling efficiency and high synchronization of the active sites indicative of an enzyme with an effective regulatory mechanism. NAD synthetase^{Yeast} exhibited moderate channeling efficiencies and poor synchronization of the synthetase and glutaminase active sites. This raises the question as to whether differences in regulation were evolved for different types of organisms. Phylogenetic analysis was performed utilizing the sequences of the glutamine-dependent NAD synthetases in order to determine if there is a correlation between the evolutionary relationship of the NAD synthetase enzymes and the extent and method of regulation.

Phylogenetic analysis involves the alignment of gene sequences to infer a phylogenetic tree. In most methods several phylogenetic trees are calculated and a consensus tree is built. The bootstrap is a method to determine the reliability of the consensus tree that has been built. This is done by replicating the data, resampling the sequence alignments and repeating the analysis. The process is performed a hundred or more times and a majority-rule consensus tree is built displaying the bootstrap for each branch of the tree showing the percentage of the calculated trees that agrees with the consensus tree. There are several methods for building a phylogenetic tree which vary in the model used, the number of sequences that can be analyzed and the calculation time. The software used to build a phylogenetic tree for glutamine-dependent NAD synthetases was PHYML using the maximum likelihood method (*150*). This method has been shown to perform best on simulated data and is capable of analyzing large numbers of sequences. However, this method is calculation intensive and, therefore, slower than other methods.

The amino acid sequences of 37 glutamine-dependent NAD synthetases were utilized in the phylogenetic analysis. Of the NAD synthetase sequences used 26 were Bacteria, 10 were Eucarya and 1 was Archaea. The number of Bacteria and Archaea sequences used in the analysis was limited by the fact that most bacterial and archaeal NAD synthetases are ammonia dependent. Also the calculation intensive maximum likelihood method limited the number of sequences due to the length of time of the analysis. The phylogenetic tree has a consensus for the majority of the braches over 50% and only two branches are below 30% (Figure 4.1). Three groups of enzymes were identified with sequence similarities below 30%. Group A contains NAD synthetase^{TB} as well as various types of Bacteria: pathogenic actinobacteria and proteobacteria, plant-symbiotic nitrogen fixing proteobacteria, human associated verrucomicrobia, soil proteobacteria and clostridia. The glutamine-dependent NAD synthetases in group A are closely related to the enzyme in group B, which contain the Eukaryotic enzymes including NAD synthetase^{Yeast}. Groups A and B are only distantly related to group C, which contain extremophiles such as thermatogae, aquificae, deinococcus–thermus and the archaeaon methanomicrobia; photosynthetic bacteria such as rhodobacter, chloroflexi, and cyanobacteria; nitrogen fixing and nitrifying bacteria such as azobacter and nitrospira. It is important to note that the type of tree obtained from this phylogenetic analysis is unrooted. This means that there is not time-line information that can be derived and therefore cannot infer the evolution of glutamine-dependent NAD synthetase from the tree alone. However, evolutionary information can be inferred from the information known about the organisms in each group. Group C contains the only Archaea, *M. thermophila* as well

as NAD synthetase from *T. maritima* (NAD synthetase^{TM}) a deep-branching Bacteria. Therefore, it is proposed that the members of group C are the ancestral form of glutamine-dependent NAD synthetases. This is confirmed by the fact that in group C also includes NAD synthetase from *T. thermophilus*, which codes for two separate polypeptide chains with glutaminase and synthetase activities i.e the ancestral form of the enzyme before a Rosetta Stone event fused the two subunits together. If the NAD synthetases of group C are an ancestral form of the enzyme then it can be proposed that the enzymes of this group would be less efficiently regulated the enzymes from group A and B. Therefore, NAD synthetase^{TM} was chosen for kinetic analysis were it was expected that the enzyme would have low channeling efficiency and active site communication.

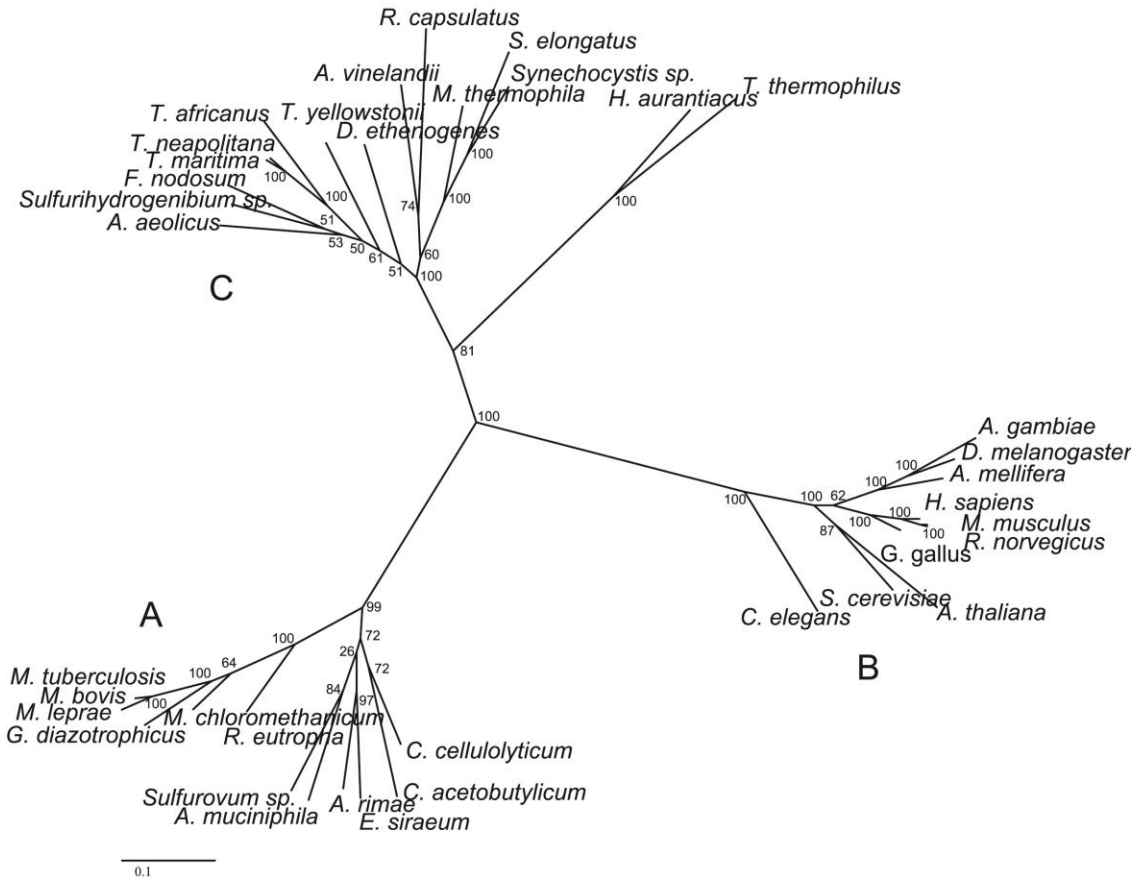

Figure 4.1 The phylogenetic tree for glutamine-dependent NAD synthetase.

4.4 Cloning, Expression and Purification of NAD Synthetase^{TM}

The gene for NAD synthetase, *nadE*, was cloned from the genomic DNA of *T. maritima*. The gene was digested with BamHI and HindIII then ligated into pSMT3 vector. The enzyme was expressed in BL21 (DE3) cells and induced with 0.2% lactose at 20 ºC for 48 hrs. The purification of the enzyme was performed in the same manner as NAD synthetase^{TB} with the exception that none of the buffers contained glycerol. It was determined that the inclusion of glycerol in the purification process had no effect on the stability of the enzyme as determine by measuring the activity of NAD synthetase^{TM} purified with and without glycerol. This is in contrast to what is observed with the enzyme from M. TB where the absence of glycerol results in

instability. However, during the gel filtration of the NAD synthetase^{TM} the high and low molecular weight aggregation peaks were still present with and without glycerol. This indicates that incorrect folding occurs during expression for both NAD synthetase^{TB} and NAD synthetase^{TM}. The protein was stored in -80 ºC with a purity of 90% (Figure 4.2) and a yield of 8.6 mg enzyme/ L culture (1.72 mg/ g cells).

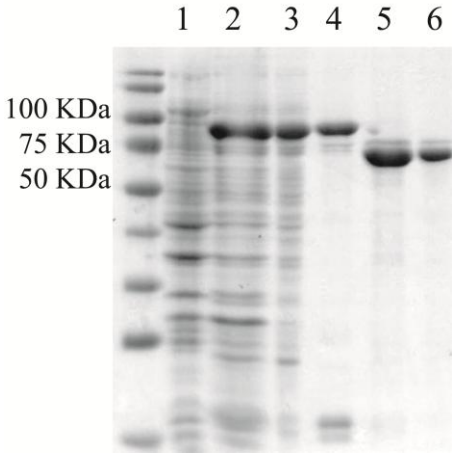

Figure 4.2 The protein gel of the purification of NAD synthetase^{TM}. Lane 1. Cells before induction. Lane 2. Cells after induction. Lane 3. After cell lysis. Lane 4. After the first nickel column. Lane 5. After the second nickel column. Lane 6. After gel filtration.

4.5 Temperature Dependence of NAD Synthetase^{TM}

The k_{obs} for NAD synthetase^{TM} were determined at a temperature range between 20 °C and 90 °C (Figure 4.3). The enzyme reaches maximum activity at 80 °C consistent with the optimum growth temperature for *T. maritima*. At temperature below 65 °C the enzyme shows similar k_{obs} for the ammonia and glutamine-dependent reactions (Figure 4.3) and similar substrate specificity for ammonia and glutamine as indicated by the k_{cat}/K_m at 37 °C (Table 4.1). At

temperatures above 65 °C the glutamine-dependent reaction becomes ~20% faster than the ammonia-dependent at 80 °C. In contrast, NAD synthetase^{TB} at 37 °C, the pathogen optimum growth temperature, is significantly more specific for glutamine rather than ammonia at the same pH.

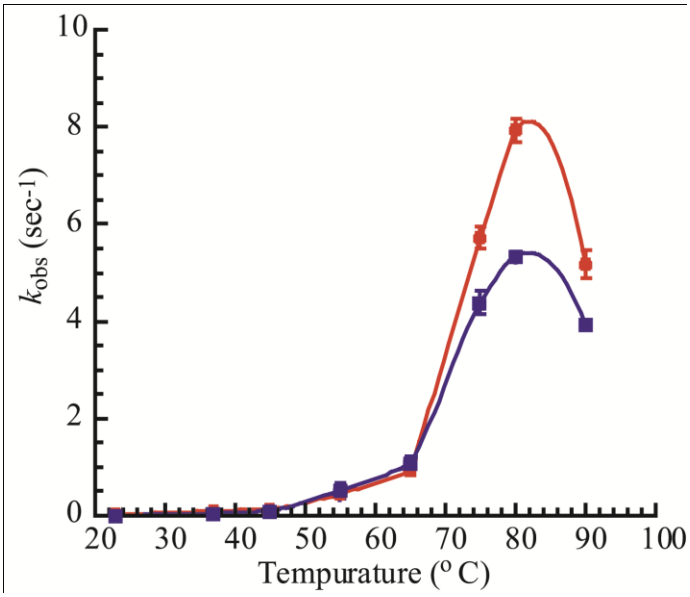

Figure 4.3 The temperature dependent profile of NAD synthetase^{TM}. The blue line is the ammonia dependent reaction monitoring NAD formation. The red line is the glutamine dependent reaction monitoring NAD formation.

4.6 Steady State Kinetic Characterization of NAD Synthetase^{TM}

A full kinetic characterization of NAD synthetase^{TM} was performed in order to compare to the mechanism of NAD synthetase^{TB} and that of the previously characterized NAD synthetase^{Yeast} (*137*). Despite the fact that the temperature of optimal activity of NAD synthetase^{TM} is 80 ºC all kinetic assay were performed at 37 ºC at pH 8.3 so to provide a direct comparison with the enzymes from M. TB and

yeast. There is a 3 fold decrease in the K_M for glutamine in the presence of synthetase substrates versus basal glutaminase activity when glutamate production is monitored (Table 4.1). The glutamine K_M values for NAD synthetase^{TB} and NAD synthetase^{Yeast} showed no or little effect due to the presence of the synthetase substrates. If one were to assume that the K_M value was an approximation of the K_d then one could surmise that NAD synthetase^{TM} is less specific for glutamine in the presence of NaAD and ATP then in the absence. NAD synthetase^{TM} has identical k_{cat}/K_m for glutamine and ammonia (Table 4.1), which means that the enzyme is not specific for either substrate. This is in contrast to what is observed for NAD synthetase^{Yeast} and NAD synthetase^{TB} which are specific for glutamine. The k_{cat} value of NAD formation is 16 fold lower than the k_{cat} value of glutamate formation (Table 4.1). Considering that the glutaminase and synthetase activities are mainly uncoupled (discussed below) and the lack of activation of the glutaminase domain in NAD synthetase^{TM}, the k_{cat} for glutamate formation includes only the microscopic rate constants of the hydrolysis of glutamine steps (discussed below) while the k_{cat} of NAD formation takes into account in addition to the hydrolysis of glutamine steps the transfer of ammonia, the NAD synthesis and any conformational change steps. This suggests that a rate limiting step occurs after glutamine hydrolysis associated with ammonia transfer to the synthetase domain or formation of NAD. However, the k_{cat} value for the ammonia dependent reaction is approximately the same as the k_{cat} value for the glutamine dependent reaction monitoring NAD formation (Table 4.1), which indicates that the rate limiting step is associated with catalytic steps in the synthetase domain or a conformational change associated to catalysis and not to the ammonia transfer step. This is in contrast

to what is observed with the NAD synthetase^{TB} where the rate limiting step of the glutamine dependent reaction is the ammonia transfer, the glutamine hydrolysis or any conformational change steps associated with them (see Chapter 2).

Table 4.1 Steady state kinetic parameters of the NAD synthetase^{TM} catalyzed reactions

Assay	Variable substrate	Fixed substrates	K_m (mM)	k_{cat} (sec^{-1})	k_{cat}/K_m ($sec^{-1}mM^{-1}$)
NAD	NaAD	Gln, ATP	0.021 ± 0.002	0.160 ± 0.002	7.6 ± 0.7
NAD	ATP	Gln, NaAD	0.095 ± 0.008	0.150 ± 0.003	1.6 ± 0.1
NAD	NH_3	NaAD, ATP	0.33 ± 0.1	0.24 ± 0.04	0.7 ± 0.3
NAD	Gln	NaAD, ATP	0.42 ± 0.05	0.288 ± 0.006	0.68 ± 0.08
Glu	Gln	NaAD, ATP	3.0 ± 0.6	4.6 ± 0.2	1.5 ± 0.3
Glu	Gln	None	11 ± 2	0.43 ± 0.03	0.04 ± 0.008
Glu	Gln	ATP	6 ± 2	1.9 ± 0.2	0.3 ± 0.1
Glu	Gln	NaAD	7 ± 2	2.4 ± 0.2	0.3 ± 0.1

[a]The enzyme assays were performed in 10 mM $MgCl_2$, 1 mM DTT and 50 mM Tris-HCl, pH 8.3, at 37°C.
[b]These values are apparent *Km* constants at saturating concentration of the other two substrates.

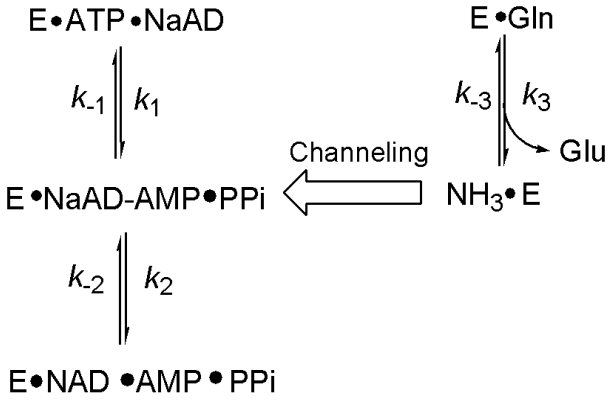

Figure 4.4 The kinetic scheme for glutamine-dependent NAD synthetase^{TM} reaction. The NAD synthetase^{TM} reaction monitoring glutamate formation takes into account k_3 and k_{-3}. The NAD synthetase^{TM} reaction monitoring NAD formation takes into account all the rates.

The activation of the glutaminase domain and channeling efficiencies for NAD synthetase^{TM} was monitored at 37 ºC and 80 ºC. A 10 fold glutaminase activation was observed at 37 °C (Table 4.1) while at 80 °C only a 2.4 fold activation of the glutaminase activity was observed (k_{obs} for the basal glutaminase = $24 \pm 2\ s^{-1}$ and k_{obs} for the glutaminase with ATP and $NaAD^{+} = 60 \pm 2\ s^{-1}$). These values are similar to that of NAD synthetase^{Yeast} (8 fold glutaminase activation in the presence of NaAD) and far below the activation seen for NAD synthetase^{TB} (179 fold, Table 2.3). This indicates that for NAD synthetase^{TM} the mechanism of active site communication was faulty leading to wasteful glutamine hydrolysis. The activation data also show that as in NAD synthetase^{Yeast} the mechanism of communication between the two active sites is different from NAD synthetase^{TB}. For NAD synthetase^{TM} and NAD synthetase^{yeast} glutaminase activity is activated by the presence of either ATP or NaAD (Table 4.1) and NaAD, respectively. While for NAD synthetase^{TB} the formation of the NaAD-AMP/pyrophosphate intermediate complex is necessary to trigger glutaminase activation. As discussed in Chapter 2, the channeling efficiency is also indicative of a lack of active site synchronization in the NAD synthetase^{TM} catalytic machinery. The channeling efficiency for NAD synthetase^{TM} is lower than for NAD synthetase^{TB} and NAD synthetase^{yeast} (Table 4.2). The maximum channeling efficiency at 37 °C is 13.5 % and 36 % at 80 °C.

Table 4.2 The channeling efficiency of NAD synthetases from *T. maritima* , *M. tuberculosis* and yeast.

Concentration Glutamine	M. TB	TM (37 °C)	TM (80 °C)	Yeast[a]
1.5 mM (1.25 mM)[b]	95 ± 5 %	13.9 ± 0.7 %	36 ± 2 %	54 %
5 mM	89 ± 12 %	9.7 ± 0.1 %	28 ± 3 %	55 %
20 mM (10 mM)[b]	73 ± 10 %	7.0 ± 0.8 %	19 ± 7 %	51 %

[a] Data obtained from (*137*).
b Concentrations in parentheses apply only to the yeast enzyme.

If NAD synthetase^{TB}, NAD synthetase^{Yeast} and NAD synthetase^{TM} were mechanistically representative of groups A, B and C, respectively, then one could draw conclusions about the mechanism of each group of enzymes (Figure 4.5). The members of group A would be the most regulated enzymes with high channeling efficiency and activation of the glutaminase domain and, therefore, have high active site synchronization. Group B consists of enzymes with moderate channeling efficiencies and low glutaminase activation. Group C represents the enzymes that are the poorest regulated with low channeling efficiencies and low glutaminase activation and, therefore, have low synchronization of the active sites.

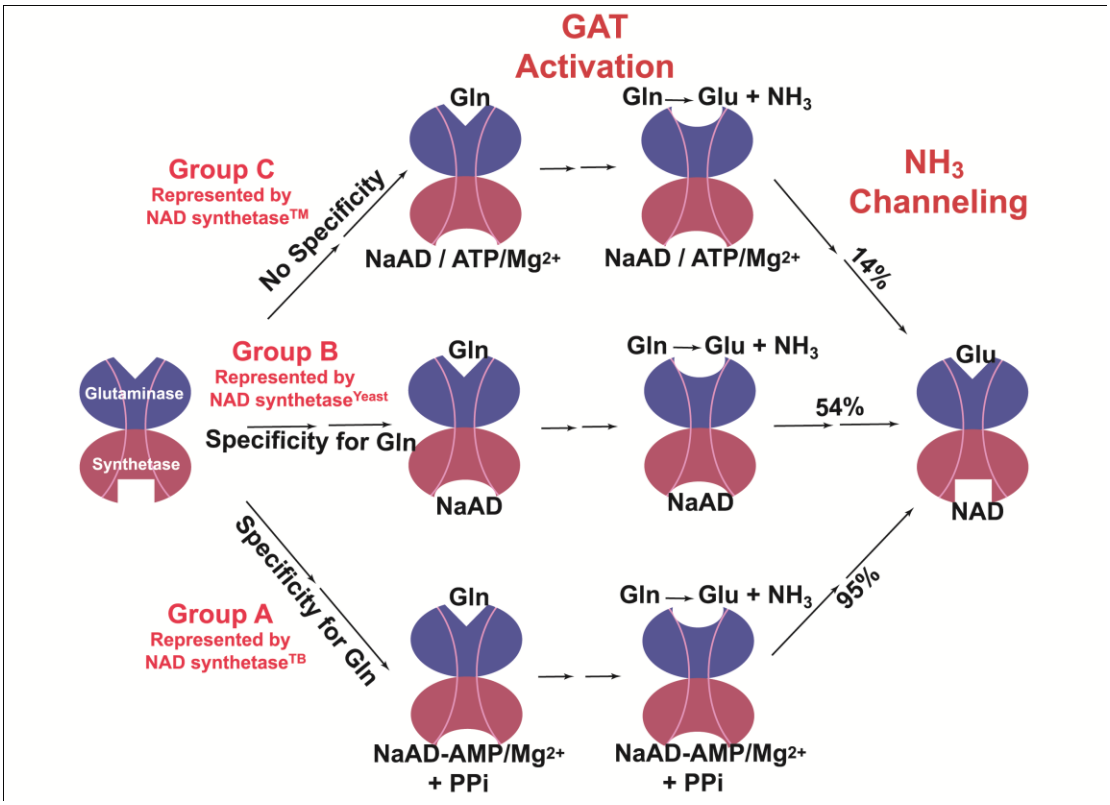

Figure 4.5 The mechanisms of groups A, B and C as represented by NAD synthetase^{TB}, NAD synthetase^{Yeast} and NAD synthetase^{TM} respectively.

4.7 Structural Studies of Glutamine-Dependent NAD synthetases

No crystal structure of any other glutamine-dependent NAD synthetase has been published except for NAD synthetase^{TB} (see Chapter 3). In the absence of any other crystal structure of a glutamine-dependent NAD synthetase the structure of NAD synthetase^{TB} can be utilized along with sequence analysis of the glutamine dependent NAD synthetases to determine what structural elements are involved in the regulation of the active site activities. As discussed in Chapter 3 the YRE loop (residues 127^{TB}-131^{TB}) contacts the DON molecule in the glutaminase active site and three sections of the ammonia tunnel, the first constriction site, the S1-G5 interface at

the glutamine and ammonia tunnel. Phe130^{TB} is part of the first hydrophobic constriction in the tunnel and Glu129^{TB} interacts with A656^{TB}. When A656^{TB} is mutated to Ala there is a severe compromise in active site communication with a 30 % channeling efficiency and only a 9 fold glutaminase activation (Chapter 3). The YRE loop residues Arg128^{TB} and Glu129^{TB}, are conserved in groups A and B but is not conserved in group C. In NAD synthetase^{TM} Glu129^{TB} is substituted by Val120^{TM} removing the potential ionic interaction (Figure 4.6). Phe130^{TB} is conserved also in groups A and C but it is not conserved in group B. None of the three residues that form the second hydrophobic constriction of the ammonia tunnel (Leu486^{TB} and Leu639^{TB}, chemically conserved and the conserved Pro640^{TB} in A) are conserved in groups B and C.

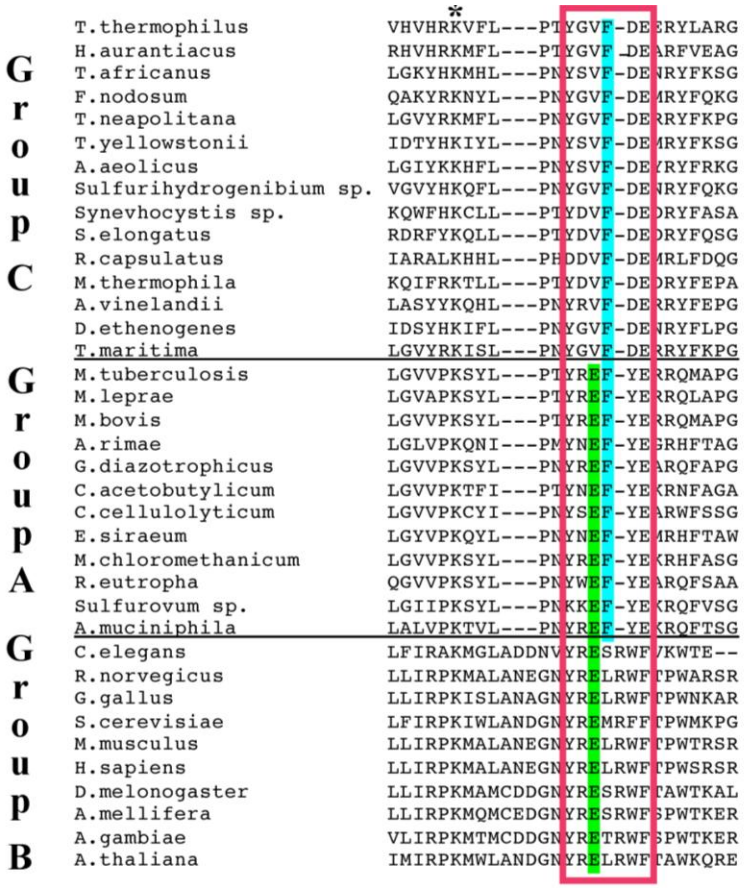

Figure 4.6 The amino acid sequence alignment of selected glutamine-dependent NAD synthetases. The YRE loop is blocked off in red and Glu129 and Phe130 are indicated in green and cyan, respectively.

In order to verify the role of the residues mentioned above in the regulation mechanism and to firmly establish the root of the differences seen in the mechanism of regulation of glutamine-dependent NAD synthetases the crystal structures of enzymes from group B and C would need to be determined. While the structures of the human and yeast enzymes are the subject of Dr. Watchalee Chuenchor's and Kati Chang's research, I have initiated crystal trials of the NAD synthetase^{TM}. DON modified NAD synthetase^{TM} bound with NaAD was crystallized under 192 different

conditions. Of these crystallization conditions several were chosen to be optimized by varying the pH, salt and cryoprotectant concentrations which produced crystals (Figure 4.7). This work is continued by Dr. Watchalee Chuenchor and Kati Chang. The next step after attaining crystals would be to utilize the diffractometer to obtain a diffraction pattern from the crystal and then analyze the data to obtain a structure.

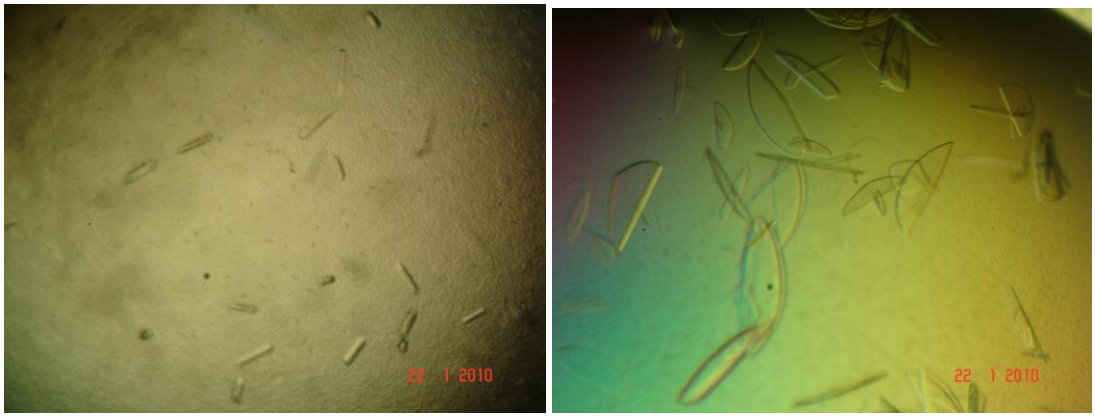

Figure 4.7 The crystals obtained from crystallization of DON modified NAD synthetase™ bound with NaAD. Crystallization conditions Left: 10% PEG8000, 10% glycerol, 0.085 M HEPES pH 7.5, Right: 8% PEG6000, 15% glycerol, 6% MPD, 0.085 M HEPES, pH 7.5.

4.8 Conclusion

Taken together the kinetic and sequence analysis indicates that the three groups of glutamine-dependent NAD synthetases have different extent of communication between active sites. These kinetic differences may be explained by any of the differences in single residues discussed or there may be significant differences in the structure of the enzymes that may account for the kinetic data.

Therefore, it is important to obtain structural data on enzymes from each group in order to determine the cause of the mechanistic differences.

Chapter 5: NaADH Assay Development

5.1 Necessity for the Development of Continuous Direct Assays

The assays monitoring the formation of the products of NAD synthetase have the disadvantage of being discontinuous indirect assays as stated in chapter 2. Therefore, a continuous direct assay was to be developed which would decrease the time it takes to run the assays and ease the determination of the inhibition of substrate and intermediate analogs to be determined. The new assay involves using NaADH as a substrate for NAD synthetase to be converted directly to NADH. In order for the formation of NADH to be monitored in real time the UV spectra of NaADH and NADH would have to be significantly different. It has been shown that NaADPH λ_{max} (λ_{max} = ~330 nm) is blue shifted compared to NADPH λ_{max} (λ_{max} = 340 nm) (*151*). Therefore, we reasoned that NaADH and NADH may have a different λ_{max}. If the absorbance is taken at the λ of greatest difference between NaADH and NADH then it would be possible to monitor the increase in NADH production. After it is established that NADH formation can be monitored it needed to be determined if NAD synthetase was able to utilize NaADH as a substrate.

NaAD is needed in order to synthesize NaADH and as a substrate for NAD synthetase. The cost of purchasing NaAD has increased over the past five years. Sigma-Aldrich is the only supplier of NaAD in the United States and sold 100 mg of the sodium salt of NaAD for $169 in 2005 and that price has increased to $230.50 as of 2010, a 36% increase in price. More worrisome is a recent 1 year backorder of NaAD from Sigma-Aldrich resulted in a loss of the only commercial NaAD supply.

Therefore, it was necessary to develop an alternative method of obtaining NaAD to ensure a supply of NaAD if another commercial NaAD shortage occurs. Most importantly developing an enzymatic synthesis would allow for the incorporation of a radiolabeled atom into the molecule. Utilizing radiolabeled ATP at the formation of ribose-5-phosphate or during the last step in the biosynthesis, a P^{32} isotope could be introduced into specific regions of NaAD. This would be important for future pre-steady state kinetic experiments that would require the monitoring of the substrates, intermediate and products of the NAD synthetase reaction. An enzymatic synthesis of NaAD was modified from the work of Rising and coworkers (*152*). ATP is the most expensive of the starting materials; therefore, ATP recycling reaction was performed involving the conversion of AMP to ADP then ATP so that ATP may be conserved. The enzymes involved in the biosynthetic reaction were cloned and purified (discussed below) with the exception of the ATP recycling enzymes, adenylate kinase and pyruvate kinase, which were purchased from Sigma.

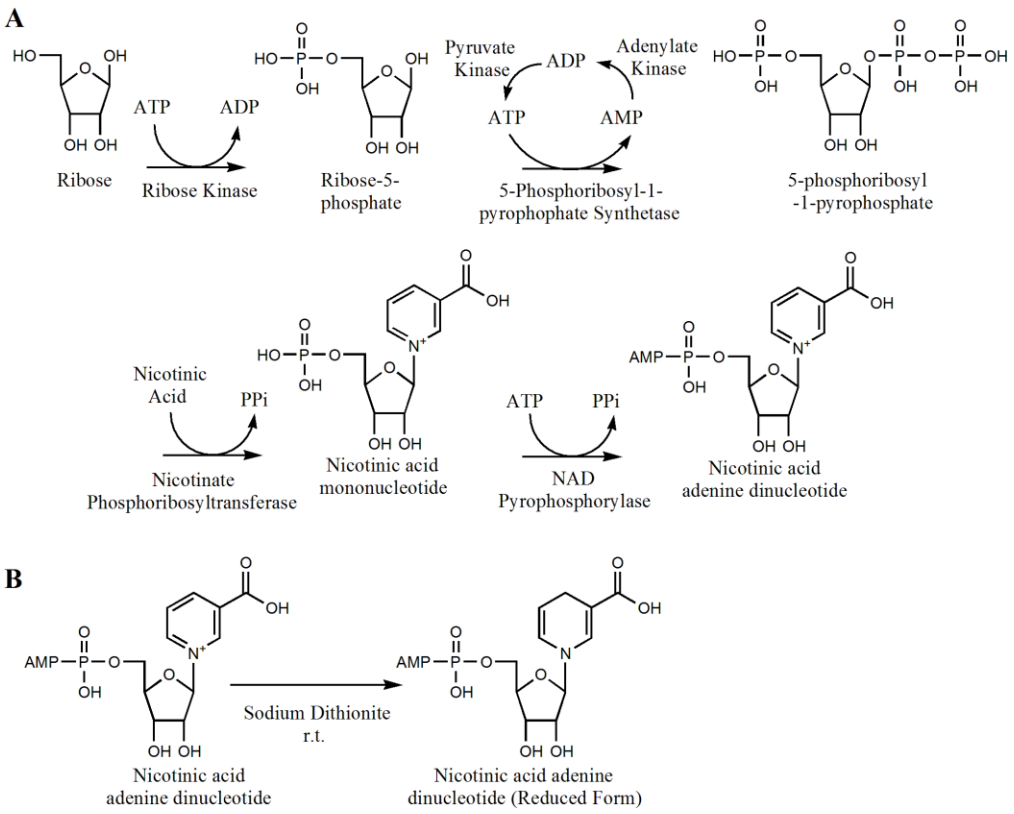

Figure 5.1 A) The biosynthetic scheme for the synthesis of NaAD. B) The 1, 4 reduction of NaAD to NaADH.

5.2 Cloning Expression and Purification of Enzymes Involved in the Biosynthesis of NaAD

Ribose kinase catalyzes the formation of ribose-5-phosphate from ribose and ATP (*153*) (Figure 5.1). The enzyme was expressed from the pBad vector donated from Evalena Andersson (Uppsala Universitet, Department of Cell and Molecular Biology, Uppsala Sweden) resulting in the enzyme with a N-terminal His_6 tag. The plasmid was expressed at an OD_{600} of 0.7 in BL21 (DE3) cells at 37 ºC with 0.2% arabinose for 4 hrs. The cells were lysed by French press at 1200 psi in 50 mM Tris pH 8.0, 300 mM NaCl, 20 mM imidazole and 1 mM PMSF then centrifuged for 30 mins at 15,000 rpm. The cell free extract was loaded on to 6 ml Ni NTA agarose

(Qiagen) resin and washed with 50 mM Tris pH 8.0, 300 mM NaCl, 20 mM imidazole. The protein was eluted over a gradient of 20 mM to 120 mM imidazole over 10 column volumes. The protein was collected and dialyzed in 50 mM Tris pH 8.0, 300 mM NaCl and 1 mM DTT and stored at -80 ºC. The ribose kinase was over 95% pure with a yield of 90 mg of enzyme/ L culture (18 mg enzyme/ gram cells). The enzyme was active for approximately 1 year under these storage conditions.

5-Phosphoribosyl-1-pyrophosphate synthetase (PRPP synthetase) converts ribose-5-phosphate and ATP to 5-phosphoribosyl-1-pyrophosphate (PRPP) and AMP (Figure 5.1). PRPP synthetase was first purified by a native purification modified from a procedure previously published (*154*). The *prpp* gene was amplified by polymerase chain reaction (PCR) from *E. coli* K12 genomic DNA. The gene was digested at the EcoRI and NdeI sites and ligated into pET24a. The gene was expressed in BL21 (DE3) cells with 1 mM IPTG at OD_{600} 0.8 at 37 ºC for 12 hrs. The cells were lysed by French press at 1200 psi in 50 mM Na_2HPO_4 pH 7.5, 1 mM DTT and 1 mM PMSF and centrifuged for 30 mins at 15,000 rpm. To the cell free extract 5% ammonium sulfate was added. The pH was adjusted to 7.5 with 1 M NaOH and stirred for 30 mins at 4 °C. The precipitation was spun at 15,000 rpm for 30 mins. The pellet was resuspended in a minimum amount of 50 mM Na_2HPO_4 pH 7.5 and 1 mM DTT. The resuspended pellet was then dialyzed in 2 L of 50 mM Na_2HPO_4 pH 7.5, 1 mM DTT and 15 % glycerol for 2 hrs at 4 °C. Glycerol is added to the solution to a concentration of 50 % and stored at –20 °C. The yield was 500 mg enzyme/ L of culture (100 mg enzyme/ gram cells). It was determined that PRPP synthetase is active for about two to three months under these storage conditions. The enzyme was

cloudy when purified and required ten times more enzyme in the biosynthesis reaction compared to the other enzymes used. The amount of enzyme needed for the assay was estimated monitoring the formation NaAD from the starting material by ion-paired HPLC (see Chapter 2). The amount of the PRPP synthetase was varied so that optimum NaAD production was achieved. It was speculated that the instability of the enzyme, which resulted in the cloudiness of the enzyme solution, resulted in low enzymatic activity. The use of larger amounts of PRPP synthetase led to the necessity of purifying PRPP synthetase frequently while optimizing the NaAD biosynthesis. Therefore, a purification method was necessary that would allow for more stable enzyme to be obtained and, therefore, higher activity. The enzyme was expressed from pET28b with an N-terminal His_6 tag donated by Dr. Kwaku Dayie. The enzyme was expressed in BL21 A2 cells with 1 mM IPTG at 37 ºC for 12 hours. The cells were lysed by French press in 50 mM Na_2HPO_4 pH 7.5, 1 mM DTT and 1 mM PMSF. The protein was stored in 50 % glycerol at -20 ºC. The PRPP synthetase (34218 Da) was clear with a yield of 200 mg enzyme/ L of culture (40 mg enzyme/ gram cells). While the yield was lower, a third of the amount of enzyme was needed to perform the biosynthesis reaction allowing for fewer preparations of the enzyme.

Nicotinate phosphoribosyltransferase catalyzes the formation of nicotinic acid mononucleotide (NaMN) and pyrophosphate from PRPP and nicotinic acid (Figure 5.1). NAD pyrophosphorylase catalyzes the subsequent formation of NaAD from NaMN and ATP. The *pncB* gene, which codes for nicotinate phosphoribosyltransferase, and the *nadD* gene, coding for NAD pyrophosphorylase, were amplified by PCR from *E. coli* K12 genomic DNA. The *pncB* and *nadD* genes

were digested with NcoI/ XhoI and NdeI/HindIII respectively. The genes were then ligated into pET28b and expressed in BL21 (DE3) cells with 1 mM IPTG at OD_{600} of 0.8 and 37 ºC for 12 hrs resulting in a protein with an N-terminal His_6 tag. The cells were lysed by French press at 1200 psi in 50 mM Tris pH 8.0, 300 mM NaCl, 20 mM imidazole and 1 mM DTT then centrifuged for 30 mins at 15,000 rpm. The cell free extracts were loaded onto 8 ml Ni NTA agarose (Qiagen) resin and washed with lysis buffer. The proteins were eluted over a gradient of 20 mM to 200 mM imidazole over 10 column volumes. The protein was collected and dialyzed in 50 mM Tris pH 8.0, 300 mM NaCl and 1 mM DTT and stored at -80 ºC. Both proteins were over 95% pure with a yield of 400 mg of enzyme/ L culture (80 mg enzyme/ gram cells) for nicotinate phosphoribosyltransferase (45897 Da) and 200 mg of enzyme/ L culture (40 mg enzyme/ gram cells) for NAD pyrophosphorylase (24528 Da). Both proteins were stable for up to 5 years under these storage conditions.

5.3 The Biosynthesis of NaAD

The reaction for the biosynthesis of NaAD contained 12 mM ribose (180 µmoles), 12 mM ATP (180 µmoles), 24 mM phosphoenolpyruvate (360 µmoles), 24 mM nicotinic acid (360 µmoles), 100 mM $MgCl_2$ (1.5 mmoles), 5 mM DTT, 50 mM KCl, 50 mM K_2HPO_4 pH 7.2. The reaction was catalyzed by 1 mg phosphoribopyrophosphate synthetase, 0.1 mg nicotinic acid phosphoribosyltransferase, 0.1 mg nicotinic acid mononucleotide adenylyltransferase, 2 U adenylate kinase (Sigma) and 4 U pyruvate kinase (Sigma) and was initiated by the addition of 0.1 mg ribose kinase for a 15 ml reaction. The reaction was incubated for 5 hrs at 37º C. It was determined that if the reaction is allowed to proceed for

more than five hours the yield of NaAD would decrease due to the reversibility of the reactions. The yield after five hours is approximately 60 %. Product formation was monitored by ion-paired HPLC described in the materials and methods. Once the reaction was quenched with 50 mM EDTA the enzymes were removed with an Amicon Ultra-15 centrifugal filter unit. Anion exchange chromatography was utilized to separate the negative nucleotides. The first resin used was the DE32 resin (Whatman) which is based on the diethylaminoethyl (DEAE) tertiary amine functional group. A 140 ml (2.5 cm X 20 cm) DE32 column was utilized with various gradients of triethylamine bicarbonate buffer pH 6.4 (TEAB buffer). However, there was low resolution between the NaAD and AMP peaks. Therefore, the DEAE sephadex A-25 resin (Sigma, donated from Dr. Dorothy Beckett) was utilized, which also utilizes DEAE in bicarbonate form on a Sephadex scaffold. A 70 ml (2.5 cm X 10 cm) column was loaded and washed with 700 ml 0.05 M TEAB buffer pH 6.4 and a gradient was performed from 0.1 M to 0.4 M TEAB buffer pH 6.4 over 1 L. It was found that better resolution of NaAD and AMP was achieved. Nicotinic acid and NaMN both eluted with 0.1 M TEAB pH 6.4 while NaAD eluted at 0.2 M and AMP eluted at 0.25 M TEAB pH 6.4. This resulted in pure NaAD confirmed by ion-paired HPLC. The NaAD triethylamine solution was rotary evaporated with methanol in order to facilitate the evaporation of the triethylamine solution. This resulted in a brown, sticky solid of NaAD triethylamine salt. In order to exchange the triethylamine cation for sodium the NaAD was then passed through an 8 ml (1 cm X 10 cm) cation exchange column C25 SP Sephadex in Na^+ form, eluted with water and lyophilized to produce a white powder. Only a 16% yield of NaAD was obtained.

Optimization of the synthesis and purification procedure is necessary in order to obtain higher yields of NaAD. Inorganic pyrophosphatase could be added to the synthesis reaction in order to prevent reversibility through the conversion of pyrophosphate to inorganic phosphate. This would allow the reaction to continue past 5 hrs resulting in a higher yield of NaAD.

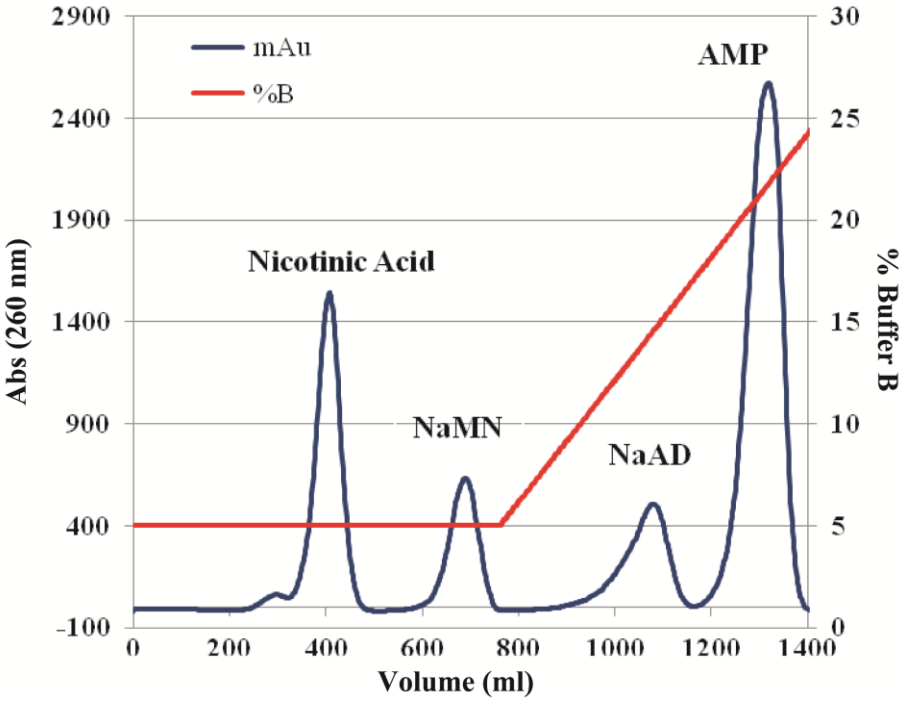

Figure 5.2 The chromatograph of the purifiaction of the NaAD synthesis reaction. The column was a DEAE sephadex A-25 resin. Buffer A was 0.05 M TEAB pH 6.4 buffer and buffer B was 1 M TEAB pH 6.5 buffer.

5.4 Reduction of NaAD

For the reduction of NaAD several reducing agents were tried such as sodium borohydride, sodium cyanoborohydride and sodium dithionite (sodium hydrosulfite). The sodium borohydride and sodium cyanoborohydride reaction did not result in full reduction and produced undesired side products. After 2 to 3 hrs the products were

degraded. The sodium dithionite reaction was performed according to a previous procedure which results in the specific formation of the 1,4 reduction product (*155*). NaAD is diluted to 30 mM (50 mg, 75 µmoles) in a solution containing 500 mM sodium bicarbonate and 500 mM sodium carbonate with a total reaction volume of 2.5 ml. The solution is bubbled under nitrogen gas in a 5 ml round bottom flask with slow stirring at room temperature. After 15 mins under nitrogen 10 equivalents of sodium dithionite is added (130.5 mg, 750 µmoles). The solution turns yellow when dithionite is added and turns clear again after an hour. The reaction is complete after 3 hrs. It was found that if the reaction was allowed to continue after 3 hrs then the product will be degraded. This reaction results in 100 % conversion of NaAD to NaADH with little side reactions (Figure 5.3). The reaction is monitored by ion-paired HPLC as described above. The formation of NaADH was confirmed by a standard NaADH formed from the reduction of NaAD by alcohol dehydrogenase, which is capable of utilizing reducing NaAD in a slow reaction over night.

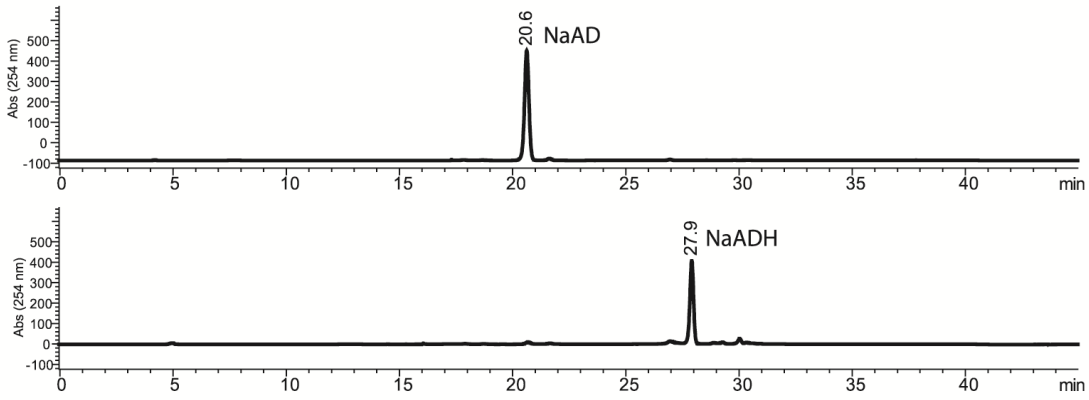

Figure 5.3 The completed reduction of NaAD to NaADH monitored by HPLC. The top panel shows the starting material at time 0. The bottom panel shows the product 3 hrs later.

Several methods for removal of the sodium dithionite were attempted. An assay for dithionite was performed in order to determine where dithionite elutes. The dithionite test was performed as follows: 20 µl of 100 mM $CuSO_4$ is added to 100 µl sample. When at least 10 mM dithionite is present the copper sulfate solution will form a dark yellow or brown precipitate (*156*). A gel filtration P2 resin was first tried. It was determined that the sodium dithionite eluted with NaADH causing degradation of the product. Therefore, the anion exchange method utilized for the purification of the NaAD synthesis product was employed. The reaction was quenched by diluting the solution by 100 times and loaded on to 70 ml of the DEAE sephadex A-25 resin. The column was washed with 0.05 M TEAB buffer pH 6.4 and NaADH eluted with a linear gradient to 0.5 M TEAB buffer pH 6.4. The product was then passed through a cation exchange column C25 SP Sephadex in Na^+ form and lyophilized to obtain NaADH sodium salt.

The UV spectra for both NaADH and NADH were measured at 0.1 mM (Figure 5.4). The concentration of NaADH and NADH was determined by measuring the absorbance at 260 nm and calculating the concentration using the extinction coefficient for NaAD. The extinction coefficient at 260 nm for NaAD and NADH are the same therefore it can be assumed that the extinction coefficient at 260 nm for NaADH would also be the same as NaAD. The maximum wavelength for NaADH (331 nm) is slightly lower than for NADH (340 nm) and the extinction coefficient is also lower. Therefore, if one were to monitor a wavelength of 340 nm one would expect to see an increase in absorbance as NaADH is converted to NADH. This is because 340 nm is the wavelength of greatest difference between the two UV spectra.

Utilizing an approximation of the difference in extinction coefficient between NADH and NaADH to estimate the lower absorbance limit of the assay, which corresponds to 0.016 mM NADH formation, the theoretical detection limit for the assay was calculated to be 0.0005 sec^{-1} as calculated in the materials and methods. This is approximately the same detection limit calculated for the alcohol dehydrogenase (0.0003 sec-1) and glutamate dehydrogenase (0.0006 sec-1) assays.

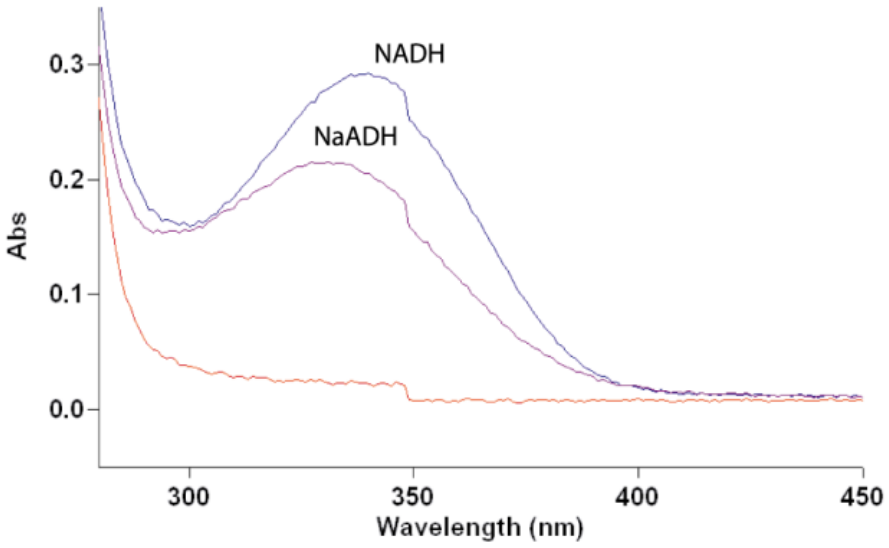

Figure 5.4 The UV scan of NaADH and NADH at 0.1 mM concentration. The maximum wavelength for NADH is 340 nm and for NaADH is 331 nm. The blue line is the spectra for NADH. The purple line is the UV spectra for NaADH. The red line is the UV spectra for the background.

In order to verify that NaADH is a substrate for NAD synthetase NaADH was utilized in an enzymatic assay. The enzyme was incubated at 37 ºC with 6 mM NaADH, saturating 4 mM ATP, 20 mM glutamine, 10 mM $MgCl_2$, 1 mM DTT and 50 mM Tris pH 8.3. The formation of NADH was monitored at 340 nm. However, the absorbance did not increase over the course of 30 mins. Ion-paired HPLC showed

that NADH was not formed in 3 hrs. Therefore, either NaADH is not a substrate for NAD synthetase or the reaction is too slow to be a useful assay.

Chapter 6: Materials and Methods

6.1 Materials

The genes encoding NAD synthetase obtained from *M. tuberculosis* genomic DNA (donated by L.Y. Gao) and from *T. maritima* MSB8 genomic DNA obtained from ATCC 43589D-5. The expression vectors pSMT3 and pUlp1were gifts from Dr. C. D. Lima, Sloan Kettering Institute. Ni-NTA agarose resin was obtained from Qiagen (Valencia, CA, USA). The Sepharose CL-6B resin and ÄKTA Prime FPLC were from Amersham Biosciences (Piscatway, NJ, USA). The Amicon filtration apparatus and Ultrafiltration Membranes were from Millipore (Billerica, MA, USA). The mass spectra were obtained on a Axima-CFR MALDI-TOF mass spectrometer from Shimadzu-Kratos (Nakagyo-ku, Kyoto, Japan). The CD spectra was obtained on a J-810 spectrometer from Jasco (Easton, MD, USA).The oligonucleotides were from Eurofins MWG Operon (Huntsville, AL, USA) except for the oligonucleotides used for the mutagenesis which were from Integrated DNA Technologies (Coralville, IA, USA). PCR components and Phosphate Sensor were from Invitrogen (Carlsbad, CA, USA). Ligation reagents and restriction enzymes were from Fermentas (Glen Burie MD, USA). The crystallization screening kits were obtained from Qiagen (Cryo and PEG Suites), Hampton Research (Index) and Emerald BioSystems (Wizard I-II). The alcohol dehydrogenase and glutamine dehydrogenase and NAD synthetase substrates were purchased from Sigma (St. Louis,MO, USA). The UV asorbances were measured on a Cary 100 Bio UV Visable Spectrophotometer from Varian (Palo Alto, CA, USA). The 1100 series High Pressure Liquid Chromatograph and Zorbax Bonus

RP C18 column (5 μm, 4.6 x 250 mm) was from Agilent (Santa Clara, Ca, USA) and the Alltima C18 column (5 μm, 4.6 x 250 mm) was from Alltech (Deerfield, Illinois, USA). The F-4500 Fluorescence Spectrophotometer was from Hitachi (Tokyo, Japan). The VP-ITC Microcalorimeter is from MicroCal (Piscataway, NJ, USA). The All other chemicals were of analytical grade.

6.2 Cloning and Expression of Wild Type and Mutant NAD Synthetases

The gene *nadE* was amplified by polymerase chain reaction (PCR) from genomic *M. tuberculosis* and *T. maritima* DNA. A 5′ BamHI site and a 3′ HindIII sites were engineered into the gene using the following primers:

nadE from *M. tuberculosis*

Forward Primer: 5′d (GGCGGCGGATCCATGAACTTTTACTCCGCC) 3′ Tm=52ºC

Reverse Primer: 5′d (GGTGGTAAGCTTCTAGCCCTTGGGCACC) 3′ Tm=54ºC

nadE from *T. maritima*

Forward Primer: 5′d (GGTGGTGGATCCATGAAAAGACTGAGAGTG) 3′ Tm=52ºC

Reverse Primer: 5′d (GGTGGTAAGCTTTCAAAGAGGTTCTTTAAATC) 3′ Tm=52ºC

The PCR products were digested with restriction enzymes BamHI and HindIII and ligated into pSMT3. The ligation reactions were transformed into electrochemically competent *E. coli* DH5α and plated on LB- kanamycin (50 μg/ml). Colonies were grown in LB- kanamycin (50 μg/ml) overnight and a plasmid miniprep was performed using Qiagen plasmid miniprep kit. All mutants were constructed using the

Quick Change Mutagenesis procedure outlined below unless otherwise noted. The primers used were (underlined is the codon mutated and bold is the mutated bases):

Mutant Y58A

Forward Primer: 5′d (GACGCTGTCGGGC**GC**CTCCATCGAGGACG) 3′ Tm=79.1ºC

Reverse Primer: 5′d (CGTCCTCGATGGAG**GC**GCCCGACAGCGTC) 3′ Tm=79.1ºC

Mutant L486A

Forward Primer: 5′d (GACCTGTCGGAG**GC**GGCACTGGGTTGGTCGACATAC) 3′ Tm=80.9ºC

Reverse Primer: 5′d (GTATGTCGACCAACCCAGTGC**GC**CTCCGACAGGTC) 3′ Tm=80.9ºC

Mutant L486F

Forward Primer: 5′d (GACCTGTCGGAG**TTC**GCACTGGGTTGGTCGACATAC) 3′ Tm=80ºC

Reverse Primer: 5′d (GTATGTCGACCAACCCAGTGC**GAA**CTCCGACAGGTC) 3′ Tm=80ºC

Mutant D656A

Forward Primer: 5′d (GTTGTCGCCGCGTGGG**CG**TGGCGGGCC) 3′ Tm=81ºC

Reverse Primer: 5′d (GGCCCGCCA**CG**CCCCACGCGGCGACAAC) 3′ Tm=81ºC

Mutant R658L

Forward Primer: 5′d (GTGGGGATTGG**CTG**GCCCCGTCGGATATG) 3′ Tm=78.8ºC

Reverse Primer: 5′d (CATATCCGACGGGGCC**AGC**CAATCCCCAC) 3′ Tm=78.8ºC

PCR was performed with 0.5 µM primers, 0.5 mM dNTPs and 10 ng/µl *nadE*/pSMT3 TB template. The polymerase used was Turbo Pfu. To each reaction 1 µl Dpn1 was added and incubated at 37 °C for 8 hrs then 10 µl transformed into electrocompetent *E. coli* Gene Hogs. Colonies were picked and inoculated into LB- kanamycin (50 µg/ml) and plasmid isolated with Fermentas Mini-Prep Kit. DNA sequencing was performed by the University of Maryland Sequencing Facility.

Plasmids were then transformed into *E. coli* BL21 (DE3). The transformation was performed with 0.5 µl plasmid and 20 µl electrocompetent BL21 (DE3) cells and plated on LB- kanamycin (50 µg/ml). One colony was inoculated into 20 mL seed culture. Of the seed culture was diluted 200 times into 1 L LB- kanamycin (50 µg/ml) and grown at 37 °C to an OD_{600} of ~0.5. The cultures were then induced with 0.2 % lactose and expressed for 48 hrs at 20 °C. The cells were harvested by centrifugation and frozen as a pellet in liquid nitrogen (yield ~8 g wet cell per liter culture). Selenomethionine labeled protein was expressed in *E. coli* BL21(DE3) in M9 SeMet high-yield media (Medicilon) containing kanamycin (50 mg ml^{-1}). The cells were induced (at an optical density at 600 nm (OD600) of 0.5) with 1 mM IPTG at 20 ºC, harvested by centrifugation 48 h after induction and frozen as a pellet in liquid nitrogen (yield of 5 g of wet cells per liter culture).

6.3 Purification of Wild Type and Mutant NAD Synthetases^{TB} and NAD Synthetases^{TM}

The purification procedure is the same for all enzymes except for the enzyme NAD Synthetases^{TM} which does not use glycerol. The approximate yields for each step refers to wild type NAD synthetase^{TB}. In 50 ml 50 mM Tris pH 8.0, 150 mM NaCl, 1 mM DTT and 20% glycerol 5 g cells lysed by French Press (12000 psi, 4 passes, new nylon ball). The cells were spun at 15000 rpm for 30 mins. The cell free extract was loaded on to 8 ml (1 cm X 10 cm) of Ni NTA agrose (Qiagen) resin pre-equilibrated with 50 mM Tris pH 8.0, 300 mM NaCl, 1 mM DTT, 20% glycerol and 20 mM imidazole. The column was washed with the 20 mM imidazole buffer for 10 column volumes (CV) or until the UV absorbance was flat. A gradient from 20 mM imidazole to 120 mM imidazole was performed over 10 CV. The column was washed with 120 mM imidazole until the absorbance reached baseline then the column was washed with 200 mM imidazole. Fractions are collected and ~50 to 60 mg of protein is normally obtained at ~1mg/ml concentration (A_{280} is ~1). For the proteolysis step a 1 to 100 ratio Ulp1 to tagged enzyme is dialyzed with the enzyme in 50 mM Tris pH 8.0, 350 mM NaCl, 1 mM DTT and 30 % glycerol for 4 hrs at 4°C. The dialysis buffer is then changed to 50 mM Tris pH 8.0, 1 mM DTT and 30% glycerol for overnight. The proteolysis reaction is then loaded on to 5 ml (1 cm X 8 cm) Ni NTA agrose (Quiagen) resin pre-equilibrated with 50 mM Tris pH 8.0, 300 mM NaCl, 1 mM DTT and 20% glycerol. The column is washed with the buffer until the UV reaches baseline. The concentration of imidazole is then increased to 200 mM to remove the protease from the column. Fractions are collected (~20 to 30 mg) and

concentrated with an Amicon filtration apparatus with Millipore Ultrafiltration Membranes 30,000 molecular weight cut off. The protein solution is then dialyzed for 2 hrs in 50 mM Tris pH 7.5, 1 mM DTT and 30 % glycerol. The protein solution is loaded on a 220 ml (2.5 cm X 45 cm) Sepharose CL-6B (Amersham) column in 5 ml aliquots and washed with 20 mM Tris pH 7.5, 1 mM DTT, 15% glycerol. The gel filtration column was repacked at the beginning of each purification (every other run) in order to maintain resolution between the peaks. The fractions are collected and concentrated to ~5 mg/ml with a yield of ~15 to 20 mg total protein (ε=1.16 ml mg^{-1} cm^{-1} ± 0.02 wild type NAD synthetase^{TB} and ε=1.02 ml mg^{-1} cm^{-1} NAD synthetase^{TM}) (Table 6.1). The protein was ~90% pure (Figure 6.1). The extinction coefficient for wild type NAD synthetase^{TB} was obtained through amino acid analysis performed by University of California (Davis) Molecular Structure Faculty and the extinction coefficient for NAD synthetase^{TM} was calculated using the ExPASy ProtParam Tool.

Table 6.1 The purification yields of the wild type and mutant NAD synthetase^{TB} and NAD synthetase^{TM}.

Enzyme	Purification Yield
NAD synthetase^{TB}	4 mg enzyme /g cells
NAD synthetase^{TM}	3 mg enzyme /g cells
Y58A NAD synthetase^{TB}	1.42 mg enzyme /g cells
L486A NAD synthetase^{TB}	2 mg enzyme /g cells
L486F NAD synthetase^{TB}	1.9 mg enzyme /g cells
R658L NAD synthetase^{TB}	1.5 mg enzyme /g cells
D656A NAD synthetase^{TB}	1.4 mg enzyme /g cells

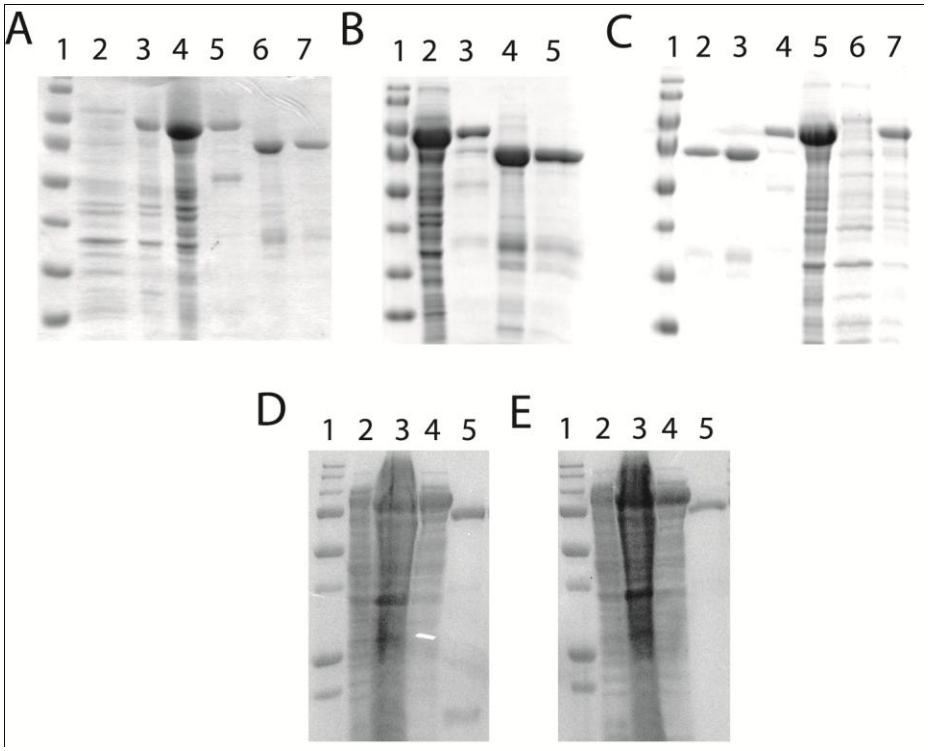

Figure 6.1 The protein gels of the mutants of NAD synthetase^{TB}. A. The protein gel of Y58A, Lane 1 is the ladder, Lane 2 the cells before induction, Lane 3 the cells after induction, Lane 4 the cells after lysis, Lane 5 the protein after the first nickel column, Lane 6 the protein after proteolysis, Lane 7 the purified protein. B. The protein gel of L486F, Lane 1 is the ladder, Lane 2 the cells after lysis, Lane 3 the protein after the first nickel column, Lane 4 the protein after the proteolysis, Lane 5 the purified protein. C. The protein gel of L486A, Lane 1 is the ladder, Lane 2 the purified proteins, Lane 3 the protein after the proteolysis, Lane 4 the protein after the first nickel column, Lane 5 the cells after lysis, Lane 6 the cells before induction, Lane 7 the cells after induction. D. The protein gel of R658L, Lane 1 is the ladder, Lane 2 the cells before induction, Lane 3 the cells after induction, Lane 4 the cells after lysis, Lane 5 the purified protein. E. The protein gel of D656A, Lane 1 is the

ladder, Lane 2 the cells before induction, Lane 3 the cells after induction, Lane 4 the cells after lysis, Lane 5 the purified protein.

The MALDI-TOF spectrum of the wild type NAD synthetase^{TB} (Figure 6.1) was obtained on a Shimadzu-Kratos Axima-CFR MALDI-TOF mass spectrometer (University of Maryland, College Park) in positive-ion mode in the presence of 3,5-dimethoxy-4-hydroxycinnaminic acid, resulting in a mass of 74,786 ±142 Da (expected 74,787 Da). The molecular mass of wild type NAD synthetase^{TB} was estimated at 4 ºC by gel-filtration chromatography on a Sepharose CL 6B column prequilibrated in 50 mM Tris, pH 7.5, 0.1 M NaCl and calibrated with High Molecular Weight Protein Standards (Amersham Biosciences). The successful full incorporation of SeMet in the protein was determined by MALDI analysis by the School of Pharmacy Mass Spectrometry Facility, University of Maryland, Baltimore (Figure 6.2). The UV CD spectra of C176A, D656A, L486A, L486F and wild type NAD synthetase^{TB} was acquired from a range of 300 nm to 185 nm at 37 ºC on a Jasco J-810 spectrometer. Protein samples were exchanged into 20 mM Na_2HPO_4/NaH_2PO_4, pH 8.5, using a G-50 spin column. The A_{280} of all the samples was 0.4.

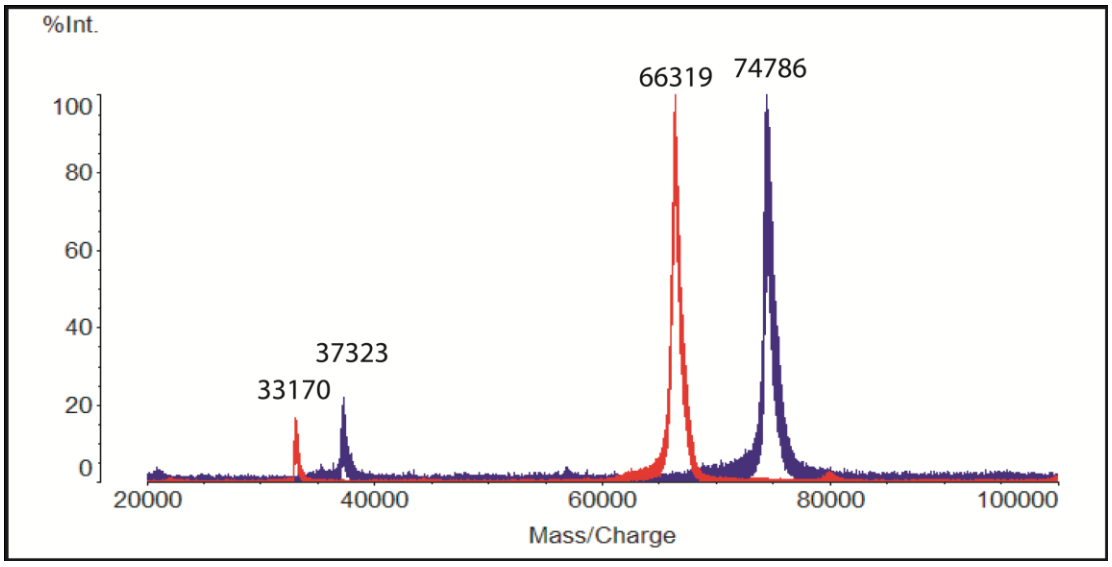

Figure 6.2. The MALDI-TOF spectrum of NAD synthetase^{TB}. The spectrum shows the molecular weight of NAD synthetase^{TB} at 74786 Da and the standard bovine serum albumin with a molecular weight of 66319 Da (expected 66382 Da).

6.4 Protein Crystallization

Before crystallization, protein samples were thawed and concentrated to 10–15 mg ml^{-1} using an Amicon Ultra 30 K centrifugal filter device (Millipore). DON-modified NAD synthetase^{TM} was co-crystallized in the presence of 2 mM DON and 3 mM NaAD at pH 8.5. Two screening conditions were tested with the sitting drop vapor diffusion method (Index and Cryo Suite). Initial screening for crystallization were carried out using a Phoenix Liquid Handling System for Crystallography (Art Robbins Instruments) with the sitting drop vapor diffusion method in 96-well microtiter plates. The sitting drop vapor diffusion method involves two drops and 90 ml of reservoir volume. One drop contained 0.4 ml of protein solution and 0.4 ml of mother liquor, whereas the other contained the same volume of protein solution and

0.2 ml of mother liquor. Crystallization plates were incubated at 20 ºC. Several conditions yielded crystals and optimization is ongoing.

6.5 NAD synthetase Activity Assays

All activity assays were end-point assays, except where noted and run at 37 ºC in 50 mM Tris, pH 8.3, 10 mM $MgCl_2$, 1 mM DTT and 0.3 mg/mL BSA at constant ionic strength (adjusted with KCl). Control reactions without the enzyme were run in parallel. The pH values of the buffers were measured at the temperature of the assays. NAD synthetase was incubated at 37 ºC for 30 mins prior to reaction initiation by the addition of substrates (incubated at 37 ºC for 10 mins). Aliquots of the NAD synthetase catalyzed reaction were removed at different times and quenched in ice with EDTA to a final concentration of 55 mM and then analyzed with one of the following assays.

NAD production. The resulting NAD is reduced to NADH by alcohol dehydrogenase in 84 mM Na_2HPO_4, pH 8.9, with 0.84% ethanol and 0.44% semicarbazide. NADH formation is measured at 340 nm (ε_{340} = 6.22 mM^{-1} cm^{-1}) after 45 minute of incubation at room temperature.

NAD formation can also be monitored by the cycling assay. The cycling assay was performed as follows: to 50 µl of the NAD synthetase reaction 100 µl of Solution 1 was added and incubated at 37°C for 10 mins. The reaction was initiated by the addition of 50 µl of Solution 2. Solution 1 contains 75 mM pipes pH 7.0, 100 mM lactate, 10 mM KCl and 1 mM WST-8. Solution 2 contains 50 mM pipes pH 7.0, 0.24 U/µl lactate dehydrogenase and 0.06 U/µl diaphorase. The reaction was incubated at 37°C for exactly 10 mins before the absorbance was taken at 450 nm. The reaction at

0 mins was used as a blank. NAD was quantified by comparison to a standard curve (Figure 6.3). The curve was constructed using solutions of NAD at 200, 100, 50 25 and 12.5 µM. This assay is only performed in the absence of DTT in the NAD synthetase reaction.

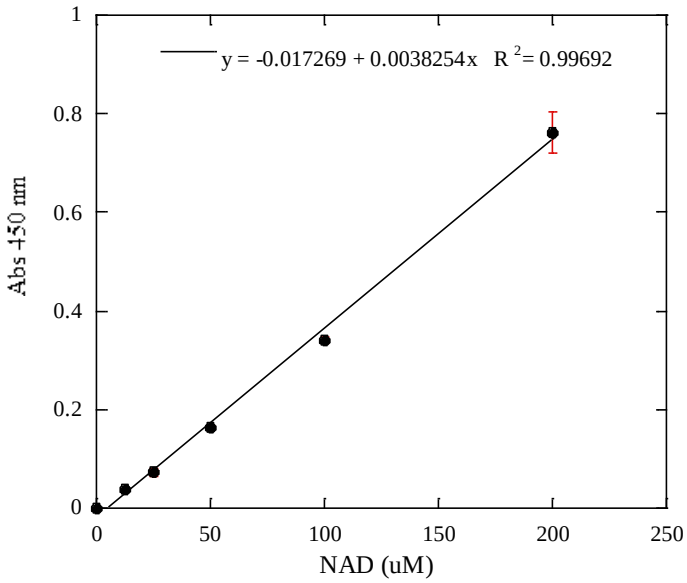

Figure 6.3 The calibration curve for the cycling assay. All reactions were performed in triplicate.

Glutamate production. Glutamate concentrations in the time aliquots were determined by measuring the absorbance at 340 nm upon reaction with glutamate dehydrogenase and by comparison to a standard curve (Figure 6.4). Reaction mixtures contained 1.5 mM NAD, 0.05 mM ADP, 0.57 M hydrazine in 50 mM Tris, pH 8.0. The reactions were incubated for 45 min at 22 ºC. The presence of the hydrazine causes the reactions to have a high background absorbance (~0.2 at 340 nm) and incubation of the reaction for more than the 1.5 hrs results in a significant increase in background (~0.5 at 340 nm).

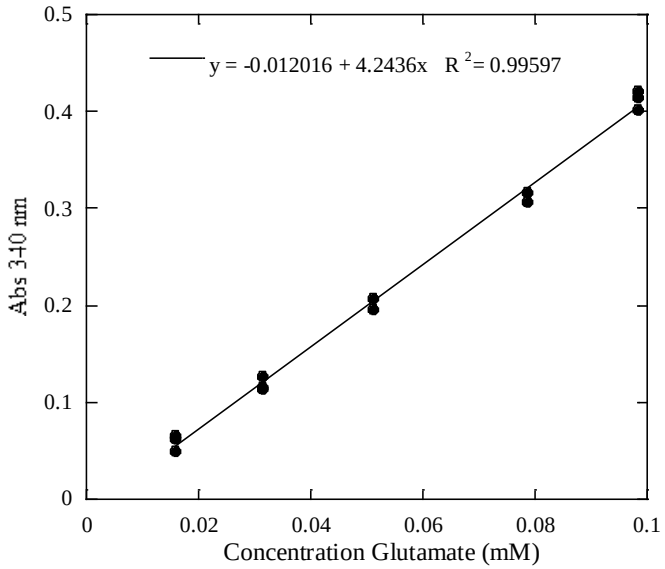

Figure 6.4 The calibration curve for the glutaminase assay. All reaction were performed in triplicate.

AMP production. Time aliquots from the NAD synthetase catalyzed reactions were analyzed on an ion-paired analytical Alltech Alltima C18 column (5 μm, 4.6 x 250 mm) preequilibrated in 100% solvent A (25 mM KH_2PO_4, pH 6.4, 4 mM tetrabutylammonium bromide, 5% methanol) at a flow rate of 1 mL/min. The various compounds, detected at 254 nm, were eluted with a linear gradient from 0-80% solvent B (25 mM KH_2PO_4, pH 6.4, 4 mM tetrabutylammonium bromide, 50% methanol) in 27 minutes and hold at 80% solvent B for 10 more minutes. Guanosine was used as an internal standard at a concentration of 0.01 mM. The retention times for NAD, AMP, NaAD, ATP and guanosine were 13.8 min, 19.5 min, 23.5 min, 28.6 min and 11 min, respectively. AMP concentration was quantified by comparison with a calibration curve (Figure 6.5). The calibration curve was obtained by plotting the ratio of the peak areas of the analyte (AMP or NAD) and of guanosine as a function

of the concentration of the analyte. This assay was used to determine the inhibition plots of NADH and to determine AMP formation in the stoichiometry analysis. A second HPLC method uses Zorbax Bonus RP C18 column (5 µm, 4.6 x 250 mm) preequilibrated in 98% solvent A (100 mM KH_2PO_4, pH 7.5) at a flow rate of 1 mL/min. The various compounds, detected at 254 nm, were eluted with a linear gradient from 2-10% solvent B (100 mM KH_2PO_4, pH 7.5, 20% methanol) in 30 minutes and hold at 10% solvent B for 10 more minutes. The retention times for NAD, AMP, NaAD and ATP were 14.9 min, 5.6 min, 10.8 min and 5.4 min, respectively.

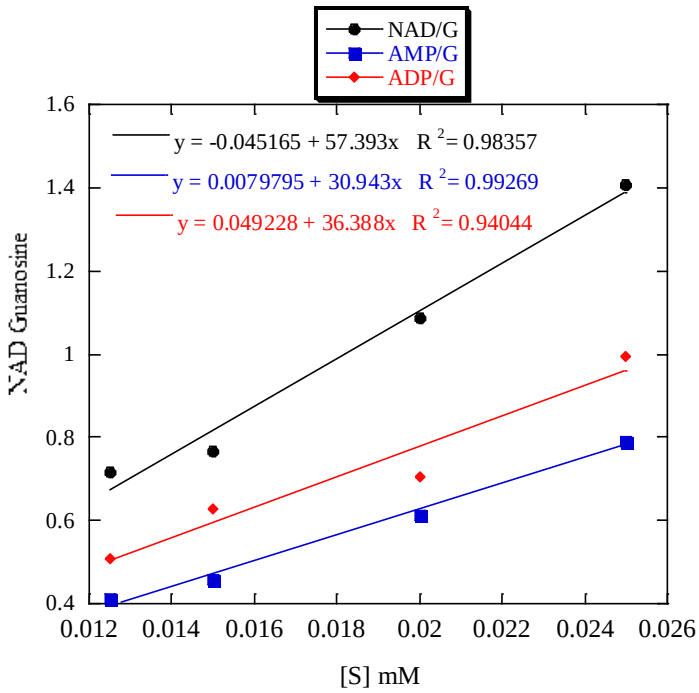

Figure 6.5 The calibration curve for the ion paired HPLC assay monitoring ADP, AMP and NAD formation. Guanosine is used as an internal standard. Each calibration curve was performed once.

Pyrophosphate/Inorganic Phosphate Assay. After quenching the NAD synthetase reaction 8 U/ µl inorganic pyrophosphatase is added. The malachite green assay is then performed on the quenched reaction with and without inorganic pyrophosphatase addition. The malachite green solution contained 0.12 % malachite green in 2 M H_2SO_4. The solution is stored in the dark. On the day of use 1 part 7.5% ammonium molybdate is added to 5 parts malachite green. Then 5 parts NAD synthetase reaction is added to 1 part malachite green/ ammonium molybdate solution. The solution is incubated at room temperature for 10 mins then the absorbance at 630 measured. The calibration curve was prepared with 0 to 20 µM potassium phosphate.

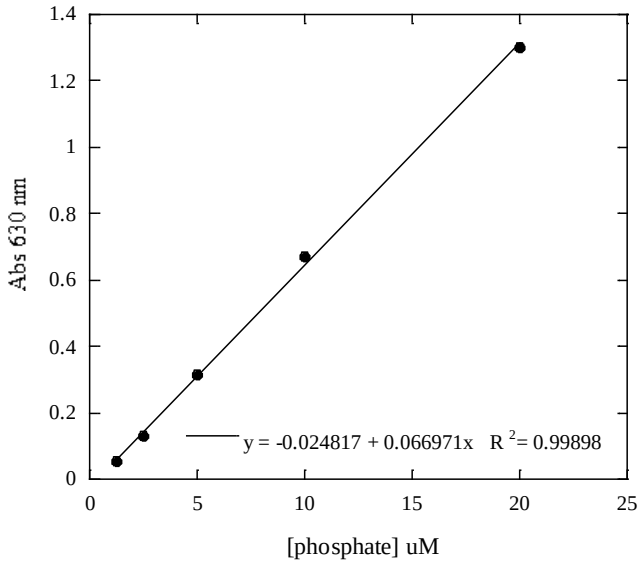

Figure 6.6 The calibration curve for the malachite green assay. All reaction performed in triplicate.

The phosphate sensor assay was performed on a Perkin Elmer LS55 Luminescence Spectrophotometer with a plate reader. The excitation wavelength was 430 nm and the emission wavelength was 450 and 480 nm. The total assay volume

was 200 µl with 40 µl of phosphate sensor (2.5 µM total concentration). The phosphate standards concentrations ranged from 0 to 1 µM.

6.6 Calculation for Assay Detection Limits

The detection limit of the alcohol dehydrogenase, NAD cycling and glutamate dehydrogenase assays were calculated from a theoretical volume of the NAD synthetase reaction of 600 µl total reaction using the maximum possible amount of enzyme, 350 µl NAD synthetase at 10 mg/ml concentration. The minimum absorbance that would be considered above background for each assay is 0.06 in a 10 min reaction. 1) The absorbance of 0.06 is used to calculate the moles of product utilizing an extinction coefficient or the equation of a calibration curve. 2) The slope is obtained for the moles product produced over 10 mins. 3) The slope is then multiplied by the dilution factor of the theoretical NAD synthetase reaction (1.7) and the dilution factor of the particular coupling assay, the U/ml is obtained. 4) The specific activity (U/mg) is then obtained by diving by the concentration of the enzyme (10 mg/ml). 5) The turnover per min is obtained by multiplying the specific activity by the enzyme molecular weight divided by 1000. 6) The turnover per sec is obtained by dividing by 60 sec/min. The sample calculation for the glutamine dehydrogenase assay is shown below:

1) Obtain mmoles glutamate from calibration curve equation (y= -0.012016 + 4.2436x).

(0.06-0.012016)/4.2436 = 0.011307 mmols glu/

2) Obtain slope of mmoles glutamate over 10 mins.

0.011307 mmoles glu/10 mins = 0.0011307 mM /min

3) Obtain the activity (U/ml) by multiplying by the dilution factors (2.68 for glutamine dyhydrogenase assay and 1.7 for NAD synthetase reaction).

0.0011307 mM/min*2.68*1.7 = 0.005152 U/ml

4) Obtain the specific activity (U/mg) by dividing by the enzyme concentration (10 mg/ml)

0.005152 U/ml /10 mg/ml = 0.000515 U/mg

5) Obtain the turnover (min^{-1}) by multiplying by the molecular weight of the enzyme.

0.000515 U/mg*74.6825 mg/mmole = 0.038474 min^{-1}

6) Obtain the turnover (sec^{-1}) by dividing by 60 sec/min.

0.038474 min^{-1} /60 sec/min = 0.00064 sec^{-1}

6.7 Initial Velocity Studies

The ionic strengths of the glutamine-dependent and ammonia-dependent reactions were kept constant with KCl at 0.012 M and 0.1 M (calculated without including the $MgCl_2$ concentration that is kept constant in all assays), respectively. Initial velocities were measured using the NAD and/or glutamate assays as specified. All reactions were performed in triplicate. ATP, NaAD, glutamine and ammonia concentrations were, respectively, 4 mM, 3 mM, 20 mM and 100 mM when held constant for wild type NAD synthetase^{TB}, L486A, L486F, C176A variants and NAD synthetase^{TM} catalyzed reactions. In the reaction catalyzed by D656A ATP and NaAD concentrations were 8 mM and 6 mM, respectively, when held constant. The concentrations for ATP, NaAD, and glutamine when varied in the wild type NAD synthetase^{TB}, L486A, L486F variants and NAD synthetase^{TM} glutamine-dependent reactions were 0.05-4 mM, 0.02-3 mM and 0.5-30 mM, respectively. The

concentration of glutamine when varied in the D656A glutamine-dependent reactions was 0-50 mM. The concentrations for ATP, NaAD, and NH_4Cl when varied in the wild type NAD synthetase^{TB}, L486A, L486F, C176A variants and NAD synthetase^{TM} ammonia dependent reactions were 0.5-5 mM, 0.1-6 mM and 1-100 mM, respectively. The concentration of NH_4Cl when varied in the D656A ammonia-dependent reactions was 0-1 mM NH_4Cl. The ionic strength of the ammonia dependent reactions were all adjusted to 0.1 M with KCl. Five different concentrations for the varied substrate were chosen in the specified range. All reactions were run in triplicate.

6.8 Temperature Dependent Studies

The temperature dependence assays for NAD synthetase^{TM} were performed at temperatures between 20 °C and 90 °C. The assay was performed under the same conditions as the specific activity assay in the presence of either 20 mM glutamine or 100 mM ammonia. Controls were performed to ensure no degradation of the substrates due to high temperatures. A solution of 4 mM ATP and 3 mM NaAD at pH 8.3 was incubated at 90 °C for 45min and analyzed before and after incubation by ion-paired HPLC.

6.9 Inhibition Studies

The NAD activity assay was used in these experiments for AMPCPP and the ion-paired HPLC assay was used for NADH. Inhibition experiments were carried out in a reaction with two of the three substrates at saturating conditions and with varying the concentration of the third substrate with several fixed inhibitor concentrations. All

reactions were performed in triplicate. ATP, NaAD and glutamine concentrations when held constant were at 4 mM, 3 mM and 20 mM, respectively. The concentrations of ATP and NaAD were varied from 0.05 to 4 mM and from 0.02 to 3 mM, respectively. The concentrations of AMPCPP and NADH were varied from 0 mM to 2 mM, and from 0 to 1.5 mM (vs. ATP) and from 0 to 0.5 mM (vs. NaAD), respectively. The concentration of acetyl-NAD was varied from 0 mM to 2 mM (vs. NaAD).

6.10 Binding Studies

Fluorescent titration experiments were performed on a F-4500 Fluorescence Spectrophotometer (Hitachi). For the intrinsic fluorescence experiments solutions of 0.5 µM enzyme or 1 µM DON modified enzyme, 50 mM tris pH 8.5, 10 mM $MgCl_2$ and 1 mM DTT were placed in a 1 cm pathlength cuvette. Ligand was then titrated into the cuvette. The excitation wavelength was 295 nm and the emission spectrum monitored from 200 to 400 nm. The excitation and emission slit width was 5 nm. The fluorescence at the maximum emission wavelength of 337 nm would be plotted verses ligand concentration to construct the binding curve. As a control ligand was titrated into solution without enzyme to ensure no fluorescence. The concentration of the ligands titrated into the solution is as follows 0 to 10 mM ATP, 0 to 50 mM ornithine, 0 to 6 mM NaAD and 0 to 30 mM Gln (Figure 2.12). The ligands were titrated in to the solution over a period of 30 mins at room temperature. Due to the slow basal glutaminase activity at 37 ºC under the conditions of the experiment the hydrolysis of glutamine would be negligible. To ensure no reaction the fluorescence of enzyme and 30 mM Gln was monitored over the course of 30 mins, no change in

fluorescence was observed. For the NADH fluorescence experiment a solution of 6 µM enzyme in 50 mM Tris pH 8.5, 1 mM DTT and 10 mM $MgCl_2$ was titrated with NADH (0 to 3 mM). A control without enzyme was also titrated with NADH (Figure 2.13). The excitation wavelength was 340 nm. The emission spectrum was monitored from 300 to 550 nm. The excitation and emission slit width was 5 nm. The difference in fluorescence (enzyme solution – control solution) at the maximum emission wavelength of 470 nm would be plotted versus ligand concentration to construct the binding curve.

Isothermal titration calorimetry was performed on a VP-ITC Microcalorimeter (MicroCal). The sample consists of 50 mM Tris pH 8.3 (at 37 °C), 10 mM $MgCl_2$, 1 mM DTT, 20 mM Gln and 1.7 µM enzyme previously dialyzed into 50 mM Tris pH 8.3 and 1 mM DTT. As a control ATP and NaAD were titrated into sample without enzyme. The concentrations of ATP and NaAD are 0.04 mM to 1 mM., in the same buffer as the enzyme, titrated into the enzyme solution in 10 µl aliquots over 30 injections while stirring. Data is collected for 200 sec with a 400 sec delay. Under the conditions of the experiment the enzyme precipitated possibly due to the removal of glycerol.

6.11 Steady-State Kinetic Analysis

All data were fitted using the Enzymes Kinetics software package (Systat). Initial velocity and competitive inhibition patterns were fitted to eqs. 1 and 2 respectively.

$$v/[E_o] = k_{cat}S/[K_M + S]$$

Equation 6.1

$$v/[E_o] = k_{cat}S/[K_M (1 + I/K_i) + S]$$

Equation 6.2

6.12 Stoichiometry Analysis

Reactions were run at 37 ºC in 50 mM Tris, pH 8.3, 10 mM $MgCl_2$, 1 mM DTT, 0.3 mg/mL BSA at constant ionic strength (0.012 M). The concentration of NAD synthetase was 0.23 μM. ATP and NaAD concentrations were 4 mM and 3 mM, respectively. Stoichiometry analysis was performed on three different reactions with 1.5 mM, 5 mM and 20 mM glutamine. The formation of NAD, glutamate and AMP was quantified as described above. The channel efficiency is calculated from the ratio of the amount of NAD to glutamate formed (Equation 1.1).

6.13 Glutaminase Effectors

The glutamate assay with 20 mM L-glutamine was used to determine the activation effect of dead-end inhibitors and synthetase substrate on the glutaminase domain. The assay was performed in 50 mM Tris pH 8.3, 10 mM $MgCl_2$, 1 mM DTT at 37 ºC. When present, the concentrations of ATP, NaAD, AMPCPP, NAD, Acetyl-NAD, PPi, AMP and intermediate analog 1 were 4 mM, 3 mM, 10 mM, 6 mM, 6 mM, 2.5 mM, 4 mM and 5 mM respectively.

6.14 DON Progress Curve

Progress curves for DON inactivation reactions were generated using the alcohol dehydrogenase assay continuously coupled to the NAD synthetase^{TB} reaction. We were able to run this assay continuously under saturating concentration of these two synthetase substrates because, even though NADH is an inhibitor, it was found to be a competitive inhibitor against both ATP and NaAD. The alcohol dehydrogenase

assay was performed continuously in 50 mM Tris, pH 8.3, at 37 °C with 4 mM ATP, 3 mM NaAD, 20 mM glutamine, 10 mM MgCl2, 0.8 % (v/v) ethanol, 0.44 % (w/v) semicarbazide, 1 mM DTT, alcohol dehydrogenase and 0-5 mM DON. After incubating at 37°C for 30 minutes the solution was initiated with 0.65 μM NAD synthetase and followed at 340 nm. Progress curves were fitted to eq. 6.3. The k_{obs} values obtained were plotted versus the concentrations of DON and fitted to eq. 6.4 to obtain k_{inact}, maximal rate of inactivation, and $K_{i\ app}$, the apparent inhibition constant.

$$[P] = [P]_{\infty} (1\text{-}e^{(\text{-}kt)})$$

Equation 6.3

$$k = k_{inact}\,[I]/\,K_I\,(1 + [S]/K_m + [I]/K_I)$$

Equation 6.4

6.15 Inactivation by DON

The inactivation reaction consisted of 4 mM ATP, 3 mM NaAD, 10 mM $MgCl_2$, 1 mM DTT, 20 mM DON and NAD synthetase^{TB}. After the reaction was incubated at 37°C in 50 mM Tris pH 8.3, for 1.5 hrs, small ligands were removed by using Sepharose G-50 (Sigma) spin column. Lack of glutaminase activity in the presence of the synthetase substrates confirmed the complete inactivation of the enzyme. The enzyme thus modified was tested for its ability to catalyze the ammonia-dependent formation of NAD in the presence of 100 mM ammonia, 3 mM NaAD and 4 mM ATP/Mg^{2+}. This inactivated enzyme was also used for structural determination.

6.16 Phylogenetic analysis

ClustalW was used to align the whole amino acid sequences of 37 glutamine-dependent NAD synthetases from different organisms obtained from NCBI. The sequence of the *T. thermophilus* used included both the glutaminase and the synthetase subunits. The sequence alignment was manually edited with SEAVIEW. A phylogenetic tree was constructed using the maximum likelihood method in PHYML. Bootstrapping was achieved by constructing 100 trees. The tree was visualized using Phylodendron v0.8 (© 1997 by D.G. Gilbert).

A list of ammonia and glutamine dependent NAD synthetases was provided by Andrei Osterman. The 37 genes used for the phylogenetic analysis were chosen out of 337 glutamine dependent enzymes which represented organisms from different species of bacteria and eukarya. The genes use to construct the tree are as follows: *Anopheles gambiae*, XP_311035.1; *Apis mellifera*, XP_392994.1; *Aquifex aeolicus* VF5, NP_213654.1; *Arabidopsis thaliana*, NP_175906.1; *Atopobium rimae* ATCC 49626, ZP_03568401.1; *Azotobacter vinelandii* DJ, YP_002798395.1; *Akkermansia muciniphila* ATCC BAA-835, ACD04457.1; *Caenorhabditis elegans*, NP_501866.1; *Clostridium acetobutylicum* ATCC 824, NP_348407.1; *Clostridium cellulolyticum* H10, YP_002505537.1; *Dehalococcoides ethenogenes*, YP_181837.1; *Drosophila melanogaster*, NP_572913.1; *Eubacterium siraeum* DSM 15702, ZP_02423806.1; *Fervidobacterium nodosum* Rt17-B1, YP_001410277.1; *Gallus gallus*, NP_001006465.1; *Gluconacetobacter diazotrophicus* PAl 5, YP_001601200.1; *Herpetosiphon aurantiacus* ATCC 23779, YP_001547049.1; *Homo sapiens*, BAA91722.1; *Methanosaeta thermophila* PT, YP_843157.1; *Methylobacterium*

chloromethanicum CM4, YP_002423109.1; *Mus musculus*, NP_084497.1; *Mycobacterium bovis* AF2122/97, NP_856111.1; *Mycobacterium leprae* TN, NP_302028.1; *Mycobacterium tuberculosis* C, YP_002079654.1; *Thermotoga maritima* MSB8, NP_229058.1; *Ralstonia eutropha* H16, YP_725265.1; *Rhodobacter capsulatus*, Q03638.1; *Rattus norvegicus*, BAC57897.1; *Saccharomyces cerevisiae*, NP_011941.1; *Sulfurihydrogenibium sp*. YO3AOP1, YP_001930207.1; *Sulfurovum sp.* NBC37-1, YP_001359756.1; *Synechococcus elongatus* PCC 6301, YP_654197.1; *Synechocystis sp.* PCC 6803, YP_680420.1; *Thermodesulfovibrio yellowstonii* DSM 11347, YP_002249082.1; *Thermosipho africanus* TCF52B, YP_002335497.1; *Thermotoga neapolitana* DSM 4359, YP_002534863.1; *Thermus thermophilus* HB8, YP_145167.1, YP_005507.1.

Bibliography

(1) Nagradova, N. (2003) Interdomain communications in bifunctional enzymes: How are different activities coordinated? *Iubmb Life 55*, 459-466.

(2) Dunn, M. F., Niks, D., Ngo, H., Barends, T. R. M., and Schlichting, I. (2008) Tryptophan synthase: the workings of a channeling nanomachine. *Trends In Biochemical Sciences 33*, 254-264.

(3) van den Heuvel, R. H. H., Curti, B., Vanoni, M. A., and Mattevi, A. (2004) Glutamate synthase: a fascinating pathway from L-glutamine to L-glutamate. *Cellular and Molecular Life Sciences 61*, 669-681.

(4) Lunn, F. A., and Bearne, S. L. (2004) Alternative substrates for wild-type and L109A E-coli CTP synthases - Kinetic evidence for a constricted ammonia tunnel. *European Journal of Biochemistry 271*, 4204-4212.

(5) Bieganowski, P., Pace, H. C., and Brenner, C. (2003) Eukaryotic NAD^+ synthetase Qns1 contains an essential, obligate intramolecular thiol glutamine amidotransferase domain related to nitrilase. *Journal of Biological Chemistry 278*, 33049-33055.

(6) Okar, D. O., Manzano, A., Navarro-Sabate, A., Riera, L., Bartrons, R., and Lange, A. J. (2001) PFK-2/FBPase-2: maker and breaker of the essential biofactor fructose-2, 6-bisphosphate. *Trends in Biochemical Sciences 26*, 30-35.

(7) Zhang, W. L., Fisher, J. F., and Mobashery, S. (2009) The bifunctional enzymes of antibiotic resistance. *Current Opinion in Microbiology 12*, 505-511.

(8) Moore, B. D. (2004) Bifunctional and moonlighting enzymes: lighting the way to regulatory control. *Trends in Plant Science 9*, 221-228.

(9) Perham, R. N. (2000) Swinging arms and swinging domains in multifunctional enzymes: Catalytic machines for multistep reactions. *Annual Review of Biochemistry 69*, 961-1004.

(10) Raushel, F. M., Thoden, J. B., and Holden, H. M. (2003) Enzymes with molecular tunnels. *Accounts of Chemical Research 36*, 539-548.

(11) Hoskins, A. A., Anand, R., Ealick, S. E., and Stubbe, J. (2004) The formylglycinamide ribonucleotide amidotransferase complex from *Bacillus subtilis*: Metabolite-mediated complex formation. *Biochemistry 43*, 10314-10327.

(12) An, S. G., Kumar, R., Sheets, E. D., and Benkovic, S. J. (2008) Reversible compartmentalization of de novo purine biosynthetic complexes in living cells. *Science 320*, 103-106.

(13) Bulock, K. G., Beardsley, G. P., and Anderson, K. S. (2002) The kinetic mechanism of the human bifunctional enzyme ATIC (5-amino-4-imidazolecarboxamide ribonucleotide transformylase/inosine 5 '-monophosphate cyclohydrolase) - A surprising lack of substrate channeling. *Journal of Biological Chemistry 277*, 22168-22174.

(14) Huang, X. Y., Holden, H. M., and Raushel, F. M. (2001) Channeling of substrates and intermediates in enzyme-catalyzed reactions. *Annual Review of Biochemistry 70*, 149-180.

(15) Mouilleron, S., and Golinelli-Pimpaneau, B. (2007) Conformational changes in ammonia-channeling glutamine amidotransferases. *Current Opinion in Structural Biology 17*, 653-664.

(16) Thoden, J. B., Huang, X., Raushel, F. M., and Holden, H. M. (2002) Carbamoyl-phosphate synthetase. Creation of an escape route for ammonia. *Journal of Biological Chemistry 277*, 39722-7.

(17) Miles, B. W., and Raushel, F. M. (2000) Synchronization of the three reaction centers within carbamoyl phosphate synthetase. *Biochemistry 39*, 5051-5056.

(18) Hyde, C. C., Ahmed, S. A., Padlan, E. A., Miles, E. W., and Davies, D. R. (1988) 3-Dimensional structure of the tryptophan synthase α-2-β-2 multienzyme complex from *Salmonella-thyphimurium*. *Journal of Biological Chemistry 263*, 17857-17871.

(19) Huang, X. Y., and Raushel, F. M. (2000) An engineered blockage within the ammonia tunnel of carbamoyl phosphate synthetase prevents the use of glutamine as a substrate but not ammonia. *Biochemistry 39*, 3240-3247.

(20) Huang, X. Y., and Raushel, F. M. (2000) Restricted passage of reaction intermediates through the ammonia tunnel of carbamoyl phosphate synthetase. *Journal of Biological Chemistry 275*, 26233-26240.

(21) Mullins, L. S., and Raushel, F. M. (1999) Channeling of ammonia through the intermolecular tunnel contained within carbamoyl phosphate synthetase. *Journal of the American Chemical Society 121*, 3803-3804.

(22) Li, K. K., Beeson, W. T., Ghiviriga, I., and Richards, N. G. J. (2007) A convenient gHMQC-based NMR assay for investigating ammonia channeling in glutamine-dependent amidotransferases: Studies of Escherichia coli asparagine synthetase B. *Biochemistry 46*, 4840-4849.

(23) Barends, T. R. M., Dunn, M. F., and Schlichting, I. (2008) Tryptophan synthase, an allosteric molecular factory. *Current Opinion in Chemical Biology 12*, 593-600.

(24) Thoden, J. B., Holden, H. M., Wesenberg, G., Raushel, F. M., and Rayment, I. (1997) Structure of carbamoyl phosphate synthetase: A journey of 96 angstrom from substrate to product. *Biochemistry 36*, 6305-6316.

(25) Doukov, T. I., Blasiak, L. C., Seravalli, J., Ragsdale, S. W., and Drennan, C. L. (2008) Xenon in and at the end of the tunnel of bifunctional carbon monoxide dehydrogenase/acetyl-CoA synthase. *Biochemistry 47*, 3474-3483.

(26) Horiuchi, K. Y., Harpel, M. R., Shen, L., Luo, Y., Rogers, K. C., and Copeland, R. A. (2001) Mechanistic studies of reaction coupling in Glu-tRNA(Gln) amidotransferase. *Biochemistry 40*, 6450-6457.

(27) Larsen, T. M., Boehlein, S. K., Schuster, S. M., Richards, N. G. J., Thoden, J. B., Holden, H. M., and Rayment, I. (1999) Three-dimensional structure of *Escherichia coli* asparagine synthetase B: A short journey from substrate to product. *Biochemistry 38*, 16146-16157.

(28) Kim, J. H., Krahn, J. M., Tomchick, D. R., Smith, J. L., and Zalkin, H. (1996) Structure and function of the glutamine phosphoribosylpyrophosphate amidotransferase glutamine site and communication with the phosphoribosylpyrophosphate site. *Journal of Biological Chemistry 271*, 15549-15557.

(29) Binda, C., Bossi, R. T., Wakatsuki, S., Arzt, S., Coda, A., Curti, B., Vanoni, M. A., and Mattevi, A. (2000) Cross-talk and ammonia channeling between active centers in the unexpected domain arrangement of glutamate synthase. *Structure 8*, 1299-1308.

(30) Moser, J., Schubert, W. D., Beier, V., Bringemeier, I., Jahn, D., and Heinz, D. W. (2001) V-shaped structure of glutamyl-tRNA reductase, the first enzyme of tRNA-dependent tetrapyrrole biosynthesis. *Embo Journal 20*, 6583-6590.

(31) Liang, P. H., and Anderson, K. S. (1998) Substrate channeling and domain - Domain interactions in bifunctional thymidylate synthase - Dihydrofolate reductase. *Biochemistry 37*, 12195-12205.

(32) Krahn, J. M., Kim, J. H., Burns, M. R., Parry, R. J., Zalkin, H., and Smith, J. L. (1997) Coupled formation of an amidotransferase interdomain ammonia channel and a phosphoribosyltransferase active site. *Biochemistry 36*, 11061-11068.

(33) Tesmer, J. G., Klem, T. J., Deras, M. L., Davisson, V. J., and Smith, J. L. (1996) The crystal structure of GMP synthetase reveals a novel catalytic triad and is a structural paradigm for two enzyme families. *Nature Structural Biology 3*, 74-86.

(34) Zalkin, H., and Smith, J. L. (1998) Enzymes utilizing glutamine as an amide donor. *Advances in Enzymology Related Areas of Molecular Biology 72*, 87-144.

(35) Fan, Y., Lund, L., Yang, L. J., Raushel, F. M., and Gao, Y. Q. (2008) Mechanism for the transport of ammonia within carbamoyl phosphate synthetase determined by molecular dynamics simulations. *Biochemistry 47*, 2935-2944.

(36) Fan, Y. B., Lund, L., Shao, Q., Gao, Y. Q., and Raushel, F. M. (2009) A combined theoretical and experimental study of the ammonia tunnel in carbamoyl phosphate synthetase. *Journal of the American Chemical Society 131*, 10211-10219.

(37) Floquet, N., Mouilleron, S., Daher, R., Maigret, B., Badet, B., and Badet-Denisot, M. A. (2007) Ammonia channeling in bacterial glucosamine-6-phosphate synthase (Glms): Molecular dynamics simulations and kinetic studies of protein mutants. *FEBS Letters 581*, 2981-2987.

(38) Goodey, N. M., and Benkovic, S. J. (2008) Allosteric regulation and catalysis emerge via a common route. *Nature Chemical Biology 4*, 474-482.

(39) Ovadi, J. (1991) Physiological significance of metabolic channeling. *Journal of Theoretical Biology 152*, 1-22.

(40) van den Heuvel, R. H., Ferrari, D., Bossi, R. T., Ravasio, S., Curti, B., Vanoni, M. A., Florencio, F. J., and Mattevi, A. (2002) Structural studies on the synchronization of catalytic centers in glutamate synthase. *Journal of Biological Chemistry 277*, 24579-83.

(41) Raushel, F. M., Thoden, J. B., Reinhart, G. D., and Holden, H. M. (1998) Carbamoyl phosphate synthetase: a crooked path from substrates to products. *Current Opinion in Chemical Biology 2*, 624-632.

(42) Myers, R. S., Jensen, J. R., Deras, I. L., Smith, J. L., and Davisson, V. J. (2003) Substrate-induced changes in the ammonia channel for imidazole glycerol phosphate synthase. *Biochemistry 42,* 7013-7022.

(43) Ravasio, S., Dossena, L., Martin-Figueroa, E., Florencio, F. J., Mattevi, A., Morandi, P., Curti, B., and Vanoni, M. A. (2002) Properties of the recombinant ferredoxin-dependent glutamate synthase of *Synechocystis* PCC6803. comparison with the *Azospirillum brasilense* NADPH-dependent enzyme and its isolated alpha subunit. *Biochemistry 41*, 8120-8133.

(44) Durand, P., Golinelli-Pimpaneau, B., Mouilleron, S., Badet, B., and Badet-Denisot, M. A. (2008) Highlights of glucosamine-6P synthase catalysis. *Archives of Biochemistry and Biophysics 474*, 302-317.

(45) Mouilleron, S., Badet-Denisot, M. A., and Golinelli-Pimpaneau, B. (2008) Ordering of C-terminal loop and glutaminase domains of glucosamine-6-phosphate synthase promotes sugar ring opening and formation of the ammonia channel. *Journal of Molecular Biology 377*, 1174-1185.

(46) Schmitt, E., Panvert, M., Blanquet, S., and Mechulam, Y. (2005) Structural basis for tRNA-dependent amidotransferase function. *Structure 13*, 1421-1433.

(47) Tesson, A. R., Soper, T. S, Ciustea, and Richards, N. G. J. (2003) Revisiting the steady state kinetic mechanism of glutamine-dependent asparagine

synthetase from *Escherichia coli*. *Archives of Biochemistry and Biophysics 413*, 23-31.

(48) Rizzi, M., Nessi, C., Bolognesi, M., Coda, A., and Galizzi, A. (1996) Crystallization of NAD^+ synthetase from *Bacillus subtilis*. *Proteins-Structure Function and Genetics 26*, 236-238.

(49) Cantoni, R., Branzoni, M., Labo, M., Rizzi, M., and Riccardi, G. (1998) The MTCY428.08 gene of *Mycobacterium tuberculosis* codes for NAD^+ synthetase. *Journal of Bacteriology 180*, 3218-3221.

(50) Rizzi, M., Nessi, C., Mattevi, A., Coda, A., Bolognesi, M., and Galizzi, A. (1996) Crystal structure of NH_3-dependent NAD^+ synthetase from *Bacillus subtilis. Embo Journal 15*, 5125-5134.

(51) Preiss, J., and Handler, P. (1958) Biosynthesis of diphosphopyridine nucleotide.2. Enzymatic aspects. *Journal of Biological Chemistry 233*, 493-500.

(52) Devedjiev, Y., Symersky, J., Singh, R., Jedrzejas, M., Brouillette, C., Brouillette, W., Muccio, D., Chattopadhyay, D., and DeLucas, L. (2001) Stabilization of active-site loops in NH_3-dependent NAD^+ synthetase from *Bacillus subtilis. Acta Crystallographica Section D-Biological Crystallography 57*, 806-812.

(53) Kang, G. B., Kim, Y. S., Im, Y. J., Rho, S. H., Lee, J. H., and Eom, S. H. (2005) Crystal structure of NH_3-dependent NAD^+ synthetase from *Helicobacter pylori*. *Proteins-Structure Function and Bioinformatics 58*, 985-988.

(54) Jauch, R., Humm, A., Huber, R., and Wahl, M. C. (2005) Structures of *Escherichia coli* NAD synthetase with substrates and products reveal mechanistic rearrangements. *Journal of Biological Chemistry 280*, 15131-15140.

(55) McDonald, H. M., Pruett, P. S., Deivanayagam, C., Protasevich, II, Carson, W. M., DeLucas, L. J., Brouillette, W. J., and Brouillette, C. G. (2007) Structural adaptation of an interacting non-native C-terminal helical extension revealed in the crystal structure of NAD^+ synthetase from *Bacillus anthracis*. *Acta Crystallographica Section D-Biological Crystallography 63*, 891-905.

(56) Rizzi, M., Bolognesi, M., and Coda, A. (1998) A novel deamido-NAD^+-binding site revealed by the trapped NAD-adenylate intermediate in the NAD^+ synthetase structure. *Structure 6*, 1129-40.

(57) Symersky, J., Devedjiev, Y., Moore, K., Brouillette, C., and DeLucas, L. (2002) NH_3-dependent NAD^+ synthetase from *Bacillus subtilis* at 1 angstrom resolution. *Acta Crystallographica Section D-Biological Crystallography 58*, 1138-1146.

(58) Pace, H. C., and Brenner, C. (2001) The nitrilase superfamily: classification, structure and function. *Genome Biology 2*, reviews0001.1- 0001.9.

(59) Brenner, C. (2002) Catalysis in the nitrilase superfamily. *Current Opinion in Structural Biology 12*, 775-782.

(60) Spencer, R. L., and Preiss, J. (1967) Biosynthesis of diphosphopyridine nucleotide - purification and properties of diphosphopyridine nucleotide

synthetase from *Escherichia Coli* B. *Journal of Biological Chemistry 242*, 385-392.

(61) Nessi, C., Albertini, A. M., Speranza, M. L., and Galizzi, A. (1995) The outB gene of *Bacillus subtilis* codes for NAD synthetase. *Journal of Biolological Chemistry 270*, 6181-5.

(62) Schneider, B. L., and Reitzer, L. J. (1998) *Salmonella typhimurium* nit is nadE: Defective nitrogen utilization and ammonia-dependent NAD synthetase. *Journal of Bacteriology 180*, 4739-4741.

(63) Yamaguchi, F., Koga, S., Yoshioka, I., Takahashi, M., Sakuraba, H., and Ohshima, T. (2002) Stable ammonia-specific NAD synthetase from *Bacillus stearothermophilus*: Purification, characterization, gene cloning, and applications. *Bioscience Biotechnology and Biochemistry 66*, 2052-2059.

(64) Sutherland, S. (2003) New antibiotics for anthrax? *Drug Discovery Today 8*, 335-336.

(65) Jedrzejas, M. J. (2002) The structure and function of novel proteins of *Bacillus anthracis* and other spore-forming bacteria: Development of novel prophylactic and therapeutic agents. *Critical Reviews in Biochemistry and Molecular Biology 37*, 339-373.

(66) Khan, J. A., Forouhar, F., Tao, X., and Tong, L. (2007) Nicotinamide adenine dinucleotide metabolism as an attractive target for drug discovery. *Expert Opinion on Therapeutic Targets 11*, 695-705.

(67) Velu, S. E., Cristofoli, W. A., Garcia, G. J., Brouillette, C. G., Pierson, M. C., Luan, C. H., DeLucas, L. J., and Brouillette, W. J. (2003) Tethered dimers as

NAD synthetase inhibitors with antibacterial activity. *Journal of Medicinal Chemistry 46*, 3371-81.

(68) Velu, S. E., Luan, C. H., Delucas, L. J., Brouillette, C. G., and Brouillette, W. J. (2005) Tethered dimer inhibitors of NAD synthetase: parallel synthesis of an aryl-substituted SAR library. *Jouranl of Combinatrial Chemistry 7*, 898-904.

(69) Tiruviluamala, P., and Reichman, L. B. (2002) Tuberculosis. *Annual Review of Public Health 23*, 403-426.

(70) Russell, D. G. (2001) Mycobacterium tuberculosis: Here today, and here tomorrow. *Nature Reviews Molecular Cell Biology 2*, 569-577.

(71) Clark-Curtiss, J. E., and Haydel, S. E. (2003) Molecular genetics of Mycobacterium tuberculosis pathogenesis. *Annual Review of Microbiology 57*, 517-549.

(72) Drevets, D. A., Leenen, P. J. M., and Greenfield, R. A. (2004) Invasion of the central nervous system by intracellular bacteria. *Clinical Microbiology Reviews 17*, 323-347.

(73) Comas, I., and Gagneux, S. (2009) The past and future of tuberculosis research. *Plos Pathogens 5*.

(74) Golden, M. P., and Vikram, H. R. (2005) Extrapulmonary tuberculosis: An overview. *American Family Physician 72*, 1761-1768.

(75) Barry, C. E., Boshoff, H. I., Dartois, V., Dick, T., Ehrt, S., Flynn, J., Schnappinger, D., Wilkinson, R. J., and Young, D. (2009) The spectrum of

latent tuberculosis: rethinking the biology and intervention strategies. *Nature Reviews Microbiology 7*, 845-855.

(76) Dorman, S. E., and Chaisson, R. E. (2007) From magic bullets back to the Magic Mountain: the rise of extensively drug-resistant tuberculosis. *Nature Medicine 13*, 295-298.

(77) Sefton, A. M. (2002) Mechanisms of antimicrobial resistance - Their clinical relevance in the new millennium. *Drugs 62*, 557-566.

(78) Fischbach, M. A., and Walsh, C. T. (2009) Antibiotics for Emerging Pathogens. *Science 325*, 1089-1093.

(79) Iseman, M. D. (1993) Treatment of multidrug-resistant tuberculosis. *New England Journal of Medicine 329*, 784 - 791.

(80) (July 4, 2007) in *http://www.cnn.com/2007/HEALTH/07/03/tb.speaker/index.html*, CNN.com.

(81) Hitti, M. (July 26, 2007) in *http://www.webmd.com/news/20070726/andrew-speaker-released-from-hospital*, WebMd.com.

(82) Denu, J. M. (2007) Vitamins and aging: Pathways to NAD^+ synthesis. *Cell 129*, 453-454.

(83) Noctor, G., Queval, G., and Gakiere, B. (2006) NAD(P) synthesis and pyridine nucleotide cycling in plants and their potential importance in stress conditions. *Journal of Experimental Botany 57*, 1603-1620.

(84) Lin, H. (2007) Nicotinamide adenine dinucleotide: beyond a redox coenzyme. *Organic & Biomolecular Chemistry 5*, 2541-2554.

(85) Magni, G., Amici, A., Emanuelli, M., Orsomando, G., Raffaelli, N., and Ruggieri, S. (2004) Enzymology of NAD plus homeostasis in man. *Cellular and Molecular Life Sciences 61*, 19-34.

(86) Lin, S. J., Defossez, P. A., and Guarente, L. (2000) Requirement of NAD and SIR2 for life-span extension by calorie restriction in *Saccharomyces cerevisiae. Science 289*, 2126-2128.

(87) Sauve, A. A., and Schramm, V. L. (2003) Sir2 regulation by nicotinamide results from switching between base exchange and deacetylation chemistry. *Biochemistry 42*, 9249-9256.

(88) Belenky, P., Racette, F. G., Bogan, K. L., McClure, J. M., Smith, J. S., and Brenner, C. (2007) Nicotinamide riboside promotes Sir2 silencing and extends lifespan via Nrk and Urh1/Pnp1/Meu1 pathways to NAD^+. *Cell 129*, 473-484.

(89) Belenky, P., Bogan, K. L., and Brenner, C. (2007) NAD^+ metabolism in health and disease. *Trends in Biochemical Science 32*, 12-9.

(90) Ziegler, M. (2000) New functions of a long-known molecule - Emerging roles of NAD in cellular signaling. *European Journal of Biochemistry 267*, 1550-1564.

(91) Diefenbach, J., and Burkle, A. (2005) Introduction to poly(ADP-ribose) metabolism. *Cellular and Molecular Life Sciences 62*, 721-730.

(92) Jacobson, E. L., Shieh, W. M., and Huang, A. C. (1999) Mapping the role of NAD metabolism in prevention and treatment of carcinogenesis. *Molecular and Cellular Biochemistry 193*, 69-74.

(93) Lee, H. C. (2005) Nicotinic acid adenine dinucleotide phosphate (NAADP)-mediated calcium signaling. *Journal of Biological Chemistry 280,* 33693-33696.

(94) Boshoff, H. I., Xu, X., Tahlan, K., Dowd, C. S., Pethe, K., Camacho, L. R., Park, T. H., Yun, C. S., Schnappinger, D., Ehrt, S., Williams, K. J., and Barry, C. E., 3rd. (2008) Biosynthesis and recycling of nicotinamide cofactors in mycobacterium tuberculosis. An essential role for NAD in nonreplicating bacilli. *Journal of Biological Chemistry 283,* 19329-41.

(95) Mattevi, A. (2006) A close look at NAD biosynthesis. *Nature Structural & Molecular Biology 13,* 563-564.

(96) Kurnasov, O., Goral, V., Colabroy, K., Gerdes, S., Anantha, S., Osterman, A., and Begley, T. P. (2003) NAD biosynthesis: Identification of the tryptophan to quinolinate pathway in bacteria. *Chemistry & Biology 10,* 1195-1204.

(97) Bieganowski, P., and Brenner, C. (2004) Discoveries of nicotinamide riboside as a nutrient and conserved NRK genes establish a Preiss-Handler independent route to NAD^+ in fungi and humans. *Cell 117*, 495-502.

(98) Tempel, W., Rabeh, W. M., Bogan, K. L., Belenky, P., Wojcik, M., Heather, F. S., Nedyalkova, L., Yang, T., Sauve, A. A., Park, H. W., and Brenner, C. (2007) Nicotinamide riboside kinase structures reveal new pathways to NAD. *Plos Biology 5*, 2220-2230.

(99) Bellinzoni, M., De Rossi, E., Branzoni, M., Milano, A., Peverali, F. A., Rizzi, M., and Riccardi, G. (2002) Heterologous expression, purification, and

enzymatic activity of *Mycobacterium tuberculosis* NAD^+ synthetase. *Protein Expression and Purification 25*, 547-557.

(100) Argos, P., Rossmann, M. G., Grau, U. M., Zuber, H., Frank, G., and Tratschin, J. D. (1979) Thermal-stability and protein-structure. *Biochemistry 18*, 5698-5703.

(101) Ruan, B., Fisher, K. E., Alexander, P. A., Doroshko, V., and Bryan, P. N. (2004) Engineering subtilisin into a fluoride-triggered processing protease useful for one-step protein purification. *Biochemistry 43*, 14539-14546.

(102) Kapust, R. B., and Waugh, D. S. (2000) Controlled intracellular processing of fusion proteins by TEV protease. *Protein Expression and Purification 19*, 312-318.

(103) Yu, C. K., and Dietrich, L. S. (1972) Purification and properties of yeast nicotinamide adenine-dinucleotide synthetase. *Journal of Biological Chemistry 247*, 4794-&.

(104) Mossessova, E., and Lima, C. D. (2000) Ulp1-SUMO crystal structure and genetic analysis reveal conserved interactions and a regulatory element essential for cell growth in yeast. *Molecular Cell 5*, 865-76.

(105) Rhodes, D. G., Bossio, R. E., and Laue, T. M. (2009) Determination of size, molecular weight, and presence of subunits, in *Guide to Protein Purification, Second Edition* pp 691-723.

(106) Howlett, G. J., Minton, A. P., and Rivas, G. (2006) Analytical ultracentrifugation for association and assembly the study of protein. *Current Opinion in Chemical Biology 10*, 430-436.

(107) Wen, J., Arakawa, T., and Philo, J. S. (1996) Size-exclusion chromatography with on-line light-scattering, absorbance, and refractive index detectors for studying proteins and their interactions. *Analytical Biochemistry 240*, 155-166.

(108) Racker, E. (1950) Crystalline alcohol dehydrogenase from bakers yeast. *Journal of Biological Chemistry 184*, 313-319.

(109) Ueshima, Y., Matsuda, Y., Wang, B. Y., Takase, S., and Takada, A. (1993) ethanol and acetaldehyde metabolism in cultured rat hepatocytes. *Alcohol and Alcoholism 28*, 3-10.

(110) Bembenek, M. E., Kuhn, E., Mallender, W. D., Pullen, L., Li, P., and Parsons, T. (2005) A fluorescence-based coupling reaction for monitoring the activity of recombinant human NAD synthetase. *Assay and Drug Development Technologies 3*, 533-541.

(111) Yamaguchi, F., Ohshima, T., and Sakuraba, H. (2007) An enzymatic cycling assay for nicotinic acid adenine dinucleotide phosphate using NAD synthetase. *Analytical Biochemistry 364*, 97-103.

(112) Bergmeyer, H. U. (1983) Methods of Enzymatic Analysis, 3rd Ed. pp 216-219.

(113) Baykov, A. A., Evtushenko, O. A., and Avaeva, S. M. (1988) A malachite green procedure for ortho-phosphate determination and its use in alkaline phosphatase-based enzyme-immunoassay. *Analytical Biochemistry 171*, 266-270.

(114) Josse, J. (1966) Constitutive inorganic pyrophosphatase of *Escherichia coli*.I. Purification and catalytic properties. *Journal of Biological Chemistry 241*, 1938-&.

(115) Brune, M., Hunter, J. L., Howell, S. A., Martin, S. R., Hazlett, T. L., Corrie, J. E. T., and Webb, M. R. (1998) Mechanism of inorganic phosphate interaction with phosphate binding protein from *Escherichia coli*. *Biochemistry 37*, 10370-10380.

(116) Hirshberg, M., Henrick, K., Haire, L. L., Vasisht, N., Brune, M., Corrie, J. E. T., and Webb, M. R. (1998) Crystal structure of phosphate binding protein labeled with a coumarin fluorophore, a probe for inorganic phosphate. *Biochemistry 37*, 10381-10385.

(117) Dipierro, D., Tavazzi, B., Perno, C. F., Bartolini, M., Balestra, E., Calio, R., Giardina, B., and Lazzarino, G. (1995) An ion-pairing high-performance liquid-chromatographic method for the direct simultaneous determination of nucleotides, deoxynucleotides, nicotinic coenzymes, oxypurines, nucleosides, and bases in perchloric-acid cell-extracts. *Analytical Biochemistry 231*, 407-412.

(118) Busch, K., Piehler, J., and Fromm, H. (2000) Plant succinic semialdehyde dehydrogenase: Dissection of nucleotide binding by surface plasmon resonance and fluorescence spectroscopy. *Biochemistry 39*, 10110-10117.

(119) Blaner, W. S., and Churchich, J. E. (1980) The binding of NADH to succinic semi-aldehyde dehydrogenase. *European Journal of Biochemistry 109*, 431-437.

(120) Stinson, R. A., and Holbrook, J. J. (1973) Equilibrium binding of nicotinamide nucleotides to lactate dehydrogenases. *Biochemical Journal 131*, 719-728.

(121) Dammersdeklerk, A. (1958) Concentration quenching in fluorescent acene solutions. *Molecular Physics 1*, 141-150.

(122) Combs, C. A., and Balaban, R. (2004) Enzyme-dependent fluorescence recovery after photobleaching of NADH: In vivo and in vitro applications to the study of enzyme kinetics, in *Imaging in Biological Research, Pt A* pp 257-645.

(123) Cleland, W. W. (1963) Kinetics of enzyme-catalyzed reactions with 2 or more substrates or products.3. prediction of initial velocity and inhibition patterns by inspection. *Biochimica et Biophysica Acta 67*, 188-&.

(124) Cleland, W. W. (1977) Determining the chemical mechanisms of enzyme-catalyzed reactions by kinetic studies. *Advances in Enzymology Related Areas of Molecular Biology 45*, 273 - 387.

(125) Cook, P. F., and Clelalnd, W. W. (2007) *Enzyme Kinetics and Mechanism*, Garland Science, New York.

(126) Cleland, W. W. (1970) Steady State Kinetics, in *The Enzymes* pp 1- 65, Academic Press Inc.

(127) Tullius, M. V., Harth, G., and Horwitz, M. A. (2003) Glutamine synthetase GlnA1 is essential for growth of *Mycobacterium tuberculosis* in human THP-1 macrophages and guinea pigs. *Infection and Immunity 71*, 3927-3936.

(128) Gray, P. J., and Duggleby, R. G. (1989) Analysis of kinetic data for irreversible enzyme-inhibition. *Biochemical Journal 257,* 419-424.

(129) Duggleby, R. G., Attwood, P. V., Wallace, J. C., and Keech, D. B. (1982) Avidin is a slow-binding inhibitor of pyruvate-carboxylase. *Biochemistry 21*, 3364-3370.

(130) Sakai, N., Tajika, Y., Yao, M., Watanabe, N., and Tanaka, I. (2004) Crystal structure of hypothetical protein PH0642 from *Pyrococcus horikoshii* at 1.6 angstrom resolution. *Proteins-Structure Function and Bioinformatics 57,* 869-873.

(131) Krissinel, E., and Henrick, K. (2004) Secondary-structure matching (SSM), a new tool for fast protein structure alignment in three dimensions. *Acta Crystallographica Section D-Biological Crystallography 60,* 2256-2268.

(132) Hung, C. L., Liu, J. H., Chiu, W. C., Huang, S. W., Hwang, J. K., and Wang, W. C. (2007) Crystal structure of *Helicobacter pylori* formamidase AmiF reveals a cysteine-glutamate-lysine catalytic triad. *Journal of Biological Chemistry 282*, 12220-12229.

(133) Endrizzi, J. A., Kim, H. S., Anderson, P. M., and Baldwin, E. P. (2004) Crystal structure of *Escherichia coli* cytidine triphosphate synthetase, a nucleotide-regulated glutamine amidotransferase/ATP-dependent amidoligase fusion protein and homologue of anticancer and antiparasitic drug targets. *Biochemistry 43,* 6447-6463.

(134) Nakamura, A., Yao, M., Chimnaronk, S., Sakai, N., and Tanaka, I. (2006) Ammonia channel couples glutaminase with transamidase reactions in GatCAB. *Science 312*, 1954-1958.

(135) Mouilleron, S., Badet-Denisot, M. A., and Golinelli-Pimpaneau, B. (2006) Glutamine binding opens the ammonia channel and activates glucosamine-6P synthase. *Journal of Biological Chemistry 281*, 4404-4412.

(136) Bieganowski, P., and Brenner, C. (2003) The reported human *NADsyn2* is ammonia-dependent NAD synthetase from a pseudomonad. *Journal of Biological Chemistry 278*, 33056-33059.

(137) Wojcik, M., Seidle, H. F., Bieganowski, P., and Brenner, C. (2006) Glutamine-dependent NAD^+ synthetase - How a two-domain, three-substrate enzyme avoids waste. *Journal of Biological Chemistry 281,* 33395-33402.

(138) Luke, K. A., Higgins, C. L., and Wittung-Stafshedel, P. (2007) Thermodynamic stability and folding of proteins from hyperthermophilic organisms. *FEBS Journal 274*, 4023-4033.

(139) Eichler, J. (2001) Biotechnological uses of archaeal extremozymes. *Biotechnology Advances 19*, 261-278.

(140) Stetter, K. O. (1996) Hyperthermophilic procaryotes. *FEMS Microbiology Reviews 18*, 149-158.

(141) Razvi, A., and Scholtz, J. M. (2006) Lessons in stability from thermophilic proteins. *Protein Science 15*, 1569-1578.

(142) Saiki, R. K., Gelfand, D. H., Stoffel, S., Scharf, S. J., Higuchi, R., Horn, G. T., Mullis, K. B., and Erlich, H. A. (1988) Primer-directed enzymatic

amplification of DNA with a thermostable DNA-polymerase. *Science 239*, 487-491.

(143) Unsworth, L. D., van der Oost, J., and Koutsopoulos, S. (2007) Hyperthermophilic enzymes - stability, activity and implementation strategies for high temperature applications. *FEBS Journal 274*, 4044-4056.

(144) Matsui, I., and Harata, K. (2007) Implication for buried polar contacts and ion pairs in hyperthermostalble enzymes. *FEBS Journal 274*, 4012-4022.

(145) Vieille, C., and Zeikus, G. J. (2001) Hyperthermophilic enzymes: Sources, uses, and molecular mechanisms for thermostability. *Microbiology and Molecular Biology Reviews 65*, 1-43.

(146) Mukaiyama, A., Haruki, M., Ota, M., Koga, Y., Takano, K., and Kanaya, S. (2006) A hyperthermophilic protein acquires function at the cost of stability. *Biochemistry 45*, 12673-12679.

(147) Conners, S. B., Mongodin, E. F., Johnson, M. R., Montero, C. I., Nelson, K. E., and Kelly, R. M. (2006) Microbial biochemistry, physiology, and biotechnology of hyperthermophilic Thermotoga species. *FEMS Microbiology Reviews 30*, 872-905.

(148) Nelson, K. E., Clayton, R. A., Gill, S. R., Gwinn, M. L., Dodson, R. J., Haft, D. H., Hickey, E. K., Peterson, L. D., Nelson, W. C., Ketchum, K. A., McDonald, L., Utterback, T. R., Malek, J. A., Linher, K. D., Garrett, M. M., Stewart, A. M., Cotton, M. D., Pratt, M. S., Phillips, C. A., Richardson, D., Heidelberg, J., Sutton, G. G., Fleischmann, R. D., Eisen, J. A., White, O., Salzberg, S. L., Smith, H. O., Venter, J. C., and Fraser, C. M. (1999) Evidence

for lateral gene transfer between Archaea and Bacteria from genome sequence of *Thermotoga maritima*. *Nature 399*, 323-329.

(149) Logsdon, J. M., and Faguy, D. M. (1999) Evolutionary genomics: Thermotoga heats up lateral gene transfer. *Current Biology 9*, R747-R751.

(150) Guindon, S., Lethiec, F., Duroux, P., and Gascuel, O. (2005) PHYML Online - a web server for fast maximum likelihood-based phylogenetic inference. *Nucleic Acids Research 33*, W557-W559.

(151) Billington, R. A., Thuring, J. W., Conway, S. J., Packman, L., Holmes, A. B., and Genazzani, A. A. (2004) Production and characterization of reduced NAADP (nicotinic acid-adenine dinucleotide phosphate). *Biochemical Journal 378*, 275-280.

(152) Rising, K. A., and Schramm, V. L. (1994) Enzymatic-synthesis of NAD^+ with the specific incorporation of atomic labels. *Journal of the American Chemical Society 116*, 6531-6536.

(153) Andersson, C. E., and Mowbray, S. L. (2002) Activation of ribokinase by monovalent cations. *Journal of Molecular Biology 315*, 409-419.

(154) Switzer, R. L. (1969) Regulation and mechanism of phosphoribosylpyrophosphate synthetase.I. Purification and properties of enzyme from *Salmonella typhimurium*. *Journal of Biological Chemistry 244*, 2854-2863.

(155) Davies, L. C. (1995) Simple synthesis of the 5-O-benzoylriboside of 1,4-dihydronicotinic acid - a cofactor for dt diaphorase and nitroreductase enzymes. *Nucleosides & Nucleotides 14*, 311-312.

(156) Gaines, P. C., and Woodriff, R. (1949) Qualitative separation of copper and cadmium by sodium dithionite ($Na_2S_2O_4$). *Journal of Chemical Education 26*, 166-167.